Nanofinishing and Surface Integrity Enhancement of Inertial Sensor Microstructures using Medium Pressure Plasma Process

A thesis submitted
in partial fulfillment of the requirements
for the degree of

Doctor of Philosophy

By

D Sam Dayala Dev
Roll No. 146103034

Department of Mechanical Engineering
Indian Institute of Technology Guwahati
Guwahati, India

March, 2019

Department of Mechanical Engineering
Indian Institute of Technology Guwahati
Guwahati-781039
INDIA

CERTIFICATE

It is certified that the work contained in the thesis entitled "**Nanofinishing and Surface Integrity Enhancement of Inertial Sensor Microstructures using Medium Pressure Plasma Process**", submitted by **D Sam Dayala Dev**, Roll No. 146103034 to the Indian Institute of Technology Guwahati for the degree of Doctor of Philosophy has been carried out under my supervision in the Department of Mechanical Engineering,Indian Institute of Technology Guwahati.This work has not been submitted elsewhere for the award of any other degree or diploma.

The thesis in my opinion, has reached the standard fulfilling the requirements for the award of degree of Doctor of Philosophy in accordance with the regulations of the institute.

Dr. Manas Das

Date: Department of Mechanical Engineering

Indian Institute of Technology Guwahati

Guwahati-781039, Assam, India

Declaration

I declare that this written submission represents my ideas in my own words and where others' ideas or words have been included, I have adequately cited and referenced the original sources. I also declare that I have adhered to all principles of academic honesty and integrity and have not misrepresented or fabricated or falsified any idea/data/fact/source in my submission. I understand that any violation of the above will be cause for disciplinary action by the Institute and can also evoke penal action from the sources which have thus not been properly cited or from whom proper permission has not been taken when needed.

Date:

D Sam Dayala Dev
Roll No. 146103034

Dedicated to

My wife Sujaya Dev

and

My children Derrish Dev Sam

&

Dr Sanchna Dev Anish

ACKNOWLEDGEMENT

I acknowledge with deep sense of gratitude and respect my Supervisor Dr. Manas Das, Department of Mechanical Engineering of Indian Institute of Technology Guwahati for his valuable support, excellent guidance and active supervision throughout this period which made all the difference in this thesis work.

I also wish to thank all my doctoral committee members Prof. S Kangaraj, Prof. Bishnupada Mandal and Dr. Ganesh Naryanan for their critical reviews, advice and encouragement for innovative ideas and unexplored technology solutions.

I express my deep sense of gratitude to Dr. K Sivan, Chairman ISRO/ Secretary Dept. of Space who had been a constant source of inspiration and encouragement to this academic research late in my professional carrier.

At this moment I recall all the help rendered by my colleagues in particular Shri Enni Krishna, Shri P B Naryanakutty and Shri Sukumaran K D in Advanced Inertial System Entity in Laser gyro laboratories to setup the polishing chamber and peripherals and carry out my research activity.

I thank my friends Bro. Asir Edwin and Bro. Richardson who constantly enquired about my progress and encouraged me to pursue in spite of my busy official engagements.

I thank my family and I recall with mixed feelings the encouragement given by my father Late Mr P Devanesan when I informed him of my academic research.

Above everything I thank the Lord Almighty and submit myself, for blessing me with wisdom and good health throughout this endeavor.

D Sam Dayala Dev

ABSTRACT

Surface integrity influences several functional parameters such as friction, wear and tear, ability of distributing and holding lubricant, thin film coating etc. It is not uncommon that aerospace inertial sensor technology demands 'zero' surface and subsurface defects up to atomic level, on sensing element microstructures. These microstructures are mostly non-metallic brittle materials such as glass, fused silica, silica etc. and are machined and polished such that the surface integrity is maintained. Non-contact type unconventional nanofinishing techniques are being developed to augment or replace chemo-mechanical polishing (CMP) techniques for finishing such microstructures.

To understand and appreciate the challenges in nanofinishing of these glass microstructures, it is essential to understand the brittle damages, such as surface cracks and plastic deformation that can occur on the surface of hard brittle materials like glass ceramics fused silica etc. when the surfaces are precision ground, lapped and polished. If the amount of material removal is controlled and reduced to a certain level, only ductile damages such as plastic deformation, densification, chemical and structural changes remain. With non-contact finishing process, if the material removal amount can be further controlled at the molecular or atomic level, both structural and chemical damage free surface and subsurface can be achieved on these components. Significant gap in literature is observed for non-contact finishing of 3D freeform surfaces without precision tool positioning requirements. Novelty of the present medium pressure plasma process is that it combines the isotropic material removal capability of low pressure plasma and atomistic material removal capability of atmospheric pressure plasma. This process is capable of simultaneously polishing entire complex 3D surfaces including cavities where no tool or beam can reach.

Plasma polishing chamber is designed and built with zerodur material with an optical window to enable optical emission spectroscopy. Components up to 40 mm diameter can be processed in this chamber. Stable plasma with processing gases such as He and Ne and reactive gases such as O_2 and SF_6 up to 30 mbar pressure is achieved by using dielectric barrier capacitive coupled RF discharge. Optical emission spectroscopy is used to identify the relative density of the excited species in the plasma and monitor the various oxidation states of silica and established correlation with respect to material removal rate and ratio of oxidation states of silica Si II and Si III and the same is used as a tool to monitor the polishing process.

With He as a processing gas and oxygen as a reactive gas, surface modification is possible by medium pressure plasma. On machined fused silica surface, the achieved improvement in surface roughness is up to 68% with He-O_2 plasma while there is 85% improvement in surface

waviness. However, reactive radicals such as Fluorine is required for sustained material removal. SF_6 as reactive gas is identified with multiple experiments. Further surface finish improvement is achieved with He-SF_6-O_2 gas mixture plasma with a material removal rate of 0.008 mm^3/min. He as plasma processing gas and O_2 and Teflon as a source of fluorine also was studied but discontinued due to carbon contamination. However, SF_6 as fluorine sources is observed to be more practical and useful. Atomistic material removal has also enabled reduction in surface residual stresses and surface cracks thereby enhancing the surface integrity.

A finite element based software i.e. Comsol® is adopted to simulate plasma processing and it is used to analyse the distribution of the radicals inside the plasma chamber with and without specimens. It also utilized to find out the ratio of free volume to the total available volume of the chamber for uniform distribution of radicals. The position of planar specimens, hemispherical shell and prisms inside plasma chamber are optimized for effective distribution of radicals which are adopted in subsequent experimentations. The shape and size of the electrodes outside plasma chamber are varied to get homogenous distribution of reactive species and ions. In the presence of hemispherical shell component, the four sided electrode provides higher density of radicals. The simulated results are validated with electron temperature measurement using experimental optical emission spectroscopy data and analytical model. The temperature calculated by simulation is approximately 550 K which can be considered as 'cold plasma' process.

The developed process is used to uniformly polish the complex shaped gyro component, a hemispherical resonator shell, which is fabricated with fused silica by a rotary ultrasonic milling process. A combination of plasma polishing and cleaning process is arrived to achieve sustained polishing of the hemispherical shell. Sustained material removal rate of 0.026 mm^3/min is achieved during this process. The uniformity of material removal is confirmed by measuring the reduction in frequency mismatch and surface integrity by enhanced Q factor after each plasma processing using Laser Doppler Vibrometer. Uniform and isotropic plasma machining is ascertained by 18% reduction in frequency mismatch between two orthogonal modes. After multiple level of plasma processing the surface roughness of 22 nm is achieved. Raman spectroscopy analysis provides clear evidence of reduction in strain bonds after plasma processing. There is significant reduction of puckered four-member and three-member rings structures indicating the reduction of surface strain caused by machining process resulting in significant improvement in Q factor of hemispherical shell.

The plasma processing method developed has been successfully applied as super finishing process post chemo-mechanical polished optical prisms. The surface chemical network analyses by Raman Spectroscopy clearly indicate reduction of distorted network structure of fused silica post plasma polishing. The increase in ratio of area under 440 to 605 cm^{-1} confirms that the chemical bond structure of the surface is becoming more like bulk material and atomic level surface and sub-surface defects are reduced distinctly. Also, the surface figure is improved as indicated by reduction of power spectral density (PSD) of higher wave length even though there is marginal degradation of surface finish from 2 to 3 Å units (Ra) as achieved by chemo-mechanical polishing (CMP) process. The Plasma treated prisms when used in Gyro device, has shown increased life span without reduction of laser intensity when compared to CMP finished prisms.

A non-contact atomistic medium plasma polishing method is conceived, polishing set up is designed and developed and is capable of polishing complex shaped glass or fused silica components. The process is fine-tuned and implemented as super finishing process to remove molecular or atomic level defects in already fine finished surfaces by finishing process such as Chemo-mechanical polishing.

TABLE OF CONTENTS

LIST OF FIGURES IX

LIST OF TABLES XIV

NOMENCLATURE XVII

1. INTRODUCTION and literature survey 1

1.1 Introduction 1

1.2 Surface integrity and surface characteristics 1

1.3 Literature review of finishing process 3

1.3.1 Abrasive finishing 3

1.3.1.1 Conventional abrasive finishing process 3

1.3.1.2 Advanced abrasive finishing process 5

1.4 Review of optical finishing techniques 6

1.4.1 Classification of glass 6

1.4.2 Classification of glass polishing methods 7

1.4.3 Full lap polishing processes (Conventional methods) 8

1.4.3.1 Conventional glass polishing 9

1.4.3.2 Chemomechanical polishing (CMP) 10

1.4.4 Sub-aperture polishing (nonconventional methods) 12

1.5 Finishing of 3D free form surfaces 15

1.6 Plasma for finishing 16

1.6.1 Capacitive coupled radio frequency discharge 18

1.6.2 Review of recent literature on atmospheric pressure plasma polishing 19

1.7 Motivation and objective of the work and work plan 21

1.7.1 Motivation 21

1.7.2 Objectives of the work 22

1.7.3 Organization of the thesis 23

2. Characterization techniques adopted in plasma processing 25

2.1 Introduction 25

2.2 Optical emission spectrometer (OES) 26

2.2.1 Atomic and molecular spectra 26

2.2.2 Spectroscopic equipment 27

2.2.3 Diagnostic methods 27
2.2.3.1 Identification of particle species 27
2.2.3.2 Measurement of plasma temperature 28
2.2.3.3 Doppler broadening 28
2.2.3.4 Absolute line method 28
2.2.3.5 Relative line method 29
2.2.3.6 Particle densities 29
2.3 Laser Doppler Vibrometer (LDV) 29
2.4 Surface characterization techniques 30
2.4.1 Contact type measurement 30
2.4.2 Non-contact measurement 31
2.4.2.1 Advantage of AFM 31
2.4.2.2 Application of AFM for fused silica substrate 32
2.4.2.3 Disadvantages 32
2.4.3 Power spectral density (PSD) of roughness profile 33
2.5 Surface chemical network analysis by Raman spectroscopy 34
2.5.1 Molecular structure 35
2.5.2 Scattering process 36
2.5.3 Basic limitation of Raman spectroscopy 37
2.5.4 Raman imaging 38
2.5.4.1 Characterization of fused silica by Raman microscopy 38
3. Experimental investigation of medium pressure plasma 39
3.1 Introduction 39
3.2 System design and methodology 39
3.3 Preliminary experiments 41
3.3.1 Experiments with Teflon 45
3.3.2 Optimization of plasma processing gases 47
3.3.2.1 Advantages of SF6 gas over O_2 gas 47
3.3.2.2 Optimization of gas concentration during plasma polishing 48
3.3.2.3 Optimization of SF_6 to O_2 ratio 51
3.4 Surface finish analysis of substrate 54
3.4.1 Plasma polishing of fine machined substrate 55
3.4.2 Raman Spectroscopic analysis 56
3.5 Summary 57

4. Simulation of plasma process 59
4.1 Introduction 59
4.2 Computational domain and boundary conditions for cylindrical substrate 60
4.2.1 Simulation results and discussion 61
4.3 Simulation for Hemispherical shell 64
4.3.1 Computational domain and boundary conditions 65
4.3.2 Simulation results of Hemispherical shell 66
4.4 Simulation for Total reflecting prism 69
4.4.1 Simulation results and discussions 69
4.5 Validation of simulation results 70
4.6 Summary 72
5. Plasma processing of free form Hemispherical shell 73
5.1 Introduction 73
5.2 Preliminary experiments 76
5.2.1 Process optimization for improving MRR 79
5.3 Study of uniform plasma processing of hemispherical shell 80
5.4 Analysis of surface strain by Raman spectrometer 83
5.5 Summary 85
6. Plasma processing of Total reflecting prisms 87
6.1 Introduction 87
6.2 Experimental Design 90
6.3 Surface inspection methodology 90
6.4 Surface characterization 91
6.5 Characterization of Chemical Network 91
6.6 Results and discussion 93
6.7 Summary 100
7. Conclusion and scope for further study 101
7.1 Conclusions 101
7.1.1 Characterization techniques adopted 101
7.1.2 Experimental investigation of medium pressure plasma 102
7.1.3 Simulation of plasma process 102
7.1.4 Plasma processing of hemispherical shell 103
7.1.5 Plasma processing of total internal reflecting prisms 104

7.2 Scope for further work 104

REFERENCES 107

PUBLICATIONS 115

List of Figures

Fig. 1.1	Classification of abrasive finishing processes	5
Fig. 1.2	Classification of glass polishing methods	9
Fig. 1.3	Mutually interacting four component polishing system	10
Fig. 1.4	Typical Chemomechanical polishing setup	10
Fig. 1.5	Principle of APPP	14
Fig. 1.6	ISRO laser gyro components	21
Fig. 1.7	Hemispherical resonator gyro (HRG) components	22
Fig. 2.1	Atomic energy level diagram of He	27
Fig. 2.2	(a) Contact type surface roughness measuring system and (b) surface roughness data collection	30
Fig. 2.3	Principle of AFM	31
Fig. 2.4	AFM images of fused silica (a) before and (b) after plasma processing	32
Fig. 2.5	(a) PSD of surface profile and (b) area surface roughness profile of CMP finished optics before plasma polishing	34
Fig. 2.6	Vibration modes of molecule	35
Fig. 2.7	Typical Raman scattering of sample	36
Fig. 2.8	Raman spectra with one molecular vibration	36
Fig. 2.9	Typical Raman spectrum of fused silica	37
Fig. 3.1	Plasma polishing setup	40
Fig. 3.2	Photograph of (a) plasma polishing system and (b) plasma chamber	41
Fig. 3.3	Spectrographs of wavelength (a) 735 to 780 nm and (b) 780 to 810 nm while processing fused silica substrate with He and Ne plasma in the presence of trace amount of oxygen	42
Fig. 3.4	Comparison between O_2 plasma with He plasma having trace amount of O_2	43
Fig. 3.5	Silicone oxidation states (a) neutral ground state, (b) Si II (first ionization) and Si III (second ionization) and (c) Si IV (third ionization) and Si V (fourth ionization)	44
Fig. 3.6	Spectrographs of He and O_2 plasma in the presence of Teflon pieces; Spectrographs at (a) 440 nm, (b) 519 nm and (c) 775 to 840 nm	46
Fig. 3.7	Spectrograph of He plasma at 70W in the presence of Teflon pieces and trace amount of O_2	46

Fig. 3.8	Spectrograph of He plasma in the presence of SF_6 and O_2 gas	47
Fig. 3.9	Spectrograph of He plasma in the presence of SF_6 gas for different time interval	48
Fig. 3.10	Spectrograph of He Plasma in the presence of O_2 gas for different time interval	48
Fig. 3.11	Spectrograph of He 30 mbar, O_2 0.20 mbar and SF_6 0.5 mbar plasma for different time interval	49
Fig. 3.12	Variation of MRR with total plasma pressure	50
Fig 3.13	Variation of carbon monoxide intensity at different total pressure and input power	51
Fig 3.14	Si III variation with composition	52
Fig 3.15	Variation of Si III intensity for cases 3, 4 and 5	52
Fig 3.16	Variation of Si II and Si III intensity for cases 3 and 5	53
Fig 3.17	Weight loss vs. ratio of SF_6 / O_2	53
Fig 3.18	Silicone ions and SiF transitions with time	54
Fig 3.19	Surface profile (a) before (Ra = 1.099 µm, Rz = 9.663 µm, Wa = 0.234 µm, Rmr = 11.5%) and (b) before (Ra = 0.358 µm, Rz = 3.379 µm, Wa = 0.035 µm, Rmr = 36.2%) plasma processing	54
Fig 3.20	Surface profile (a) before (Ra = 0.256 µm, Rz = 5.352 µm, Wa = 0.226 µm, Rmr = 91.1 %) and (b) before (Ra = 0.169 µm, Rz = 1.386 µm, Wa = 0.02 µm, Rmr = 96.5%) plasma polishing on fine machined surface	55
Fig 3.21	AFM surface profile (a) before and (b) after plasma polishing on fine machined surface	56
Fig 3.21a	AFM results of (a) before and (b) after plasma processing	56
Fig 3.22	Magnified image (100X) of the specimen surface (1.5 × 1.5 mm^2) inspected (a) before and (b) after plasma processing	56
Fig 3.22a	Average surface roughness of various kind of samples before and after plasma processing.	57
Fig 3.23	Comparison of Raman spectrum of fine machined surface of fused silica before and after plasma polishing	56
Fig 4.1	2D Computational domain of the plasma chamber	61
Fig 4.2	Electron density (a) without and (b) with specimen inside plasma chamber	62

Fig 4.3	Electron density when specimen sizes are (a) three-fourth, (b) half and (c) one-fourth of chamber size	63
Fig 4.4	Variation of O 1s radical number density with increasing O_2 concentration (a) 1%, (b) 1.5%, (c) 2% and (d) 5%	63
Fig 4.5	2D Computational domain of the plasma chamber with two (a) parallel electrodes at top and bottom and (b) L shaped four sided electrodes	64
Fig 4.6	Distribution of number density of O_2b 1s radicals inside plasma chamber with (a) two parallel electrodes at top and bottom, and (b) four sided electrodes	64
Fig 4.7	2D Computational domain of the plasma chamber with hemispherical shell having two (a) top and bottom and (b) L shaped electrodes	65
Fig 4.8	Distribution of O2b1s radical density inside plasma chamber while hemispherical shell is (a) centred in the chamber without support and (b) placed at the bottom	67
Fig 4.9	Distribution of O2b1s radical density inside plasma chamber while hemispherical shell is supported by a (a) metallic and (b) dielectric stand	67
Fig 4.10	Distribution of O2b1s radical density inside plasma chamber while hemispherical shell is supported by dielectric stand with L shaped electrode	68
Fig 4.11	Distribution of O2b1s radicals having upside down hemispherical shell with modified dielectric stand for (a) top and bottom and (b) L shaped electrodes	68
Fig 4.12	A 2D Computational domain of the plasma chamber for total reflecting prism	69
Fig 4.13	(a) Electron density, (b) O1s Density, (c) O2b1s density and (d) Electron temperature	70
Fig 4.14	Electron temperature distribution of hemispherical shell	71
Fig 5.1	Cross sectional view of a typical hemispherical shell (all dimensions are in mm)	74
Fig 5.2	MRR of the substrate at different time interval	78
Fig 5.3	Vibration modes of hemispherical shell having two identical characteristics of natural frequencies in two mutually orthogonal mode shapes (a) Mode 1 and (b) Mode 2	80

Fig 5.4	Electron density when specimen sizes are (a) three-fourth, (b) half, and (c) one-fourth of chamber size	81
Fig 5.5	Laser Doppler Vibrometer (LDV) frequency plots of hemispherical shell (a) before plasma processing (as machined) and (b) after plasma processing with top and bottom electrode configuration	82
Fig 5.6	Frequency plots (a) before and (b) after plasma processing with L shaped electrode configuration	83
Fig 5.7	Raman spectrum of hemispherical shell before and after processing	84
Fig 5.8	Hemispherical shell of fused silica after plasma polishing	85
Fig 5.9	Area surface roughness plot of hemispherical shell (a) before (Ra=37 nm and Rq=53 nm) and (b) after (Ra=22 nm and Rq=33 nm) plasma processing	85
Fig 6.1	(a) Photograph and (b) line diagram of TIR prism	88
Fig 6.2	Typical (a) mechanical, (b & c) structural and (d) chemical defects on fused silica specimen	89
Fig 6.3	Typical Raman Spectrum of Fused Silica	92
Fig 6.4	(a) EDX image of TIR optics and (b) elemental concentration of contamination	93
Fig 6.5	Raman spectroscopy of optics A before plasma polishing at peak (a) 440 cm^{-1} and (b) 603cm^{-1}	94
Fig 6.6	Raman spectroscopy of optics A after plasma polishing at peak (a) 440 cm^{-1} and (b) 603cm^{-1}	94
Fig 6.7	Raman spectroscopy of optics B before plasma polishing at peak (a) 440 cm^{-1} and (b) 603cm^{-1}	94
Fig 6.8	Raman spectroscopy of optics B after plasma polishing at peak (a) 440 cm^{-1} and (b) 603 cm^{-1}	95
Fig 6.9	(a) PSD of surface profile and (b) area surface roughness profile of CMP finished Optics A before plasma polishing	96
Fig 6.10	(a) PSD of surface profile and (b) area surface roughness profile of CMP finished Optics A after plasma polishing	96
Fig 6.11	(a) PSD of surface profile and (b) area surface roughness profile of CMP finished Optics B before plasma polishing	97
Fig 6.12	(a) PSD of surface profile and (b) area surface roughness profile of CMP finished Optics B after plasma processing	98

Fig 6.13	(a) Laser light inspection set up and zoomed view of specimen A (b) before and (c) after plasma polishing	99
Fig 6.14	Laser light inspection of Optics B (b) before and (c) after plasma polishing	99
Fig 6.15	Reflected output power variation of gyro device with time period	100

LIST OF TABLES

Table 1.1	Plasma material removal mechanism spectrum	16
Table 1.2	Plasma Pressure Vs polishing applications	17
Table 1.3	Chemical plasma gases for various materials	18
Table 3.1	Transitions from 780 nm to 810 nm wavelength	42
Table 3.2	Transitions from 735 nm to 775 nm wavelength	42
Table 3.3	Surface finish achieved on fused quartz specimens	44
Table 3.4	Transitions from 440 nm to 520 nm	45
Table 3.5	Observed Silica ion, Flourine and SiF transition	47
Table 3.6	Experiments with different gas compositions	49
Table 3.7	Plasma experiments with different gas compositions for constant total pressure and power	51
Table 4.1	Main reactions occurring inside the plasma chamber	60
Table 4.2	Measured plasma temperature from Comsol® simulation and optical emission spectroscopy	71
Table 5.1	MRR of fused silica substrate at different plasma excitation power and total pressure	77
Table 5.2	Different processing sets with different stages of plasma cleaning and plasma processing	79
Table 5.3	Area under Raman peaks before and after processing	84
Table 6.1	Area and ratio of Raman spectroscopy peaks before and after plasma processing	94

NOMENCLATURES

$\mathring{A}$	Angstrom
A_p	Powered electrode
A_g	Grounded electrode
T_e	Electron temperature
T_i	Ion temperature
K_B	Boltzmann's constant
e_v	Electron volt
h	Plank's constant
λ	Wavelength
v	Frequency
A	Einstein's coefficient
E	Energy of transition
g	Degeneracy of states
I	Intensity of transition
λo	The central wavelength
λ_d	Width of the wave length
me	Mass of the electron
mi	Mass of the ion
T_{gas}	Temperature of the gas
c	Speed of the light
m	mass

ACRONYM

AFM	Abrasive flow machining
MAF	Magnetic abrasive finishing
MRAFF	Magnetorheological abrasive flow finishing
MFP	Magnetic float polishing
MRF	Magnetorheological finishing

MRR	Material removal rate
SSD	Sub-surface damage
RAP	Reactive atom plasma machining
APPP	Atmospheric pressure plasma polishing
APPJ	Atmospheric pressure plasma jet
HER	High etching rate
LER	Low etching rate
MWP	Microwave plasma
OES	Optical emission spectrometer
NIST	National institute of standards and testing
LIDT	Laser induced damage threshold
CRM	Collision radiative model
HF	Hydrofluoric acid
NIST	National Institute of standards and Testing
PSD	Power Spectral Density
CMP	Chemo Mechanical polishing
RF	Radio frequency
ISRO	Indian Space Research Organization
HRG	Hemi Spherical Shell
LDV	Laser Doppler Vibrometer
FEM	Finite Element Method
AFM	Atomic Force Microcopy
FWHM	Full Width Half Maximum
PTFE	Poly Tetra Fluro Ethylene
U V	Ultra Violate
EDX	Energy Dispersive X ray spectrometer
TIR	Total Internal Refractive
EMM	Elastic Emission Machining
DBD	Dielectric Barrier Discharge
MWP	Micro Wave Polishing

Chapter 1

INTRODUCTION AND LITERATURE SURVEY

1.1 Introduction
1.2 Surface integrity and surface characteristics
1.3 Literature review of finishing processes
1.3.1 Abrasive finishing
1.3.1.1 Conventional abrasive finishing processes
1.3.1.2 Advanced abrasive finishing processes
1.4 Review of optical finishing techniques
1.4.1 Classification of glass
1.4.2 Classifications of glass polishing methods
1.4.3.1 Conventional glass polishing
1.4.3.2 Chemomechanical polishing (CMP)
1.4.4 Sub-aperture polishing (nonconventional methods)
1.5 Finishing 3D free form surfaces
1.6 Plasma for finishing
1.6.1 Capacitive coupled radio frequency discharge
1.6.2 Review of recent literature on atmospheric pressure Plasma polishing
1.7 Motivation and objectives of the work and work plan
1.7.1 Motivation
1.7.2 Objectives of the work

1.1 Introduction

Over past many decades, human kind has consistently improved their surface finishing (polishing) ability of the order of few nanometer (nm) and currently few order of angstrom ($\mathring{A}$). As the human race is developed, surface quality is transformed from decorative to an essential function for certain applications such as telescopes. Modern measurements on 17^{th} century telescope lenses had been found to be of superb quality for that time. Copper and silicon polishing has been the key of interest over last twenty years due to the necessity of finishing for the manufacture of integrated circuit chips. The majority of the polishing, however, still lies in the realm of glass and glass ceramic substrates which are used in different applications like for optics in lithographic machines, laser systems and for an array of microstructures in aerospace sensors.

1.2 Surface integrity and surface characteristics

Advanced processing technologies are promised to have enhanced functional performance with improved product quality. The quality and reliability of the components

mostly depend on the material removal mechanism during fabrication. The quality of a surface is defined as surface integrity. Product performance correlation with various material removal as well as surface finishing mechanism is highly essential. Typical modifications of surface are recognized as phase transformations, plastic deformation, micro-cracking, surface impregnation of polishing powders, hardness variations, elastic modulus variations, tears and laps, residual stress distribution, loss of quality factor of resonating structures etc.

Various components of advanced engineering materials such as fused silica, silicon carbide and aluminum oxide with low surface roughness value and high form accuracy are vital in advanced engineering industries, especially, in ultra-precision manufacturing industries. These advanced materials and super alloys such as titanium, ceramics, glasses and nickel based super alloys are being used due to their high strength to weight ratio, resistance to heat, wear, corrosion and good toughness. These materials play a vital role in various manufacturing sectors such as aerospace, automotive, semiconductor etc. These materials are difficult–to-machine by conventional manufacturing methods.

Finishing operations of these advanced engineering materials are most critical and expensive part in global production process. Fine abrasives processes are in use for finishing purposes since long back. Abrasive finishing is mostly used in the realization of components with high quality surface topography and integrity. The finishing operation is employed as a last operation on high-value added engineering components. Surface integrity has a critical role in most of the engineering components.

Modern sensor technology demands ‘zero defect’ surface for their functional performance and reliability. Subsurface damage and nano-stress induced effects dominate the performance degradation as the size of the micro structures shrink further. As the thrust on miniaturization and complexity of components/ microstructures grow rapidly, demand on new capabilities in surface finishing processes also rises multifold. This has put forth the need of advanced characterization tools to analyze the surface with very thin sublayers of the finished products.

It is imperative that the microstructures used in aerospace sensors are highly complicated and miniaturized with freeform surfaces. These components demand very high level of surface integrity. Hence, the need for developing newer finishing processes which can enhance the surface integrity of such microstructures and thereby achieving improved performance.

The scope of present chapter is the literature review of all finishing processes and in particular on glass or glass ceramic materials and also to identify gap in the literature.

Fundamental information on plasma and the mechanism involved in material removal on various materials by wide spectrum of plasma with varying characteristics are studied. Recent research activities in Atmospheric Pressure Plasma Polishing (APPP) are reviewed in details to generate maximum input for the proposed research work. Finally, the experimental investigations are carried out at IISU, Trivandrum in tune with the objectives of the present work and further work plan is charted out for research in the area of Nano finishing and enhancement of surface integrity of inertial sensor microstructures.

1.3 Literature review of finishing processes

In order to discuss the advanced ultraprecision finishing processes, it is essential to understand traditional finishing processes. Abrasive finishing operations are amongst the oldest ones employed in manufacturing utilized to achieve required geometrical accuracy and surface properties by removing material from the workpiece surface.

1.3.1 Abrasive finishing

Abrasive finishing processes can be categorized into two classes; bonded abrasive finishing processes (grinding, honing etc.) and free flowing abrasive finishing processes (abrasive flow machining, magnetic abrasive finishing, etc.). The first category is usually called "conventional (abrasive) finishing processes" while the second one is named as "advanced (abrasive) finishing processes". Abrasive finishing process are used primarily because of low force and low penetration depth and simultaneous material removal in the presence of abrasive's random cutting edges with random orientation and geometry. Because of micron/submicron chips being produced in abrasive finishing, it results in a better surface finish with close dimensional tolerances and allows machining of difficult-to-cut materials.

1.3.1.1 Conventional abrasive finishing processes

In the manufacturing industries, **grinding** is a common method used for finishing parts to provide a reasonably good surface finish and close tolerances. Although, grinding is more efficient for removing material than other finishing processes, it is difficult to achieve desired fine finish by grinding alone. The problem associated with grinding is that the grinding wheel fine grits get loaded heavily with the debris removed from the workpiece material. It frequently requires dressing of the grinding wheel. The grinding process develops localized heat generation causing thermal stresses with potentially harmful effects on surface integrity.

Lapping is performed by pressing a lap against the work surface and moving back and forth over it. Lapping is a low pressure abrading process which is used to produce a geometrically true surface, to correct minor surface imperfections and to improve the fit between two matching surfaces (Chang et al., 2000). Lapping process does not produce much heat or high stresses as unlike grinding process. Thus, it avoids the chances of burning of the surface or the formation of the grinding cracks. Lapping is a slow process of material removal and it is relatively expensive. To avoid micro cracks on the finished surface, it is essential to apply suitable lapping pressure. The rate of stock removal is low due to low cutting speed and small penetration of abrasive grains into the workpiece. Abrasive particles are embedded in the lap or may be carried through slurry.

Honing is an abrading process carried out at low velocity with the help of bonded abrasives. Commonly, it is employed for finishing round and curved surfaces. It not only produces a high finish, but also corrects the slight out-of-roundness, taper and axial distortion in the workpiece.

In honing operation, generally rotary and reciprocating motions are provided to the hone tool. The honing gives a smooth finish with a characteristic cross hatched appearance. Typical applications of honing are finishing of automobile engine cylinders, bearings, gun barrels, piston pins and shafts. Tough non-ferrous metals cause clogging of the voids of the abrasive sticks, thus difficult to hone. Conventional machining while adopting to advance engineering materials, these suffers from long lead time as well as high production cost. Figure 1.1 shows the classification of various abrasive fine finishing processes (conventional as well as advanced) as proposed by Komanduri et al. (1993).

Hardest materials like hardened steel, glasses, ceramics, titanium and nickel super alloys provide manufacturing challenges for given size, shape and finish. It is essential to process these materials under benign conditions. Also, finishing of these materials being used in high-tech industries has to be effective. This demands the development of non-traditional (or advanced) finishing processes.

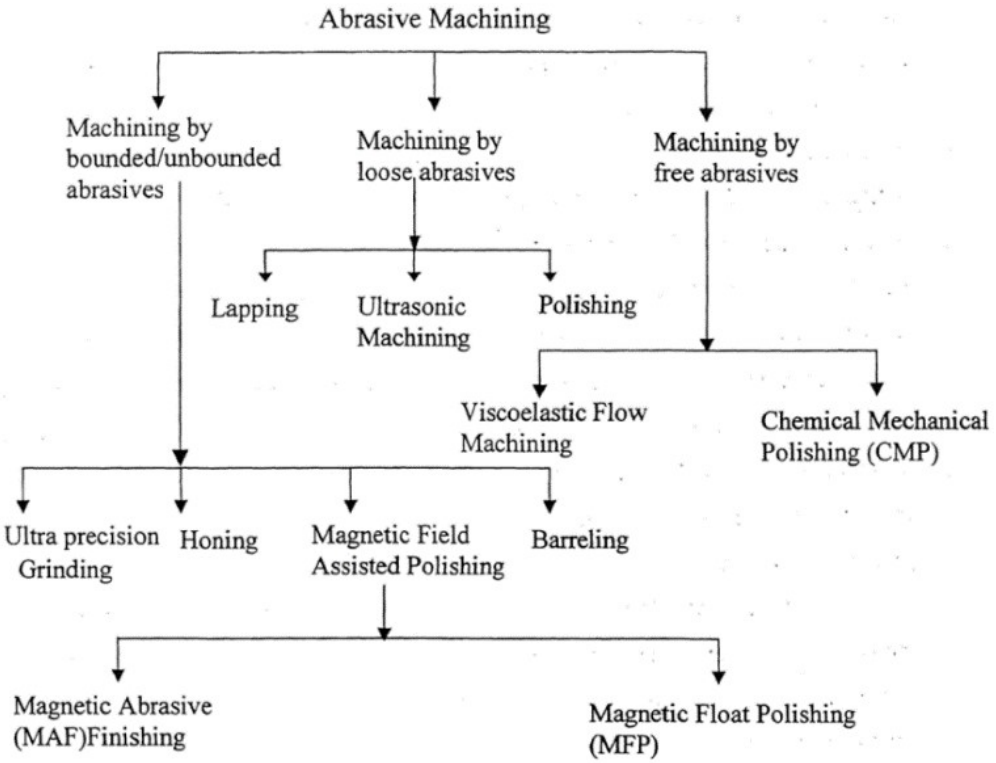

Fig. 1.1 Classification of abrasive finishing processes (Komanduri et al., 1997; Copyright from Elsevier with license No. 4635910093434)

1.3.1.2 Advanced abrasive finishing processes

Conventional abrasives are used for final processing i.e. post milling or cutting operation, but the geometry undergoes continuous change during processing. There are many measures under taken for fine finishing and producing nanometer surface finish. Hence, abrasives are being used in various forms such as loose abrasives for polishing and lapping and bonded form in grinding wheels for realizing required surface finish and integrity. Also, abrasive laden viscoelastic polymeric medium is used in Abrasive flow machining (AFM) for advanced finishing.

Abrasive flow machining (AFM)

Abrasive flow machining (AFM) was first developed by Extrude Hone Corporation, USA in 1960 (Rhoades, 1988). In AFM (Jain et al., 1999), finishing is performed by flowing a semisolid abrasive laden medium over the surface to be finished. The rheological property of the media determines the level and quality of polishing.

Przyklenk (1986) observed that the material removal capacity of high viscous base medium was around 300 times greater than that of less viscous base medium. The important

parameters which influence stock removal and medium velocity are abrasive percent concentration, grain size and viscosity of the base medium. The two possible means of increasing viscosity suggested are either by increasing percent contribution of abrasives in the medium or by using more viscous base medium. Loveless et al. (1994) also concluded from their experimental study that initial surface roughness and viscosity significantly affect the improvement in surface finish for a certain finishing cycles.

Magnetic field assisted advanced finishing processes (AFPs)

In contact type fine finishing process, accurate control of forces is essential to avoid damage surface topography and fine tolerances. The draw back in existing finishing technology is the lack of control in abrasive forces. The nature and strength of bonded abrasive material decides the level of abrasion and quality of final surface. Few newly developed magnetic field assisted finishing processes are Magnetic Float Polishing (MFP), Magnetic Abrasive Finishing (MAF), Magnetorheological Abrasive Flow Finishing (MRAFF) and Magnetorheological Finishing (MRF) (Gessenharter et al., 2003; Seok et al., 2007 and Kim et al., 2005).

1.4 Review of optical finishing techniques

Advanced optical designers require shapes and materials that are challenging to finish. As design become more intricate, new fabrication tools and techniques are needed. A general overview of some precision polishing methods and advanced surface finishing methods that enable precision fabrication of flat and surfaces and increasingly complex optics, such as aspheric and freeform shapes are highlighted. In order to understand and appreciate the challenges in optical polishing, the basic classification of most commonly used optical glass with the precision and advanced applications are to be studied.

1.4.1 Classification of glass

(a) Fused Silica is the purest form of Silicon dioxide (SiO_2). This glass has superior transmission in both the UV and IR spectra, a very low dielectric coefficient and excellent properties where fluorescence or solarization are an issue. Unlike sapphire (a crystalline structure, not amorphous), fused silica can be shaped to different forms and produce extremely high grade (pure) fused silica glasses that exhibit excellent ultraviolet and infrared performance. For applications requiring purity i.e. a non-reactive, durable substrate and

homogeneity between melts (uniform optical properties), this high quality material is the likely choice.

(b) Bk 7 is a barium borosilicate glass known for its high transmission, clean and clear appearance. It is most common material for many optical glass applications as it offers good optical properties at a reasonable price. It is mostly used as a standard to compare with other glass materials.

(c) Borofloat is a particular schott borosilicate glass. It is characterized by its excellent flatness and better resistance to heat. These characteristics make borofloat costlier than float glass. However, borosilicate retains its shape and can handle thermal shock better than other less expensive glasses.

(d) B270/crown glass/water white has good optical transmission and appears crystal clear as a result of fewer impurities. It can be easily polished and readily accepts all types of coating**.**

(**e) GE 124 & NSG OZ** are fused quartz glasses. Fused quartz is used in applications where good ultraviolet light transmission, very good thermal stability and chemical inertness (resistance to stains) are required. Fused quartz is harder and more difficult to polish than borosilicate, hence, costlier. For application where prolonged or periodic temperatures are more extremely prevailed or there is a need for higher purity, fused quartz is an appropriate choice.

(f) Soda lime / float glass is a common, inexpensive substrate. Float glass is a sheet of glass made by floating molten glass on a bed of molten tin. This method gives the sheet uniform thickness and very flat surface. The oldest glass float, can appear with a slight greenish or blue tin, depending upon the amount of iron and other elements. It is easily tempered to increase strength.

(g) Zerodur is a glass-ceramic developed by A G Schott. It has both amorphous (vitreous) and crystalline components. It is mainly used in many optical devices such as telescope and laser gyro cavity where near-zero coefficient of thermal expansion ($\sim 0.02 \times 16^{-6}$/K at 0–50 ^{0}C) and /or excellent thermal shock resistance of the substrate material is required.

1.4.2 Classifications of glass polishing methods

The following classification chart provides an idea of basic processes for precision polishing of glass.

1.4.3 Full lap polishing processes (conventional methods)

There are three popular theories of glass polishing. Hooke, Newton and Rayleigh proposed 'wear theory', which says that the polishing takes place by the mechanical wear of the abrasives with glass surface. In short, it is an extension of grinding. This is also called the 'hypothesis of abrasion'. The other theory is 'flow theory' or 'flow hypothesis', and it was proposed by Beilby. It says that the polishing compounds can be used to form amorphous layer of glass that can be smeared to fill the void of the glass surface. Finally, Preston (1930) and Grebenshchikov (1931) had advanced the 'chemical theory' or 'chemical hypothesis'. The actual material removal rate in the glass depends on chemical durability of glass rather than micro-hardness or softening point of glass. As stated by Izumitani (1988), there is no bulk material removal, instead, only soft hydrated layer is removed. There is a chemical reactivity between glasses, sometimes with lap and always with polishing slurry which is a mixture of water, polishing powder and additives. However, as the wear on the polishing pads takes place, the amount of energy put in is reduced. Hence, MRR is also reduced. The SiO_2 film surface first reacts with cerium oxide (CeO_2) particles and a bonding of Si-O-Ce is formed. Further, mechanical tearing of those bonds leads to the removal of SiO_2 instead of lump Silicon hydroxide ($Si(OH)_4$).

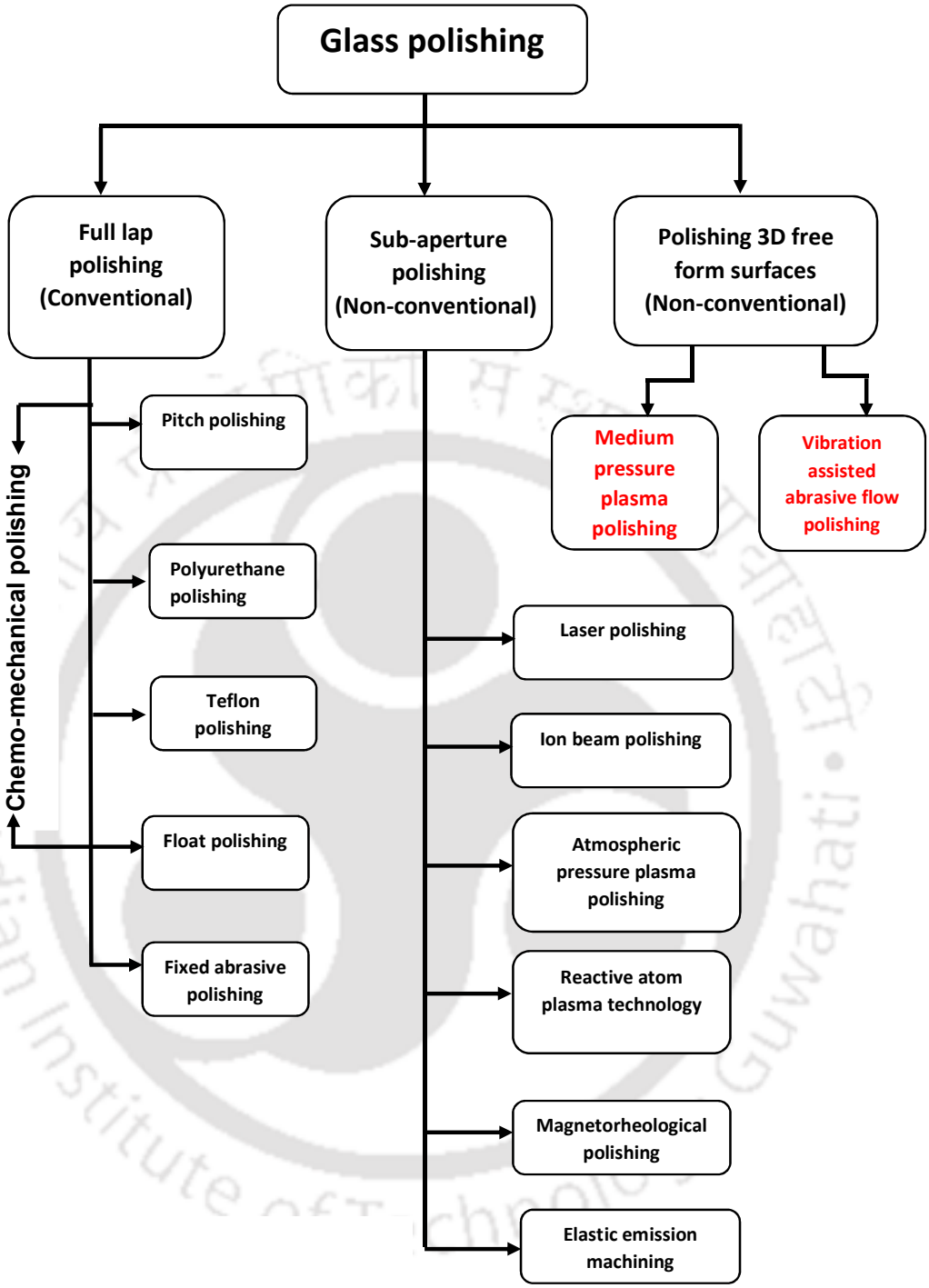

Fig. 1.2 Classification of glass polishing methods

1.4.3.1 Conventional glass polishing

Lapping and polishing are inherent conventional processes to fabricate optics of desired shape, size, surface figures and quality. These processes basically involve interaction of workpiece with the lap through solid granular particles (slurry) mixed with a fluid in a four-component-mutually-interacting system as shown in Fig. 1.3.

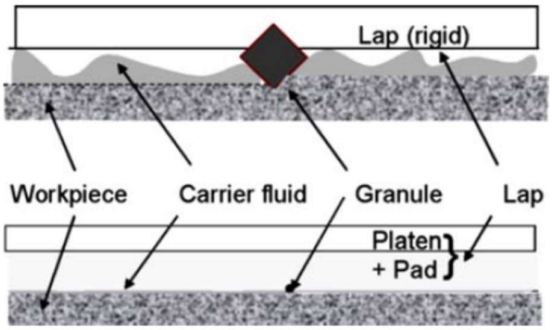

Fig. 1.3 Mutually interacting four components polishing system

1.4.3.2 Chemomechanical polishing (CMP)

Chemomechanical polishing process is most widely used and is most matured among non/less-damaging polishing technologies. Super-smooth polished surface can be successfully obtained through mechanical and chemical reactions among abrasive, workpiece and environment (Jairath et al.1994, Xie, Y and Bhushan, B (1996)). These interactions can be in macroscopic scale like ductile cutting using fine diamond to remove material in the micron range and affects the workpiece property up to 100 of μm depth. Also, in microscopic scale like dissolution, the workpiece affected in the nanometer level laterally as well as vertically. The outcome of these interactions is given in terms of MRR, surface figures (flatness and roughness) and sub-surface damage (SSD) of the workpiece.

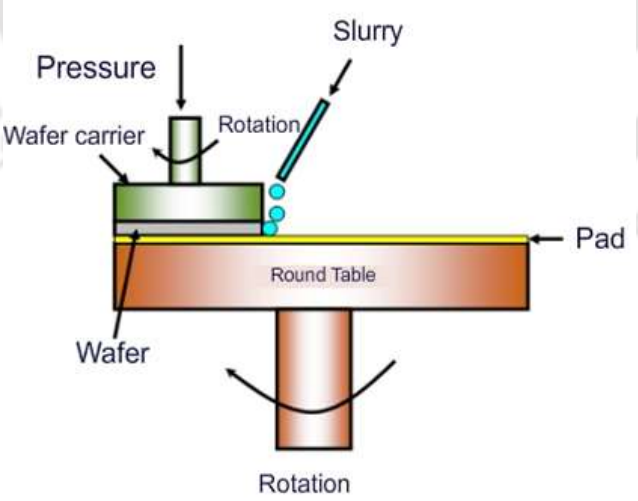

Fig. 1.4 Typical chemomechanical polishing set up

Pitch polishing

It is one of the most historic processes and is used since ages. Pitch is a very complex material. Limited information is available in the literature regarding composition and properties

of optical polishing pitch (Gillman, B. E and Tinker, F (1999), Sutton, S (2004)). Compositions are mostly proprietary in nature. It is generally understood that the material consists of various amounts of the following: residues distilled from tar, oil or wood; rosin, a derivate of turpentine which comes from sap of pine trees or stumps to increase melting point and tackiness; beeswax or linseed oil to lower melting point: asphalt; flake shellac; paraffin wax; wood flour; or walnut shell flour. Important properties are viscosity (stared to be in the range of 10^7 to 10^9 Pa.s), softening temperature in the range of 55-70^{0}C, penetration hardness (shore D by 60-80), coefficient of friction (tackiness), and groove pattern. After the glass is ground, it is integrated to a spherical viscoplastic pitch lap. Now, any tangential force that will be applied to the workpiece will cause it to slide on the lap surface which is wetted with a slurry containing abrasives. Here, the high spots are under more pressure and hence, they are removed preferentially. Therefore, the spherical surface is obtained almost automatically. The abrasives could be silicon carbide (SiC) used for rough grinding, aluminum oxide (Al_2O_3) which is used for fine grinding, and other compounds like cerium oxide (CeO_2), zirconium oxide also used for ultrafine grinding. The surface roughness that is achieved is ~5.7 Å RMS for BK 7 with Al_2O_3 abrasives and 2.6 Å with CeO_2, 8Å for flint glass with Al_2O_3 abrasives and 0.8 Å with CeO_2 abrasives (Achim, J et al., 1992).

High metal removal rate and easy lap preparation are the advantages of pitch polishing. Lap has to be frequently checked and corrected. Also, the pitch is volatile and sometimes acts as a fluid. Also, the abrasive media can sometimes be reactive with the surface. These are some of the disadvantages of pitch polishing method.

Polyurethane polishing

Basically introduced in 80's by Carl Zeiss optics, it was developed due to the need for high speed and finer accuracy in advanced field of engineering. Pitch and cloth were replaced by highly wear resistant polyurethane polishing pads. The polyurethane lap is trued to the desired shape on workpiece surface (Xu et al., 2010). During polishing this master shape is copied on the workpiece at high speed. The rigid lap does not flow and so a fairly high number of workpieces can be polished by one lap before regrinding. Same slurry as the one used in pitch polishing is used here. Polyurethane is expected to perform better than pitch in comparison of MRR. The MRR for BK 7 and fused silica are 10 and 4 µm/h respectively (Yaguo Li and Jian Wang 2009). The polishing pad used here is polyurethane pad and the same slurry of pitch polishing is used. Better MRR and surface finish than pitch polishing is

observed, however, occasionally small pits and depression are also introduced during the process.

Teflon polishing

It is one of the fine finishing processes where really low MRR is achieved. Before polishing a workpiece surface on Teflon, it must be polished using a pitch so that all imperfections and grinding marks can be removed (Leistner, 1979).

Float polishing

Float polishing is done by rotating a tin lap with aqueous polishing slurry of colloidal silicon oxide at high speed (Namba, Y and Tsuwa, H (1987)). Non-porous tin lap is one of the essential elements for the success of float polishing. The size of these abrasive polishing particles is in the range of 4-7 nm, in contrast to the conventional polishing particles of the order of 1 μm. The elastic bombardment by the polishing grain on the workpiece leads to the contact bonding and removal of weakly bonded atoms from the surface. The average surface roughness that can be experimentally obtained for some glass are as follows: Zerodur 8.5Å, fused quartz 11Å, Cer-Vit 3.2Å (Jean M. Bennett et al., 1987).

Fixed abrasive polishing

When lower quality lenses are to be finished in large numbers, this process can be adopted. Plastic laps with pure water as lubricant and sub-micron sized CeO_2 as abrasives are used (Li et al., 2012). No chemical unpredicted slurry is required; it has distinct advantage over polyurethane polishing apart from higher MRR CeO_2 is selected as abrasives due to its high polishing efficiency for soft and moderately hard glasses. The average RMS that can be achieved is 2 nm. The advantages of this process are high polishing efficiency (high MRR per stroke of polisher), temperature stability, low cost of consumables; compatibility which reduces overall production time when employed in mass production. The main disadvantages of this process are tool life is in hours and tool has to be checked for shape accuracy frequently.

1.4.4 Sub-aperture polishing (nonconventional methods)

With the advances in the technology and new invention in the space technology, there was a need to develop optical surfaces of free form components. This was not possible with the conventional full aperture polishing methods and computer control was necessary to generate aspheric and freeform surfaces. This led to the development of non-conventional processes.

Ion Beam Polishing

The surface atoms are removed by the impact of energetic ions and atoms (Wilson and Mcneil, 1987). It needs vacuum pumping facility, gas medium lines, loading of workpiece, cooling of system and ion beam source. During sputtering process, ions collide with the substrate resulting in cascade collision of atoms. The distance between the ion source and the workpiece holder is smaller than the mean free path length of ions so that the extracted ions will reach the workpiece without collision. A typical system may have a vacuum of 2×10^{-6} Torr or lower. The workpiece holder can be made with all the possible advances in mechanisms and with all the possible degrees of freedom. The best performance (cascade collision) happens when ion beam incidence angle is between 45^0 and 60^0. The average surface roughness of 0.2 nm can be achieved by this process. The beam diameters can be 5 to 0.5 μm. the MRR can reach up to 1.050 $\mu m^3/s$ (Rauschenbach, B et al., 2008). It is suitable for special purpose application, although it is expensive with limited availability and long polishing cycles.

Reactive atom plasma (RAP) machining

The chemically reactive jet of plasma is used to precisely shape optical and semiconductor surfaces by reactive atom plasma (RAP) method. Basically, it is dry chemical etching process. As material removal is done chemically there is no subsurface damage. Computer numerical control RAP process can polish or correct precisely complex shape. Energy associates with this process is considerably large, approximately 1 keV compared to plasma process which is typically less than 100 eV.

Atmospheric pressure plasma polishing (APPP)

Chemical reaction between the plasma and surface atoms are engineered to achieve atom by atom material removal. As this process is purely chemical in nature, hence surface and subsurface defects which are usually appear in conventional machine process are absent in APPP. Uniform low temperature plasma can be generated over a large surface at low cost and more extensive application range. Also due to the presence of more active and multifarious species than those generated from wet chemical reactions, it easily reacts with surface. The reactive gas and plasma process gas with optimum ratio is mixed and fed to the plasma torch. High energy reactive radicals are generated by ionization through RF excitation which cause chemical reaction with the surface atoms. Atomic scale material removal can be achieved by

this process. For different materials, different combinations of plasma and reactive gas are used. Like for silicon, He is used as plasma and carbon tetrafluoride (CF_4) is used as reactive gas. This gives a radical F*and SiF_4 both of which are volatile and machined surface is left with no contaminant. The principle of APPP is shown in Fig.1.5 which shows how the reactive radicals combine with the workpiece surface atoms and volatile products are formed. The APPP method uses cold (low temperature plasma) to avoid localized high temperature on the substrate. The temperature is just 90 ^{0}C as compared to 800-900 ^{0}C in ion beam polishing.

The system consists of gas supply lines, RF excitation power supply, corresponding impedance matching network, motion control system, hermetic chamber and removal mechanism of generated residual gas. Surface average roughness around 0.631 nm or 6.31Å is achieved by this process. This process is capable of achieving sub nanometer average surface roughness. Also, the MRR is 32 mm^3/min that is better than ion beam polishing (Zhang et al., 2008).

Advantage of this process includes the surface defects left behind for brittle materials like glass and ceramics by conventional contact polishing method are removed by APPP without inducing further defects.

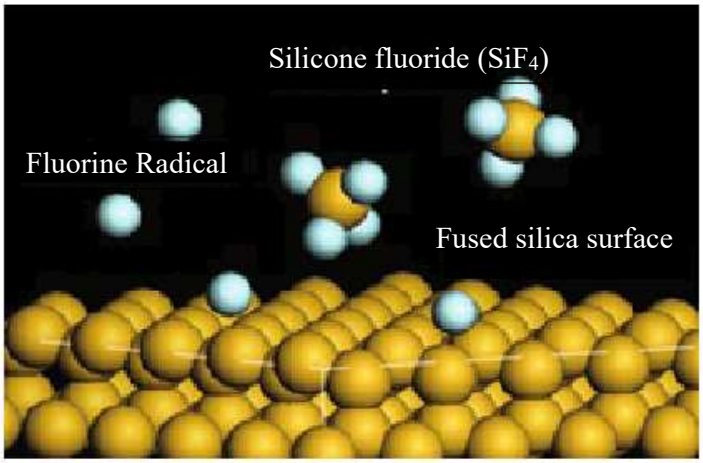

Fig. 1.5 Principle of APPP (Zhang et al., 2008).

Magnetorheological Finishing (MRF)

Magnetorheological finishing (MRF) was developed by the Center for Optics Manufacturing (COM) and QED Technologies in Rochester, N.Y. to automate high-precision optics polishing (Kordonski, 1996). Using MRF, surface roughness better than 300 Å Ra and less than 5 Å RMS are achieved while polishing optical glass and glass ceramics, respectively. The process depends on smart fluid called magnetorheological (MR) fluid. As the MR fluid

forms a polishing tool confining workpiece, it can polish all shapes and complex geometries.

Laser polishing

Laser polishing is an advanced non-contact surface finishing technique in which surface layers of tens of microns are heated up just below evaporation temperature by a controlled small size laser beam. The reduction in viscosity of the surface layer at high temperature leads to mass flow within the laser melted layers driven by surface tension force. Thus it improves the micro roughness of the surface without loss of material or need for any polishing agent.

High precision laser ablation using a focused beam is done for locally controlled ablation with small depth by employing high speed scanning method and modulating the scan speed and laser power to remove the material locally.

Elastic Emission Machining

Pure water used as suspension medium for abrasives in elastic emission machining (EEM) and it is allowed to flow over the workpiece at high speed and chemical bond is created between abrasive particle and with a work-piece as each particle flow fast the chemically bonded atoms are removed from the surface. In EEM process as material removal occur by atom by atom very good finish can be achieved without defects. Hence, the work surface can be finished with no defects (Kubota et al., 2005).

1.5 Finishing 3D freeform surfaces

Surfaces with no area of rotational variance with itself or outside surface is defined as freeform surface. Freeform surface has obituary shape and irregular surface. Freeform optics or micro structures are utilized for designing precision sensors, however, opportunities and challenges are there in machining and surface finishing of these type of components. Freeform optics has wide application prospects in different areas such as solar energy, biomedical engineering and aerospace industries. Hemispherical shell with stem can be considered as a special case of freeform optics with an area of rotational invariants.

Freeform optics play a vital role in reflective, refractive and diffractive optical systems which demand finishing of multiple surfaces on a single microstructure or inside surfaces which cannot be accessed by any tool or jets, either abrasive jets or plasma jets. Newer and

hybrid of proven processes are being developed for nanofinishing of such freeform components used in optics and sensor micro structure.

1.6 Plasma for finishing

The word plasma is used to describe a wide variety of macroscopically neutral substance containing many interacting free electrons and ionized atom or molecules. In other words, plasma, which is called the fourth state of matter is a partially ionized gas with equal number of positive and negative particles and overall the plasma remains electrically neutral.

Ion: A positively charged particle with an electron removed.

Radical: A neutral particle (atom or molecule) that exists in a state of incomplete chemical bonding and is therefore chemically reactive. It is formed by the fracture of a gas molecule by a high energy electron collision given as

$$O_2 + e^- \longrightarrow 2O^* \qquad (1.1)$$

where O* is oxygen radicals. A typical plasma contains neutral molecules at a density of $10\times10^{16}/cm^3$, radicals $10\times10^{14}/cm^3$, electrons $10\times10^{8}/cm^3$ and positive ions $10\times10^{8}/cm^3$. There are million times more radicals than ions or electrons in plasma. Radicals form more easily and their life time is much longer. Ions do not etch or remove material. Ions affect the process by energetic (physical) bombarding of the surface, influencing the chemical process of atom by atom material removal. Radicals are responsible for dry etching or material removal process. They are chemically active and react with surfaces to produce volatile products. Table 1.1 shows plasma material removal mechanism spectrum. Table 1.2 shows plasma polishing applications at different plasma pressure. Table 1.3 shows chemical plasma gases for various materials.

Table 1.1 Plasma material removal mechanism spectrum

Decreasing pressure	Description	Increasing energy
0.1 mbar	Physical (sputtering) momentum transfer and directional Etching.	
0.2 mbar	Reactive ion etching physical and chemical variable anisotropy.	Surface damage is high due to higher energy.
0.5 mbar	Chemical plasma etching, fast and isotropic.	

1 mbar – 100 mbar	**Bulk isotropic polishing due to cold chemical plasma**	**Low energy cold plasma model assumes lower plasma temperature**
1 bar	Atmospheric pressure plasma, cold chemical isotropic jet plasma (small aperture).	Very low energy and high surface integrity

Table 1.2 Plasma Pressure Vs. polishing applications

Applications / properties	**Low Pressure Plasma**		**Medium Pressure Plasma**		**Atmospheric Plasma**	
	Advantages	Disadvantages	Advantages	Disadvantages	Advantages	Disadvantages
Generation of plasma	Plasma is evenly distributed.	Complex vacuum technology.	Plasma can be made evenly distributed inside chamber	Complex vacuum and flow control	Plasma treatment is possible directly at the conveyor belt. In-line is suitable. Vacuum set up is not required.	The treatable area is limited.
Treatment of metal	Oxidation-sensitive objects can be treated with plasma.	Microwave plasma can transfer energy to overheat.	Passivation and cleaning can be done.	Microwave plasma can transfer energy to the object.	When aluminum is treated with plasma, very thin oxide layers (passivation) are formed.	Plasma treatment of oxidation-sensitive objects is limited.
3D Objects	All items in the plasma chamber are treated simultaneo-usly. Also cavities can be treated from inside.	Not known.	All surfaces can be treated uniformly and simultane-ously. Also cavities can be treated from inside wide aperture.	Establishing isotropic chemically reactive plasma is a challenge. Custom designed chamber may be required for uniform polishing.	Local surface treatment is possible (e.g. gluing groove).	Complex robotic technologies are necessary for treatment of surfaces with deep grooves. It is a small aperture process.
Surface integrity and surface finish of optics	Isotropic polishing is possible.	Limited applications	Surface integrity is very good due to non-contact chemical reactive plasma.	Only incremental surface finish can be achieved.	Surface integrity and surface finish improves.	Only locally very small area can be covered.
Electronic/ semi-conductors	Plasma treatment of state of the art electronic devices, printed circuit boards and semiconduc-tors can be done.	Not known	To be explored.	To be studied.	Plasma treatment of metal or indium tin oxide contacts is possible directly.	Reduced ability to treat surfaces with deep grooves may limit the usages of atmospheric plasma.

Table 1.3 Chemical plasma gases for various materials

Material	Kind of gas plasma
Si	CF_4, CF_4+O_2, $CC1_2F_2$, SF_6
poly-Si	CF_4, CF_4+O_2, CF_4+N_2, SF_6
SiO_2	CF_4, CF_4+O_2, HF*, SF_6
Si_3N_4	CCl_2F_2, C_3F_8**
Mo	CF_4, CF_4+O_2
W	CF_4, CF_4+O_2
Au	$C_2Cl_2F_4$
Pt	CF_4+O_2, $C_2Cl_2F_4+O_2$, $C_2Cl_3F_3+O_2$
Ti	CF_4
Ta	CF_4
Cr	Cl_2, CCl_4, CCl_4+Air
Cr_2O_3	CI_2+Ar, CCl_4+Ar
Al	CCI_4, $CC1_4$+Ar, BCI_3
Al_2O_3	$CC1_4$, $CC1_4$+Ar, BCl_3
GaAs	CCI_2F_2

1.6.1 Capacitive coupled radio frequency discharge

Capacitive coupled radio frequency discharge consists of two typically plane parallel electrodes of either same or different surface areas. The electrodes are located within the vacuum chamber in direct contact with the plasma or isolated from the plasma by a dielectric medium. If the electrode is behind a dielectric barrier, then it is called dielectric barrier RF excited plasma.

The chamber is usually grounded. One electrode is connected to a RF generator via an impedance matching network and the electrode is connected to a RF high voltage wave form. The externally applied radio frequencies typically range between 1 to 250 MHz. The match box matches the impedance of the load (plasma) to the output impedance of the source (RF generator), which is typically 50Ω. If the surface area of the powered electrode (A_p) is equal to the surface area of the grounded electrode (A_g) including all grounded surfaces in contact with the plasma, the discharge is symmetric. If Ag ≠ Ap, then the discharge is geometrically asymmetric.

Due to the difference between electron mass (m_e) and ion mass (m_i) i.e. $m_i / m_e >> 1$, the ion inertia is much higher than the electron inertia. Since the electrons have much higher energies than ions, electrons will lose in the walls quickly, if the plasma gets in contact with the boundary wall. As a consequence, a sheath of positive space charge will develop adjacent to the wall. In the sheath an electric field accelerates ions towards the wall and repels electrons confining them in the discharge. In the sheath, quasi-neutrality is violated. In the quasi neutral bulk, an ambipolar field confines ion and electron diffusion. Depending on the choice of

electrode surface area (i.e. chamber geometry), electrode gap, applied voltage wave forms, gas mixture, pressure and power, a variety of capcitively coupled discharges can generate. Each type provides unique features useful for particular application. The gas mixture and pressure play the major role in defining the plasma characteristics. The choice of processing gas is essential for chemical processing in the plasma itself and at surfaces in contact with the plasma. Depending on the gas, the discharge might be electropositive or electronegative. Capacitive coupled dielectric barrier RF discharges can be operated at low pressures to less than 10^{-2} mbar for an isotropic etching process or at a high pressure like atmospheric pressure plasma jets. High pressure micro discharges can provide high radical density which is essential for material removal. Non-equilibrium ($T_e \neq T_i$) and low temperature (K_BT_i is ~0.03eV, $T_e >> T_i$) plasma is defined as cold plasma. Cold plasmas are of paramount importance for nanofinishing processes due to insignificant temperature induced degradation. The electron temperature is 'K_BT_e' is typically of the order of few eV, where the ion temperature T_i is close to room temperature.

1.6.2 Review of recent literature on atmospheric pressure plasma polishing

Gerhard et al. (2013) investigated the polishing of optical media by dielectric barrier discharge gas plasma at atmospheric pressure. Precision polishing of the sub-nanometer scale is achieved using dielectric barrier discharge at atmospheric pressure. The process gas used is Argon, with traces of oxygen. They reported significant topographic surface modifications on the optical media. Approximately, 20% reduction in surfaces roughness is achieved along with 80% improvement in waviness with increased surface energy on optical materials including fused silica. The material removal is explained by ion bombardment and de-excitation of argon species. It is explained that the plasma discharge causes high electric field strength at roughness peaks, initiating corrosion effects.

Wang et a1. (2011) studied surface changes in terms of surface modules and hardness, after atmospheric pressure plasma polishing and demonstrated improved surface mechanical properties. Nano indentation tests were carried out to evaluate the residual stress on the surface before and after polishing. They demonstrated a decrease of surface residual stresses as the deformed layer is removed atom by atom form the surface.

Jin et. al. (2010) investigated the impacting factors on the Zerodur material surface roughness during APPJ processing. Also, the modification of surface chemistry of Zerodur is studied as this material is based on multiphase-multi-chemical component nature. The relation

between surface roughness of the substrate and process parameters is reported based on experimental results. The processing gasses used are He, O_2 and SF_6 and the gas mixture ratio implication on surface finish is also reported.

Yao et al. (2010) reported chemical machining of Zerodur material with atmospheric pressure plasma jet (APPJ). The paper discusses the repeatability and uniform spatial distribution of chemical active part of the plasma jet. Atom emission spectroscopy is extensively used to study the distribution of activated flourine atoms (radicals) and the material removal mechanism. Also, the material removal function is studied with respect to work material, RF power, flow rate of SF_6, ratio of SF_6/O_2 and working distance.

Zhang, et al. (2008) analyzed the mechanism of ultra-smooth surface formation due to APPP. Quantum chemistry simulation is done to explain the selectively of APPP on surface topography and surface finish improvement mechanism. Optical Emission spectroscopy is used to characterize the plasma and to identify the control parameters in material removal. Low temperature is encountered on the specimen and surface finish of 0.63 nm Ra are also reported. Li et al. (2002) discussed the effects of Ar and O_2 additives on SiO_2 etching in the presence of C_4F_8. Infrared laser absorption spectroscopy is used to study the etching functions under different operating parameters.

Coburn and Winters (1979) studied the ion and electron assisted gas surface chemistry and its effect in plasma etching. An attempt has been made to independently evaluate the ion enhanced gas-surface chemistry and electron enhanced gas-surface chemistry. Wang et al. (2006) discussed novel, non-thermal atmospheric pressure plasma for polishing SiC optics. Reactive gas such as CF_4 was introduced into the plasma area to react with the molecules at the surface of the SiC optics. As the interaction is a pure chemical process, the material removal is at the atomic level and no surface damage is caused. The theoretical analysis on necessary conditions to generate the radicals is also presented.

Liu et al. (2009) reported novel plasma polishing process on fused silica used for thin film techniques and optical test in Xi'an University. This study utilizes capacitive coupled hollow cathode RF excited SF_6 and argon plasma. The factors influencing the characteristics of plasma such as gas flow rate and exciting power are studied. The reported surface finish improvement is marginal from 1.2 to 1.0 nm, however, the surface integrity is enhanced. This is the only available literature where effective plasma machining/polishing is done on bulk fused silica under low pressure (0.05 mbar). Also, the plasma source is operated in two modes such as High Etching Rate (HER) mode and Low Etching Rate mode (LER). HER mode is

used for removing surface and subsurface damaged layer and LER mode is operated to improve the surface finish.

1.7 Motivation, objectives and organization of the thesis

1.7.1 Motivation

For state of art of inertial sensors such as gyroscopes and accelerometers, for aerospace applications, the sensing microstructures demand excellent surface integrity in terms of sub nanometer surface finish, surface/ subsurface damage nano scale surface residual stresses to minimize surface losses, and activation of surface prior to thin film coating. These naturally pose demanding challenges in manufacturing such microstructures with high surface integrity. Also the microstructures are not simple planar or aspheric surfaces but mostly they are either complex surface or free form surfaces, usually made of hard brittle materials such as fused silica, Saffire, Zerodour, SiC etc. Against this background developing precision nano finishing techniques for free form surfaces for such materials gains importance. Conventional fine methods such as Magneto-rheological polishing, chemo mechanical polishing are able to achieve sub nanometer surface finish however they are not very deterministic processes when it comes to 'zero defect' surface / subsurface damage potential is concerned. Atmospheric pressure plasma polishing techniques have been developed as efficient deterministic process to meet 'zero defect' surface. However, its application is limited to planar or simple surfaces and treatable area at given time is very limited. Complex robotic technology is required to apply the same on complex/free form surfaces.

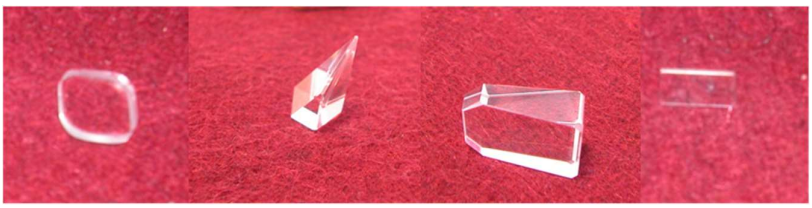

Fig. 1.6 ISRO laser gyro components

The components shown in Fig. 1.6 are realized through finer customized variants of chemo-mechanical polishing techniques. Surface finish of the order of 2-3Å units is achieved. However, in terms of surface integrity to build a long life laser resonator, the yield has been very poor as the processes are not deterministic to achieve 'zero defects' in critical surface locations. Therefore, a finishing process which enhances the surface integrity maintaining or improving the surface finish is required.

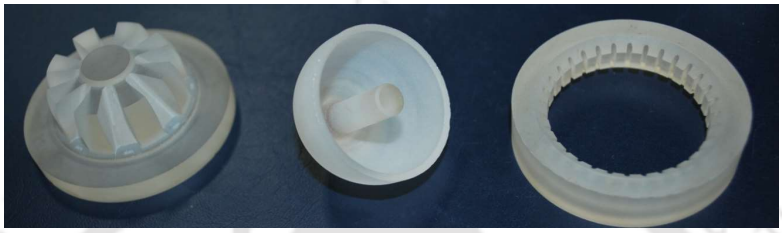

Fig. 1.7 Hemispherical Resonator Gyro (HRG) Components

The components shown in Fig 1.7 displays complex and freeform surfaces which need to be polished to sub nanometer finish while maintaining very high surface integrity levels with respect to subsurface damage, residual stresses and maintain the surface topography and geometry tolerances to enable pico-grams of unbalance. Hence, a low power medium pressure 'cold' plasma polishing process is conceived to achieve isotropic polishing of complex 3D surfaces, concurrently, including inside surfaces where no tool or beam can reach.

1.7.2 Objectives of the thesis

The following objectives are considered in the present thesis.

1. Design and development of an operational plasma polishing setup to achieve isotropic and atomistic polishing on 3D surfaces and to establish chemical plasma for achieving stress free material removal.
2. To establish the plasma characterizing setup to understand plasma polishing process, chemical dynamics of the plasma and material removal mechanism.
3. To establish surface characterization techniques to evaluate surface integrity including surface finish, surface and subsurface structure damages and chemical bond changes / damages.
4. To identify processing gases and reactive gases and their compositions to achieve atom by atom material removal for fused silica components.

5. Simulation study of plasma process using FEM based Comsol® software to substantiate the experimental studies and to fine tune parameters when actual targeted components with complex surfaces are nanofinished.
6. Process tuning to finish components with complex surfaces like hemispherical shell up to nanometre level while maintaining very high surface integrity for achieving design goals with respect to subsurface damage, residual stresses and reverting the surface structure identical to bulk structure without degrading the surface topography and geometrical tolerances while retaining the surface material properties to near one hundred percent of the bulk material including reducing of dynamic surface damping and increasing of surface energy characteristics.
7. Adopt plasma polishing technique as a super finishing deterministic process, by removing few tens of nanometre surface material, to enhance surface integrity of an optical components, which are finished up to 2-3 Å Ra by fine customized variants of chemo-mechanical polishing techniques while maintaining achieved surface finish better than 5Å. The surface integrity shall be maintained to an extra ordinary level to meet 'zero defects' at critical surfaces required for inertial sensors.

1.7.3 Organization of the thesis

The thesis is organized into seven chapters with references. The introduction to the finishing processes and related literature review is in first Chapter. The literature review of various contact and non-contact finishing processes is carried out. Also, atomistic polishing methods are discussed along with previous studies.

In Chapter 2, various characterization methods which have been adopted in the present thesis to understand plasma processing is discussed. The main characterization methods are as follows: Analysis of plasma characteristics is carried out using Optical Emission Spectrometer (OES), Laser Doppler Vibrometer (LDV) is used for establishing uniform plasma polishing of hemispherical shell, surface characterization of workpiece are conducted with Talysurf Profilometer, Atomic Force Microscopy and White Light Interferometer, Raman Microscopy is used for analyzing substrate's chemical network change during plasma processing.

Design and development of plasma polishing set up is discussed in Chapter 3. The study related to basics of plasma, their characteristics as applicable to polishing / material removal mechanism are also presented. The preliminary experiments conducted to characterize the plasma, experiments for selection of processing and reactive gases are presented. The

preliminary plasma polishing experiments along with results with fused silica specimens are discussed in this chapter.

The Comsol® model development, analysis results are discussed in Chapter 4. The Comsol® analysis result is used to fine tune the processes parameters, electrode geometry and positioning of the specimen in the chamber.

The experiments conducted with fused silica hemispherical shell and its characterization with surface characteristics and functional performance parameters and the results are discussed in Chapter 5.

The successful application of the developed plasma polishing process for fine removal of a 60 nm layer of fused silica CMP finished TIR prism and related results are discussed in Chapter 6.

Discussion on conclusions, findings and limitations of the present work with scope for future studies are presented in Chapter 7.

Chapter 2

CHARACTERIZATION TECHNIQUES ADOPTED IN PLASMA PROCESSING

2.1 Introduction
2.2 Optical Emission Spectrometer (OES)
2.2.1 Atomic and molecular spectra
2.2.2 Spectroscopic equipments
2.2.3 Diagnostic methods
2.2.3.1 Identification of particle species
2.2.3.2 Measurement of plasma temperature
2.2.3.3 Doppler broadening
2.2.3.4 Absolute line method
2.2.3.5 Relative line methods
2.2.3.6 Particle densities
2.3 Laser Doppler Vibrometer (LDV)
2.4 Surface characterization techniques
2.4.1 Contact type measurement
2.4.2 Non-contact type measurement methods
2.4.2.1 Advantages of AFM
2.4.2.2 Application of AFM for fused silica substrate
2.4.2.3 Disadvantages
2.4.3 Power spectral density (PSD) of roughness profile
2.5 Surface chemical network analysis by Raman spectroscopy
2.5.1 Molecular structure
2.5.2 Scattering process
2.5.3 Basic limitation of Raman spectroscopy
2.5.4 Raman imaging
2.5.4.1 Characterization of fused silica by Raman microscopy

2.1 Introduction

Various characterization methods which have been adopted to understand plasma processing are as follows:

- Analysis of plasma characteristics using optical emission spectrometer. It is a vital tool in this study. It helped in optimization of plasma processing parameters as well as understanding the plasma chemistry during plasma polishing.
- Laser Doppler Vibrometer (LDV) is used for establishing uniform plasma polishing of 3D freeform surfaces like hemispherical shell.
- Surface characterization techniques like Talysurf profilometer, Atomic Force Microscopy (AFM) and white light interferometer are used to analyze the surface properties before and after plasma processing.

- Raman microscopy is used for analyzing substrate's chemical network change during plasma processing.

2.2 Optical Emission Spectrometer (OES)

Plasma spectroscopy is a vital characterization tool used in astrophysics and plasma physics from long back (Griem, 1964 and Lochte, 1968). Information regarding ionizing atoms, molecules and their ions reflects the characteristics of the plasma and it helps in-situ analysis of the process. Simple and robust experimental set up makes emission spectra very reliable tool. As this method is noninvasive, it does not affect the plasma chemistry as well as does not disturb by external RF and magnetic field. Hence, this technique is proved to be one of the indispensable tool for plasma research. For both low temperature and low pressure applications, the interpretation of the spectra is a bit complex.

2.2.1 Atomic and molecular spectra

Energy level diagram is used to represent atoms and molecular spectra which correlates the emission and absorption spectra. Notation of electron energy states is given as

$$^{2S+1}L_{L+S} \tag{2.1}$$

where $2S+1$ the multiplicity of the orbit, $L+S = J$, total angular momentum. The light atoms undergo LS coupling. Electron transition follows the selection rule as: $\Delta L = 0, \pm 1$, $\Delta J = 0, \pm 1$, $\Delta S = 0$. Transition is forbidden if the angular momentum for both the states is zero.

Figure 2.1 shows the energy level diagram for helium which is a two electron systems i.e. singlet and triplet. During transition, if the spin orientation is maintained then it is a triplet state, while the spin state got reversed is called singlet state. Resonant transition which are linked with ground state shows intense peaks due to higher transition probability. Figure 2.1 shows different energy states of helium atom. The corresponding transition spectra is shown in arrow. It is worth to note that only excited state transition gives radiation in visible region.

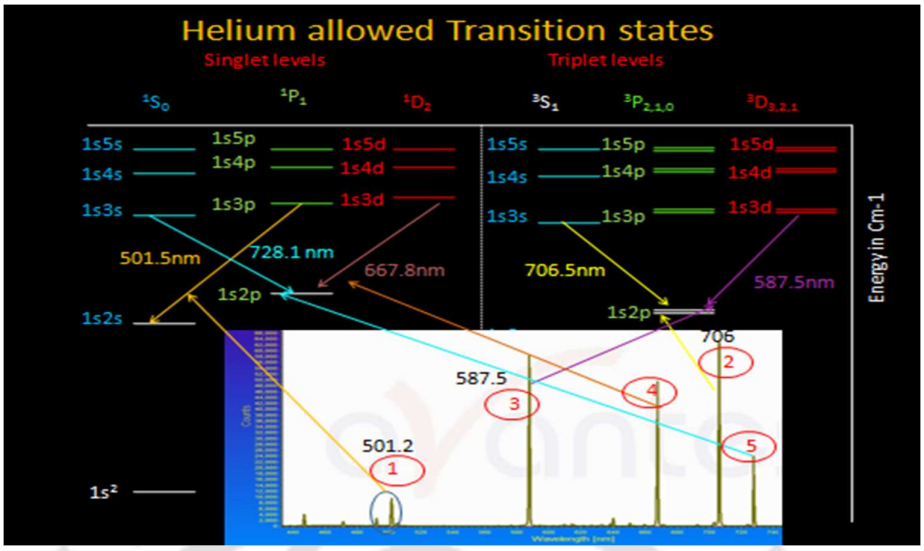

Fig. 2.1 Atomic energy level diagram of He

2.2.2 Spectroscopic equipments

In this study, two spectrometers are adopted for optimization of plasma parameters as well as gas composition analysis during plasma processing. Ava spec. 2048 by Avantes is one of the spectrometers used for optimization of total pressure and composition of gases for plasma processing. This spectrometer is adopted for total pressure optimization because of its good sensitivity with 25 µm large slit and wide spectral range from 400 to 1100 nm. Application of this spectrometer is described in Section 3.2. On the other hand, Aryelle 200 high resolution spectrometer by LTB with echelle grating is used for the analysis of plasma temperature and identification of silica oxidation states for the prediction of MRR during plasma processing. This spectrometer also helps for the validation of simulation results as discussed later (Section 4.3.2).

2.2.3 Diagnostic methods

The low temperature plasma diagnostic methods of emission spectroscopy, are described here.

2.2.3.1 Identification of particle species

Identification of particle species (atoms, ions and molecules) in the plasma is the trivial part of the emission spectroscopy. The position of the wavelength provides information about the kind of transition, and intensity revels about the concentration of the particular atom or molecule. The exact wavelength position can be obtained from National

institute of standards and Testing (NIST) data base. The high resolution spectrometer is capable of finding out Doppler shift, which is very useful for analyzing particle velocity in the system. Other than the required known filled atoms and molecules, spectrometer is also sensitive to trace impurities generated due to processing. Hence, this method is used extensively during plasma processing for optimization of processing gas composition, total pressure of gas and power of operation. In this study, Specline made software is used for identification of silicon oxidation states, which helps in in-situ prediction of MRR.

2.2.3.2 Measurement of plasma temperature

Many techniques for measuring temperature in plasmas exist. Each has its advantages and disadvantages. A method that is very useful for calculating temperature in one type of plasma may not be useful for another plasma. Indeed, the most appropriate method in one region of plasma might be different to that of another region of the same plasma. It might take several attempts to find out the right method.

2.2.3.3 Doppler broadening

Doppler broadening is the result of the Brownian motion of particles within the source. The perceived wavelength of transmission from a given atom or ion is either red-shifted or blue-shifted, depending on its motion relative to the observer. As long as there is a large number of particles involved and their energies follow a Maxwellian distribution, the result is that spectral lines become Gaussian in shape in the wavelength domain (Griem, H. R ,1997 and Marr G., 1968). The degree of broadening depends on the temperature. The width of wavelength (λ) can be calculated using peak width at the half-height (FWHM) in terms of wavelength, given as

$$\Delta\lambda_D = 2\sqrt{\ln 2}\lambda o\sqrt{\frac{2kT_{gas}}{mc^2}} \tag{2.2}$$

where, m is the mass of the atom or ion, λ_o is the central wavelength of the line, k is Boltzmann's constant, T_{gas} is gas temperature and c is the speed of light.

2.2.3.4 Absolute line method

This method is direct temperature measurement method by using absolute line radiation. Highly calibrated spectroscopy is required for analyzing wavelength accurately with the knowledge of electron density and electron temperature can be obtained. This

method is applicable for rare gases where particle density can be calculated with known electron temperature.

2.2.3.5 Relative line method

Relative line method of temperature determination involve measuring the intensity of at least two lines in the plasma. If the emission coefficients of two emission lines of the same species (lines '1' and '2') at a particular point are given by E_1 and E_2, their ratio is given by

$$T = \frac{(E_1 - E_2) \times \left(1/k\right)}{\ln\left(\frac{I_1}{I_2}\right) - \ln\left(A_1 g_1 \frac{\lambda_2}{A_2 g_2 \lambda_1}\right)} \tag{2.3}$$

where, A= Einstein's coefficient of respective transition, E= energy of transition, g= degeneracy of state, I= intensity of transition, λ= wave length. The value of the Boltzmann's constant (K) is equal to 1.38×10^{-23} J/K. The wave lengths considered here are λ_1=706.52 nm and λ_2=667.82 nm. Provided that the upper energy states of the transitions are in local thermal equilibrium with each other. The ratio is thus just dependent on known variables and temperature. This method offers significant advantages over the absolute line method. This method is used for calculating electron temperature during plasma processing and cold plasma processing condition was established as described later Section 4.3.2. However, producing a Boltzmann plot means measuring the intensity of a series of emission lines, which can be time-consuming.

2.2.3.6 Particle densities

The number density or particle density can be calculated similarly as mentioned above. Depending on the availability of spectroscopic system either line ratio or absolute line intensity method can be adopted.

2.3 Laser Doppler Vibrometer (LDV)

Laser Doppler vibrometer (LDV) is a velocity and displacement measurement technique. LDV has having various advantages because of non-contact type measurement. Therefore, the tested part stays uninfluenced during measurement bringing a much more reliable picture of its own properties. Because of this, it is possible to observe very broad scale dynamics down to micron size. As an alternative to LDV, accelerometer can be used

which supply a better sensitivity. Also, it is less sensitive to environmental vibration as they are not part of it. The basic component of a LDV aperture is a laser beam focused on the tested structure whose movement causes the presence of the Doppler effect in the laser reflection. If the object supplies a proper reflection, it is possible to calculate its displacement and velocity. As the name LDV suggests, it has two major components such as laser which induces Doppler effect and vibrometer which provides sufficient interference pattern for the analysis of dynamics of the object.

2.4 Surface characterization techniques

Surface roughness is a measure of unevenness in the machined surface. Optical/mechanical product performance depends on surface roughness. It is also very important parameter for determining the scattering of optics (Whitehouse, 1994). Accurate measurement tools are very useful for modern industry (Gadelmawla et al., 2002). Surface roughness measurement methods are the following types: contact measurement methods and non-contact measurement methods.

2.4.1 Contact type measurement

In contact type measurement, detector tip is equipped with a stylus. The stylus directly touches the sample surface, which analyses the surface of the sample. The upright movement of the stylus is detected electrically. The electrical signals go through an amplification process and digital conversion process is recorded.

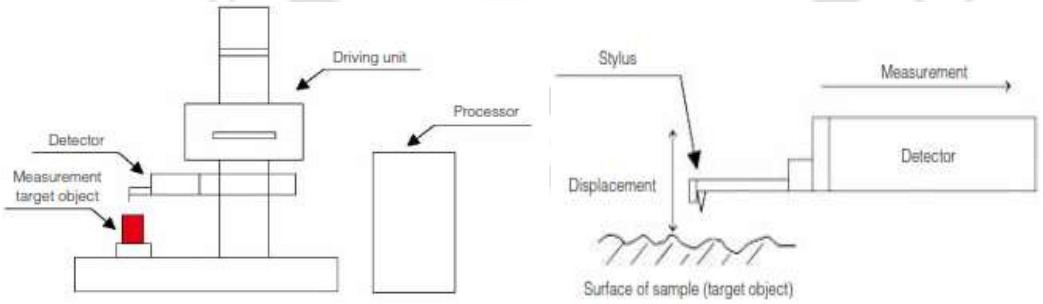

(a) (b)

Fig. 2.2 (a) Contact type surface roughness measuring system and (b) surface roughness data collection

To precisely measure delicate shapes and roughness with a contact-type surface roughness tester, the radius of the stylus tip must be as small as possible with low contact pressure. Styluses are made of sapphire or diamond and their tip radius is usually about 10

µm or smaller. A conical shape with a ballpoint tip is considered for an ideal stylus. This is a very accurate method for surface analysis, although, it suffers following short comings.

- Stylus wear
- Measuring pressure can cause scratches on the sample surface
- Inability to measure viscous samples
- Measurement is limited by radius of stylus tip
- Measurement takes time
- Difficulties in positioning and identification of subtle measuring points
- Requires sample cutting and processing for tracing by the detector

2.4.2 Atomic Force Microscopy measurement

The atomic force microscope (AFM) analyses the forces between a fine tip and a sample surface. AFM is a kind of scanning probe microscopy where probe approaches very close to the surface. The interaction between the tip and substrate is a function of fine surface undulations. The physical interaction between the sample and probe helps the construction of an image of sample surface.

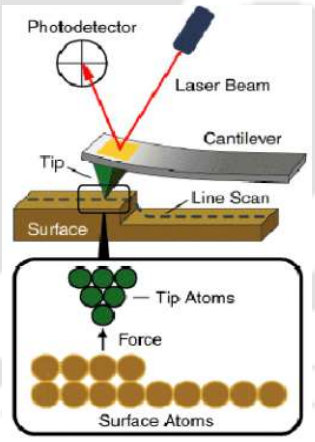

Fig. 2.3 Principle of AFM

The tip of the AFM which is attached to the cantilever allow it to move towards the substrate. Attractive or repulsive forces resulting from interactions between the tip and the surface will induce a positive or negative cantilever bending. Laser beam is used to detect the bending, which is reflected from the back side of the cantilever. Figure 2.3 shows the basic concept of AFM.

2.4.2.1 Advantages of AFM

AFM provides a 3D image along with 2D picture. It does not require any special surface treatment such as gold/carbon coating etc. Also, expensive vacuum system is not required. It gives true image of the surface with comparably higher resolution than other characterization tools.

2.4.2.2 Application of AFM for fused silica substrate

AFM is very useful method for studying surface topography of fused silica substrate. Mechanical polishing and machining induce surface cracks at the fused silica interface. In present study, plasma processing method has been adopted to mitigate the cracks developed during mechanical machining. AFM technique is used for characterizing the crack depths as well as surface finish of the fused silica substrate before and after plasma processing as shown in Fig. 2.4.

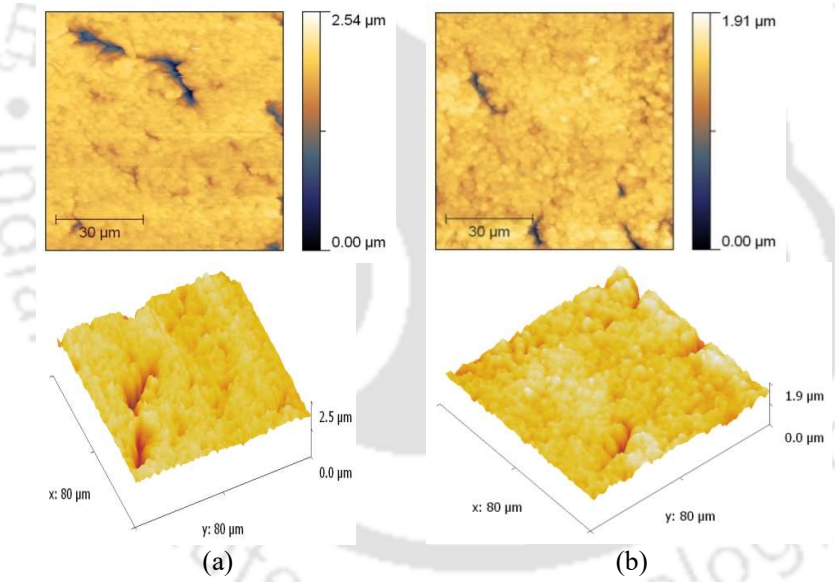

(a) (b)

Fig. 2.4 AFM images of fused silica (a) before and (b) after plasma processing. AFM results shows that after plasma processing crack depth has reduced significantly and surface finish gets improved

2.4.2.3 Disadvantages

AFM can measure only small scanning area approximately 150×150 µm and height of the order of 10-20 µm. AFM takes lot of time for imaging due to slow scanning speed. Hence, it undergoes thermal drift which makes it unsuitable for analyzing exact distance between the image and surface figure. Hysteresis of the piezoelectric material can also affect the AFM images. Software enhancement and filtering are also required for eliminating the

cross-talk between the x, y, z axes but images may get flatten due to the filtering. However, advanced versions are available for innovative solutions like orthogonal scanning to eliminate above problem. AFM probes cannot measure overhangs or steep walls. Specially tailored tools are required for analysis of such side walls which are expensive with less lateral resolution.

2.4.3 Power spectral density (PSD) of roughness profile

When different instruments are used for sample's measurement which are to be converted to a common quantity for the comparison of results. For example, while root mean square (RMS) roughness measurements are obtained with different instruments, generally, the results become different due to different spatial frequency bandwidth limits of the instruments. The power spectral density (PSD) signifies the spatial-frequency spectrum of the surface roughness measured in inverse-length units. Area under the PSD function provides roughness values of the surface and its frequency distribution (Duparre et al., 2002).

Mathematically, PSD is defined as a autocorrelation function of the Fourier transform, which contains only the power across a range of wave vectors without phase (Stover, 1995 and Leach, 2010). The PSD mostly encompasses statistical information of the surface figure which is unbiased by the scan size and kind of instrument used for characterization. PSD can be computed over any length scale with the help of any instrument. Multiple instruments and multiple measurements are also possible to reconstruct the complete image by PSD. The partial PSD is very useful even in the absence of complete measurements. This technique helps to calculate the upper and lower bounds of the roughness and enables to mitigate instrument limitations and artifacts.

The PSD can be interpreted by the following ways. The shape or optical figure can be attributed from the lower spatial frequencies (deviation of the surface from a desired shape). The roughness of the finest-grained optical coatings can be obtained from the higher spatial frequencies. Visible spectrum may not provide scattering for these frequencies but vacuum UV radiation can induce defects due to the presence of these frequencies. For ideal case, the PSD reduces from low to high spatial frequencies. The way in which it reduces depends on the process by which the surface is realized.

In this study, ultra-high finished total internal reflecting optics is used as substrate to reduce sub surface damage which cannot be identified by naked eye. The chemo-mechanical polishing (CMP) method is adopted for getting surface finish in sub nanometer range. However, CMP method in general induces surface strain as well as subsurface cracks which

result in low threshold material. These substrates deteriorate during operation with time due to formation of absorbing center. The roughness measurement alone cannot explain the reason behind this cause. However, by using PSD, surface can be analyzed with deeper sense and can be attributed to the quality of machining. Figures 2.5 (a) and (b) are the typical examples where plasma polishing improves the surface figure by the reduction in low frequency or high wavelength of spatial components.

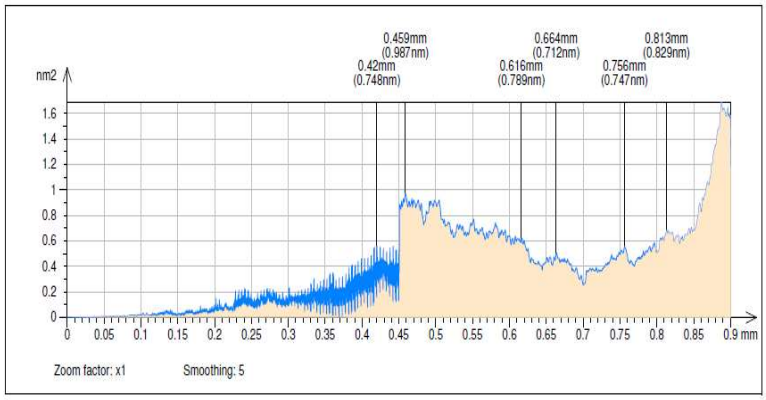

(a)

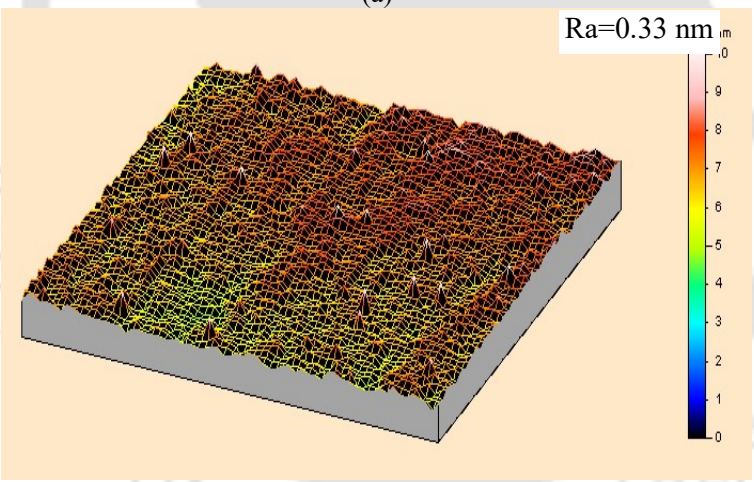

(b)

Fig. 2.5 (a) PSD of surface profile and (b) area surface roughness profile of CMP finished Optics A before plasma polishing

2.5 Surface chemical network analysis by Raman spectroscopy

Spectroscopy is the study of interaction of electromagnetic radiation with matter. Spectroscopic methods can be based on phenomena of emission, absorption, fluorescence or scattering (Skoog et al., 2006 and Settle et al., 1997). Raman spectroscopy is an optical technique for measuring vibrational energies in molecules. With Raman spectroscopy, it is

possible to identify which molecules are present in a sample. Raman spectroscopy is just one of many optical spectroscopy techniques for studying samples. The major potential of Raman spectroscopy compared to other methods is the possibility of easily identifying many different compounds in the same sample. If Raman spectroscopy is combined with imaging techniques, Raman imaging can be obtained. With Raman imaging, it is possible to obtain information about the spatial distribution of molecular species within a sample.

2.5.1 Molecular structure

A molecule consists of two or more atoms which are bonded together. According to quantum mechanics, the energy of an atom or a molecule is quantized into discrete energy states. In an atom, these energy states correspond to different arrangements of its electrons. A molecule has additional energy states beside electronic states. These energy states correspond to the vibrational and rotational motion of the molecules. The rotational motion of the molecule is defined as rotation around a principal axis and the vibrational motion of the molecule is a periodic change in the bond distances and/or the angles of the molecule. The total energy of a molecule is the sum of its electronic, vibrational and rotational energy. The separation between rotational energy states is of the order of 0.001 eV and between vibrational energy states is of the order of 0.1 eV. The vibration of a molecule is described by fundamental frequencies or modes corresponding to different types of vibrational motion. Each of these vibrational modes corresponds to a different vibrational energy level of the molecule. The normal vibrational modes in a molecule can be divided into stretching and bending modes. In stretching modes, the distance between the atoms in the molecule changes and in bending modes, the angle between the bonds changes.

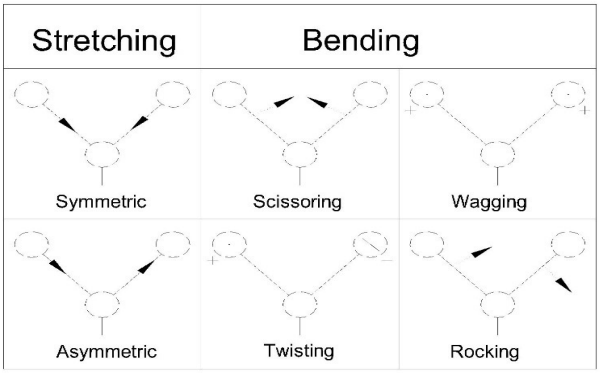

Fig. 2.6 Vibrational modes of a molecule (The + and - signs signifies movement Perpendicular to the plane of the image.)

2.5.2 Scattering process

When photons propagate through a media they have a possibility of interacting with it. The photons might be absorbed or they might be scattered. These scatterings can be either elastic or inelastic. When a photon is elastically scattered there is no net energy transfer between it and the media. The elastically scattered light keeps its original wavelength. When inelastic scattering occurs there is a net energy transfer between the photon and the media. The inelastically scattered light has a different wavelength than the incoming light. This phenomenon is described in Fig. 2.7.

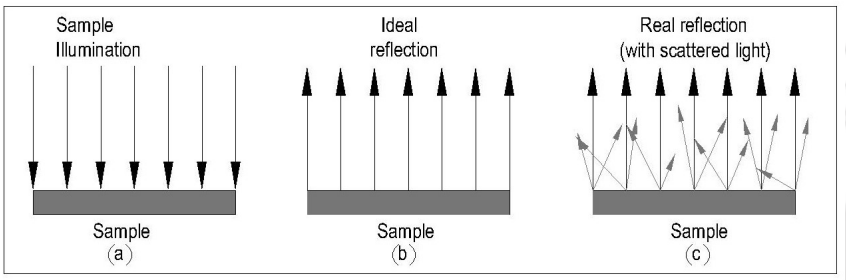

Fig. 2.7 Typical Raman scattering of sample

If the energy of the photons is not high enough to excite the molecule to a higher electronic state, Raman or Rayleigh scattering may occur. The molecule absorbs the photon and is excited up to a virtual level. The molecule then de-excites to one of the levels in the ground electronic state by emitting light. If the scattered photon preserves its energy, Rayleigh scattering is obtained. If the scattered photon has gained or lost energy, either anti-Stokes and Stokes Raman scattering is obtained. This phenomenon is described in Fig. 2.8.

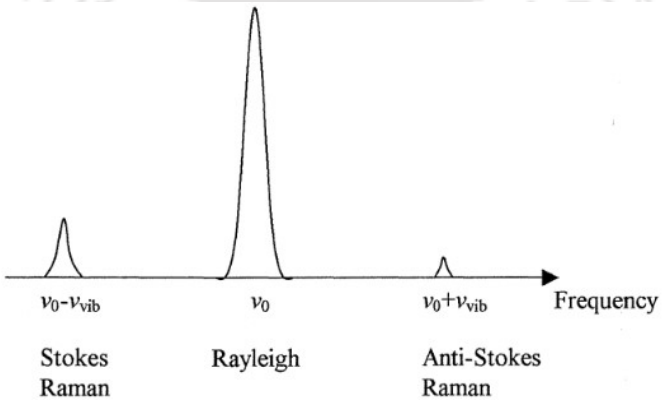

Fig. 2.8 Raman spectra with one molecular vibration

2.5.3 Basic limitation of Raman spectroscopy

Raman spectroscopy is an optical technique for measuring the vibrational energies in molecules. By using Raman spectra, it is possible to identify which chemical bonds present in a sample, and from this information regarding molecules can be obtained. The major problem when conducting Raman spectroscopy is the very low intensity of the Raman scattered light, which is due to the low probability of Raman scattering. As a result of this other scattering effects, such as fluorescence, will show a higher intensity and severely affect the possibility of measuring the Raman signals. A schematic of Raman spectrum is shown in Fig. 2.9.

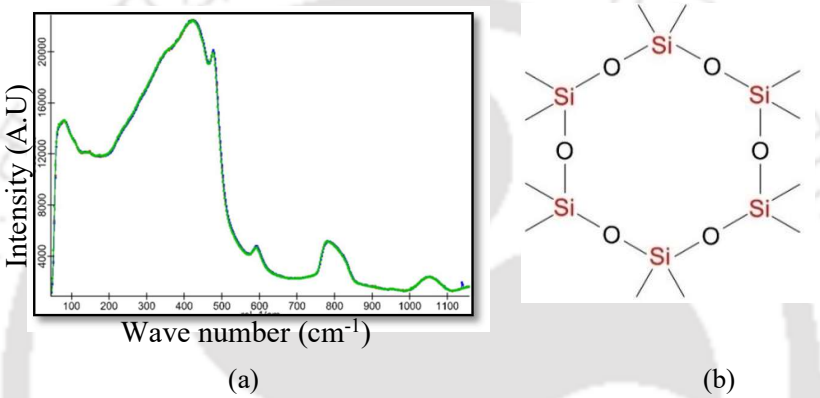

(a) (b)

Fig. 2.9 (a) Typical Raman Spectrum of fused silica and (b) six membered peak

While performing Raman spectroscopy, frequency shift from excitation light is observed. The reason for this is that the frequency shift of a Raman peak is independent of the wavelength of excitation light. As the frequency shifts are in the order of 10^{-12} s^{-1}, the frequency is usually divided by the speed of light. The resulting quantity is then a wave number, which is defined as

$$\Delta v = \frac{v}{c} = 1/\lambda \qquad (2.4)$$

where, v is the frequency, c is the speed of light and λ is the wavelength. The usually used unit of Δv is cm^{-1}. The zero frequency shift i.e. Rayleigh line, which is the elastically scattered excitation light. On either side of the Rayleigh line, Raman peaks of Stokes and anti-Stokes Raman scattering exits. The absolute frequency shifts of peaks coming from single molecular vibration are equal.

2.5.4 Raman imaging

Raman imaging, which combines Raman spectroscopy and imaging techniques, is an excellent method for obtaining information about the spatial distribution of molecular species.

2.5.4.1 Characterization of fused silica by Raman microscopy

Raman spectroscopy is one of the efficient methods for characterizing structural modification in fused silica (Xu et al., 2008). Broad bands are observed in Raman spectroscopy reflects the coupled vibration modes of the fused silica network (Galeener et al., 1983). Characteristic Raman peak centered at 440 cm^{-1} related to the Si-O-Si angle in the silica network and its width and area suggests the Si-O-Si angle distribution (Galeener & Geissberger, 1983). The SiO_2 network is ideally 6-member structure as shown in Figure 2.9 (b).

Chapter 3

EXPERIMENTAL INVESTIGATION OF MEDIUM PRESSURE PLASMA

3.1 Introduction
3.2 System design and methodology
3.3 Preliminary experiments
3.3.1 Experiments with Teflon
3.3.2 Optimization of Plasma processing gases
3.3.2.1 Advantages of SF_6 gas over O_2 gas
3.3.2.2 Optimization of SF_6 gas concentration during plasma polishing
3.3.2.3 Optimization of SF_6 to O_2 ratio
3.4 Surface finish analysis of substrate
3.4.1 Plasma polishing of fine machined substrate
3.4.2 Raman Spectroscopic analysis
3.5 Summary

3.1 Introduction

The required specification of plasma processing set up is that it should be capable of atom by atom material removal without heating up the surface or initiating micro cracks resulting in surface/sub surface damages. The process should be deterministic one for complex and freeform surfaces. Low pressure plasma (10^{-2} mbar to 0.5 mbar) finishing has been proved to be capable of producing fine surface finish on complex surfaces but not without subsurface damage due to heating and ion physical damage. Atmospheric pressure plasma with different working gases has been successfully developed for achieving sub-nanometer surface finish without surface damage but not on freeform surfaces.

3.2 System design and methodology

In this section an isotropic dielectric barrier cavity based plasma, operating at a medium pressure of 1 mbar to 100 mbar is conceived. The experiments are designed to realize a system to understand the mechanism and to develop the process for achieving the goals set forth. The higher pressure levels are chosen to eliminate the damaging effects of ion impingement. Dielectric barrier RF excitation is chosen to minimize electron heating while allowing chemical interaction of free radicals with surface atoms of workpiece. Typical plasma contains, million times more radicals than ions or electrons. Radicals form more easily and their lifetime is much longer. Ions don't etch while radicals do. Ions affect the

process by energetic (physical) bombarding of the surface, influencing chemical processes of etching. Radicals are responsible for dry etching process. They are chemically active and react with the surfaces to produce volatile products.

A Zerodur cavity shown in Fig. 3.1 is chosen as the plasma cavity and it acts as a dielectric barrier for the exciting electrodes. The plasma chamber is designed to polish components having diameer between 5 to 40 mm. Uniform generation of reactive gases is considered to enable isotropic plasma while designing the chamber. The photograph of the polishing system with vacuum system and different gas units required for plasma processing is shown in Fig. 3.2(a). The magnified view of the plasma chamber is shown in Fig. 3.2(b). Glass ceramic Zerodur is used to fabricate the plasma chamber. The chamber is sealed with a lid plate which is optically transparent for 300 to 1200 nm wavelengths. The vacuum pump is connected to the chamber with different tubes for feeding reactive and processing gases. To avoid ion impingement and to enable a true non-contact process, medium vacuum pressure is considered. Also, to minimize electron heating, dielectric barrier RF excitation is selected to permit chemical interaction by the reactive free radicals with component's surface atoms. The excitation RF frequency is selected as 40.68 MHz to minimize bombardment of ions.

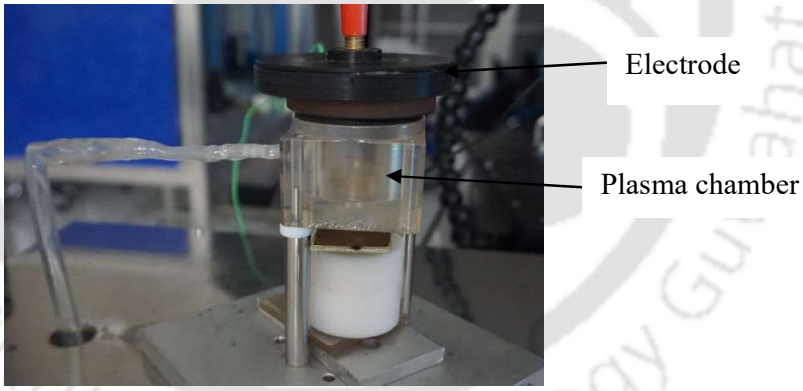

Fig. 3.1 Experimental set up of plasma polishing

The optical emission spectroscopy is applied to analyze the light emitting photons during plasma processing. In plasma, the outer shell electrons of atoms are excited to higher energy states by collision with free electrons. Excited state is unstable. Hence, the observed energy is emitted by the atom in the form of electromagnetic radiation. The emitted wavelength is related to energy as per Plank's equation given as

$$\lambda = hc/\Delta E \qquad (3.1)$$

where $\lambda =$ emission wavelength, ΔE = difference in energy between two electronic states, h is Plank's constant and c is speed of light. The relative derivatives and atomic transition of the plasma are distinguished depending on measured λ with atomic spectra database of National Institute of Standards and Technology (NIST). The emission spectroscopy analyser used during experiments is Awa spec ULS 2048 (Avante Inc. Netherland).

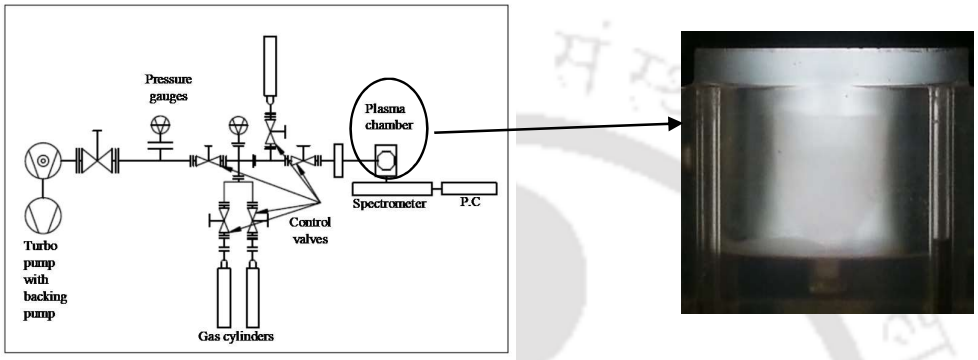

(a) (b)

Fig. 3.2 (a) Schematic of plasma polishing system and (b) photograph of plasma chamber

Plasma polishing set up consists of following sub units:

Turbo pump with backing pump is used to achieve maximum vacuum and minimum pressure of the system to avoid residual gas contamination during process. **Control valves** are used to regulate the flow of the gases. **Pressure gauges** are required for measuring pressure of the gases during filling of the gases. There are two types of pressure gauges used in the system. Full range gauge for measuring high vacuum and capacitance gauge for filling gases accurately. **Gas cylinders** act as gas reservoir. **Plasma chamber** is made up of Zerodur glass where polishing takes place.

3.3 Preliminary experiments

For preliminary experimental study, fused silica circular specimens are prepared by coarse and fine machining and surface roughness (R_a) of around 1 µm and 0.25 µm, achieved respectively. Preliminary experiments are carried out to identify the process gases (He, Ne) and the reactive gas (O_2) and their mixture ratio, working pressure, RF excitation power and duration of polishing. Experiments are carried out based on optical emission spectroscopy (OES) observations during plasma processing and verifying surface characteristics of the specimens.

It is observed that pure He or Ne plasma, does not show any sign of silica peaks. However, in the presence of trace amount of oxygen as a reactive gas in He or Ne plasma. The silica peaks are observed for He plasma significantly more as compared Ne plasma as shown in Fig. 3.3. Figures 3.3 (a) & (b) show the optical spectrographs while processing fused silica substrate with He and Ne plasma in the presence of trace amount of oxygen. There is a significant intensity of broad peaks as observed at 760 to 770 nm (Fig. 3.3 (a)) and 785 to 795 nm (Fig. 3.3 (b)) regions in He plasma as compared to Ne plasma. In this region, the more probable transitions are shown in Table 3.1 from NIST data which suggests that the He plasma effectively ionizes silica to Si III and Si II than Ne plasma. In Figure 3.3 (b) there is considerable intensity of peaks observed at 760 to 770 nm and 745 to 750 nm in He plasma than Ne plasma in the presence of trace amount of O_2. At 771 nm Si IV shows strong transition as shown in Table 3.2.

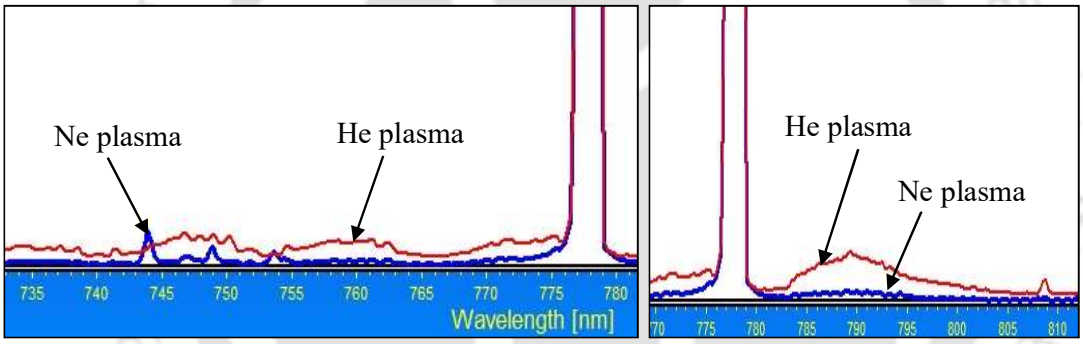

(a) (b)

Fig. 3.3 Spectrographs for wavelengths (a) 735 to 780 nm and (b) 780 to 810 nm while processing fused silica substrate with He and Ne plasma in the presence of trace amount of oxygen

Table 3.1 Transitions from 780 nm to 810 nm wavelength

Element	Line (nm)	I -rel	Energy (eV)	Transition Lower–Upper	Quantum No. Lower-Upper
Si II	784.88	540	12.53–14.10	$4d\ ^2D - 5f\ ^2F^0$	1½ – 2½
Si II	784.97	520	12.53–14.10	$4d^2D - 5f\ ^2F^0$	2½ – 3½
Si III	789.02	777	26.66–28.23	$5p^3P^0 - 5d^1D$	1 – 2
Si II	791.16	282	14.10–15.67	$5f\ ^2F - 9g^2G$	2½ – 3½
Si III	796.46	631	26.60–28.16	$5P^1P^0 - 5d^3D$	1 – 2

Table 3.2 Transitions from 735 nm to 775 nm wavelength

Element	Line (nm)	I -rel	Energy (eV)	Transition Lower – Upper	Quantum no Lower– Upper
Si I	766.97	88	6.19 – 7.81	$3d^3F - P6f[9]$	3 – 4
Si IV	771.87	14791	39.09 – 40.70	$6g^2G - 7h^2H^0$	4 ½ – 5½
Si I	774.51	15	6.08 – 7.68	$4p^3P - 5d^3P$	0 –1

Similarly, near 750 nm Si I and OI, OII and OV shows most probable transitions (not listed in the Chapter). Above results suggests that He plasma effectively ionizes Si through oxygen than the Ne plasma. It may be due to the higher electronic energy of He (ionization energy of He ~24 eV) than Ne plasma (ionization energy ~16 eV). Hence, He plasma generates higher collision energy than Ne plasma. Generation of higher excited states of oxygen in He plasma confirms these results.

Further experiments are carried out to compare plasma characteristics between He with trace amount of oxygen and only oxygen. Figure 3.4 shows that near 785 to 795 nm, 770 to 775 nm and 745 to 750 nm, there is significant intensity broad peaks observed in He plasma with trace amount of oxygen than only oxygen plasma. As shown earlier, peaks near above said regions are responsible for Si III, Si IV and Si I and O I, II and V transitions.

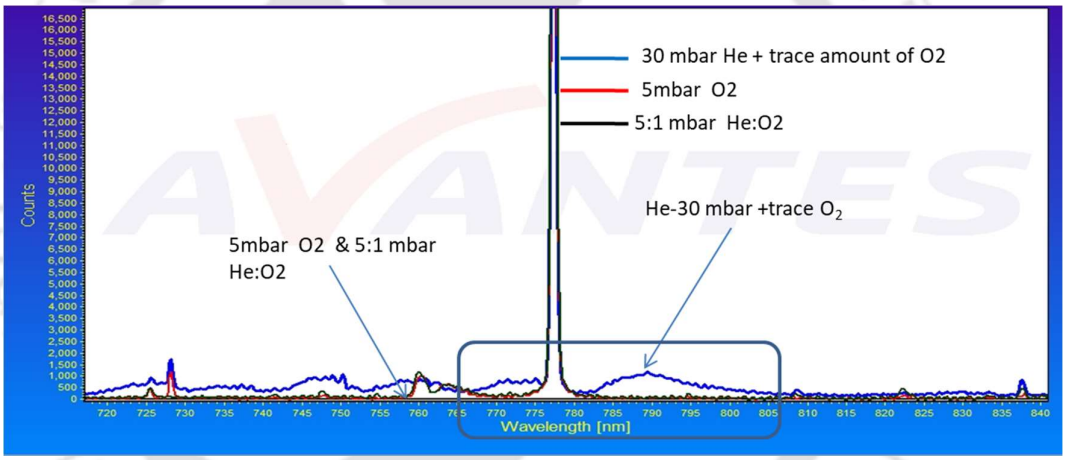

Fig. 3.4 Comparison between O_2 plasma with He plasma having trace amount of O_2

Higher concentration of oxygen in helium plasma retards silicon oxidation due to reduction in electronic energy of plasma (ionization energy of O_2 ~ 5 eV). As oxygen has higher electron affinity, it reduces electron density in the plasma. Only He plasma has not shown any sign of silica peaks (not shown). However, in the presence of trace amount of oxygen shows considerable amount of silica peaks. It suggests that although He is having higher electronic energy, it can't oxidize silicon without oxygen. Even though He can break the Si-O bond, however, in the absence of oxygen, it reforms the bond again. In the presence of oxygen, the oxide radicals readily form the bond with silicon radicals.

Figures 3.5 (a), (b), (c) explain the plausible ionic mechanism for oxidation of silicon in He plasma with trace amount of oxygen. Here oxygen stabilizes both electron deficient

center of Si and negative oxygen ion. However, in the absence of oxygen above mechanisms follow reversible route. Oxygen does not have enough electronegativity to form ionic bond with silicon. Hence, SiO and SiO_2 are not volatile compounds. However, silicon oxidation products and therefore, a silicon-based surface will not be removed by oxygen. Hence, Si V will not form during He and Oxygen plasma alone. The typical surface finish obtained with He and O_2 plasma is given in Table 3.3.

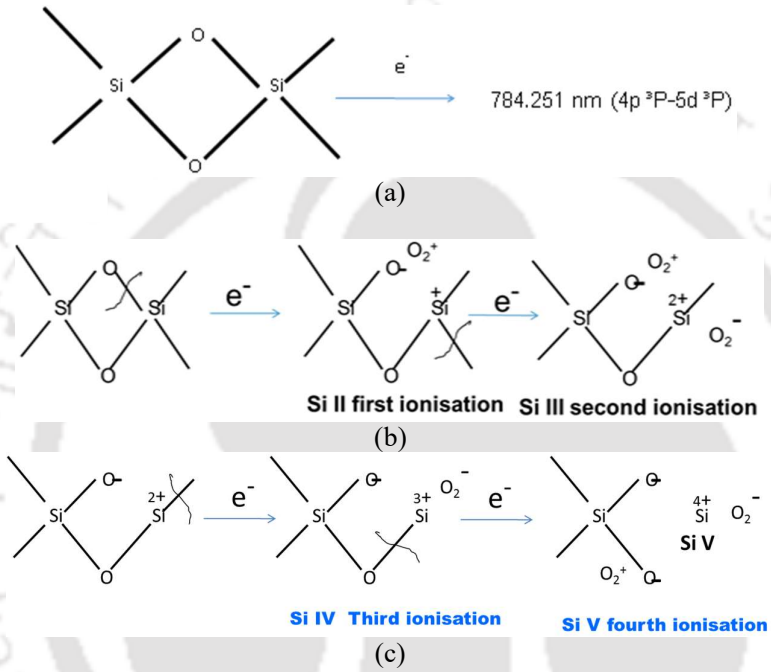

Fig. 3.5 Silicone oxidation states (a) neutral ground state, (b) Si II (first ionization) and Si III (second ionization) and (c) Si IV (third ionization) and Si V (fourth ionization)

It is observed that as machined surface shows appreciable improvement in surface finish whereas surface roughness of lapped surface remains more or less same. Another interesting observation is the polishing effect on machined surface happens irrespective of the orientation of the given surface in the plasma. Horizontal, vertical and inclined specimens displayed identical polishing effects indicating isotropic polishing effects.

Table 3.3 Surface roughness Ra achieved on fused quartz specimens

Sample No.	**Ra (µm) before polishing**		**Ra (µm) after polishing**	
	Lapped	Machined	Lapped	Machined
1	0.360	1	0.296	0.370
2	0.159	1	0.171	0.460
3	0.390	0.9	0.330	0.385

It is understood that He–O_2 plasma is able to remove material only when the surface has strained or partially broken bonds due to the machining operation. Hence, more reactive radicals such as fluorine are to be present for sustained material removal by plasma. The chemically active neutral substances (free radicals) of the F* dissociated from SF_6 reacts with silica to form volatile products as given below.

$$SiO_2 + 4F^* \rightarrow SiF_4 \uparrow + O_2 \uparrow \quad (3.2)$$

Also, positive F^+ ions react with the substrate to form volatile products as

$$4F^+ + SiO_2 + 4e^- \rightarrow SiF_4 \uparrow + O_2 \uparrow \quad (3.3)$$

3.3.1 Experiments with Teflon

Volatile SiF_4 can be removed easily during plasma processing. The current set up does not have provision for fluorine gas. In order to introduce fluorine, pieces of PTFE (Teflon) are introduced inside the chamber. Figure 3.6 shows the Spectrographs of He and O_2 plasma in the presence of Teflon for transitions at (a) 440 nm, (b) 519 nm and (c) 775 to 840 nm. The transitions from 440 to 520 nm are given in Table 3.4. As shown in Table 3.4, at region 440–450 nm, the SiF and F III give most probable emission peaks. For He and O_2 plasma, these peaks increase initially, after that start reducing with time as shown in Fig. 3.6(a). Most interestingly near 515 to 520 nm region as shown in Fig. 3.6(b), intense broad peak is observed. It is probably due to the formation of CO. However, the shoulder peak at 516 nm (Fig. 3.6(b)) is formed due to fluorine excitation. Shoulder peak disappears after 4 mins of experimentation. It suggests that the fluorine is not getting enough gain in plasma. Similarly, peaks for oxygen observed at 777 and 844 nm almost vanishes after 1 min which suggests oxygen is consumed effectively by C due to the formation of mostly CO and also CO_2. Hence, in the presence of O_2, the plasma is mostly dominated by CO.

Table 3.4 Transitions from 440 nm to 520 nm

Element	Line (nm)	I (rel.)	Energy (eV)	Transition Lower – Upper	Quantum number Lower – Upper
Si I	449.6433	1	5.08–7.84	$4s^1P–8p^3D$	1–2
SiF	449.58	600	0.00–2.84	$X^2Pi–A^2Sig+$	3–3
F III	449.5077	7763	55.12–57.88	4f 2[4]0–5g 2[6]	3–3
F I	518.991	2	14.53–16.91	3p4D°–5d 4P	2½–1½
CO	519.82	1000	8.07–10.78	$A^1Pi–B^1Sig+$	2–0

Further experiments are carried out for He and O_2 plasma at 70W RF power in the presence of Teflon pieces and the spectrograph is shown in Fig. 3.7. From Fig. 3.7, it is

observed that there is an increase in intensity (about 10 times) for peaks at 516 nm and 519 nm for 70 W RF power. It suggests that increase in power increases the probability of fluorine removal from the Teflon. But these peaks decrease after one min. During plasma processing, pressure increases inside plasma chamber. This may be due to the formation of volatile CO, CO_2 and small amount of SiF_4. Formation of CO may be responsible for the reduction in fluorine emission with time when Teflon is used as fluorine source. Formation of Si V and SiF are distinctly identified in the presence of fluorine radicals. However, in case of closed-medium pressure plasma chamber for sustained material removal, Teflon cannot be used as a fluorine source. A reactive gas such as SF_6 or CF_4 is required for continued polishing/material removal. Accordingly, SF_6 gas is introduced as reactive gas. With this chemistry of gases, the silica and fluorine peaks are predominant between 440 to 520 nm as shown in Table 3.5 from NIST database.

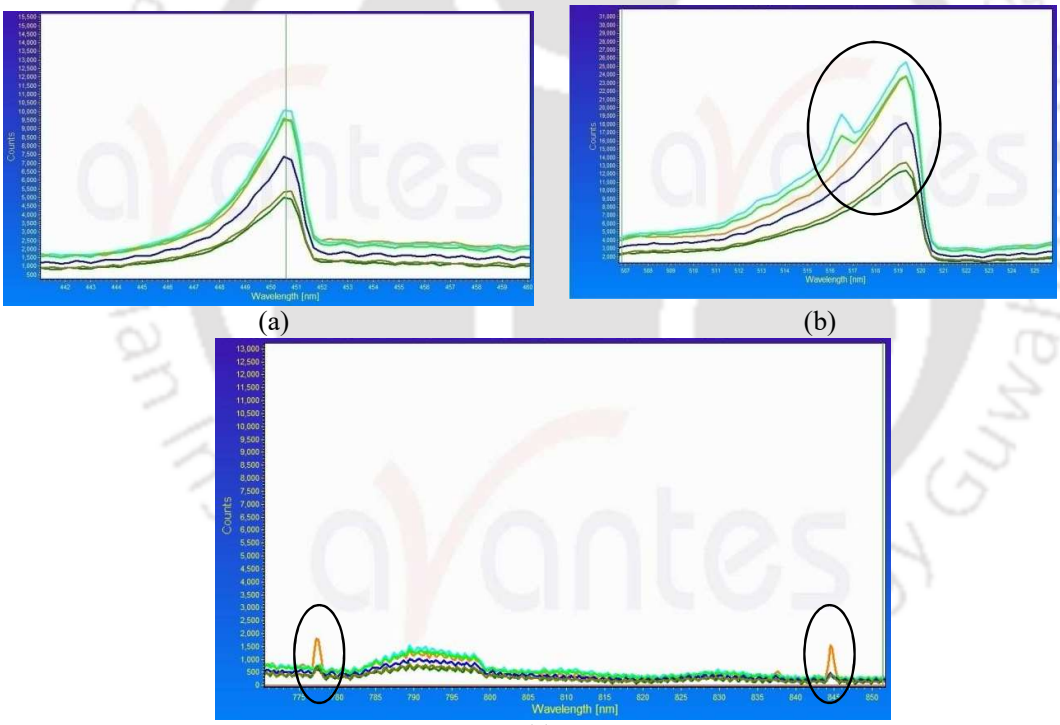

Fig. 3.6 Spectrographs of He and O_2 plasma in the presence of Teflon pieces; Spectrographs at (a) 440 nm, (b) 519 nm and (c) 775 to 840 nm

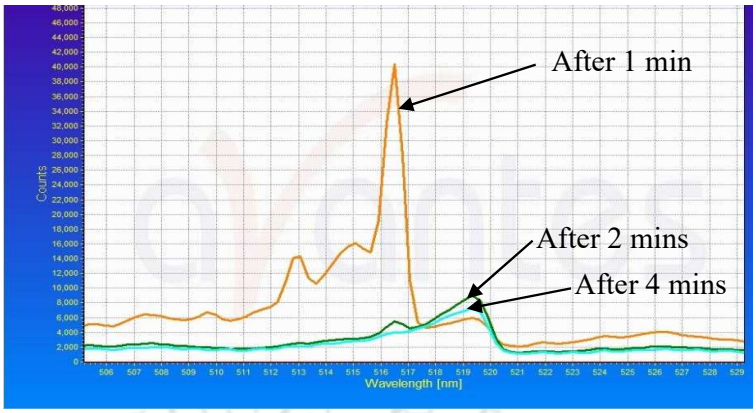

Fig. 3.7 Spectrograph of He plasma at 70W in the presene of teflon pieces and trace amount of O_2

Table 3.5 Observed Silica ion, Flourine and SiF transition

Element	Line(nm)	I -rel	Energy eV Lower – Upper	Transition Lower – Upper	Quantum no Lower – Upper
F II	450.7152	1996	33.04 - 35.79	3d' 3P0 - 4f' 2[5/2]	2 - 3
F III	449.5077	7763	55.12 - 57.88	4f 2[4]0- 5g 2[6]	9/2 - 11/2
SiF	449.58	600	0.00 - 2.84	X2Pi - A2Sig+	3 - 3
Si III	482.897	12303	25.99 - 28.55	4f 3F0 - 5g 3G	4 - 5
Si IV	480.1437	132	39.08 - 41.67	6f 2F0 - 8d 2D	7/2 - 5/2
Si II	519.286	2512	16.36 - 18.75	4p' 4D - 4d' 4F	5/2 - 7/2
Si II	518.525	1259	16.35 - 18.74	4p' 4D - 4d' 4F	3/2 - 5/2
Si II	518.19	1000	16.34 - 18.73	4p' 4D - 4d' 4F	1/2 - 3/2

3.3.2 Optimization of plasma processing gases

3.3.2.1 Advantages of SF_6 gas over O_2 gas

Figure 3.8 shows the spectrograph from 445 to 535 nm for He plasma in the presence of SF_6 and O_2 gases. When SF_6 gas is introduced in the plasma, concentration of fluorine species significantly increases as shown in Fig. 3.8.

Figures 3.9 and 3.10 show the spectrographs of He plasma in the presence of SF_6 and O_2 gas, respectively for different time interval for transitions between 445 to 535 nm. Si II, Si III and Si IV concentration increases with time in the presence of SF_6 gas. However, in the presence of O_2 gas, the concentration of Silicon states decreases with time due to reversible reaction as mentioned in Section 3.3. Above results suggest that SF_6 gas induces chemical reaction for material removal, hence, Silicon oxidation states increases with time.

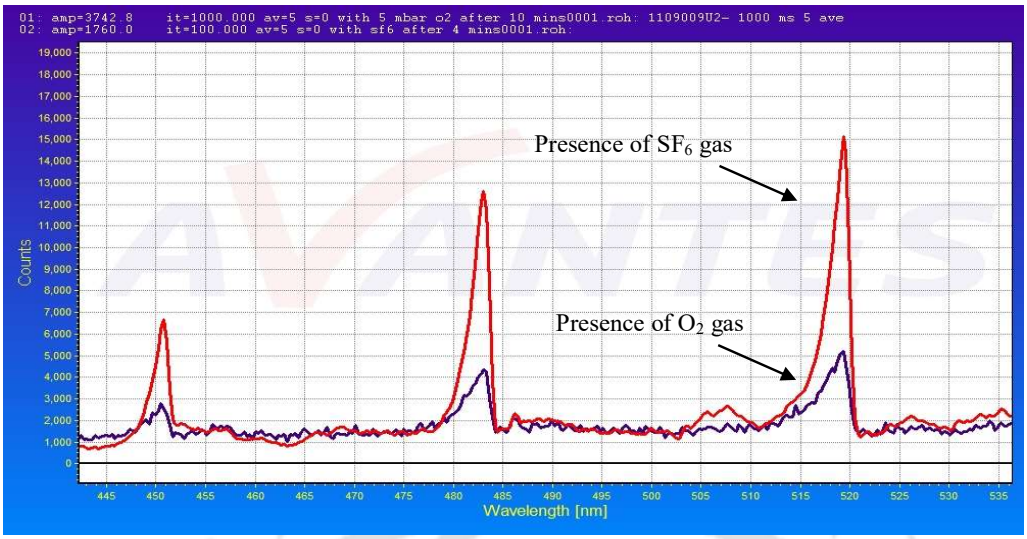

Fig. 3.8 Spectrograph of He plasma in the presence of SF_6 and O_2 gas

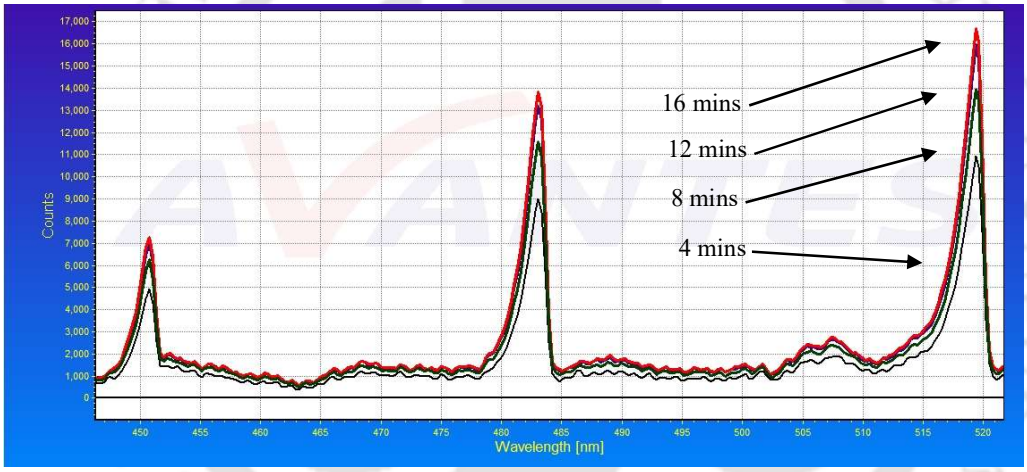

Fig. 3.9 Spectrograph of He plasma in the presence of SF_6 gas for different time interval

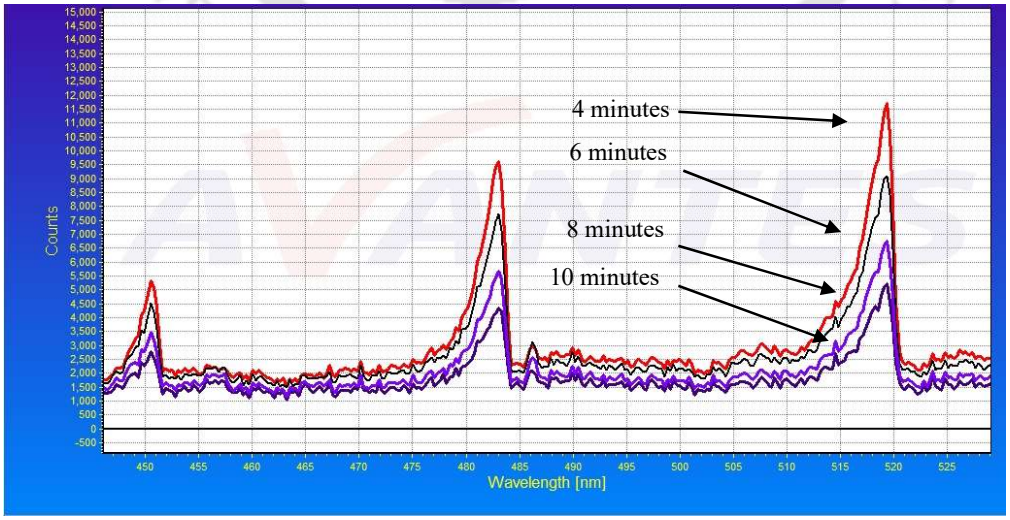

Fig. 3.10 Spectrograph of He plasma in the presence of O_2 gas for different time interval

3.3.2.2 Optimization of gas concentration during plasma polishing

Composition of gases used during experiment are He 30 mbar, O_2 0.25 mbar and SF_6 0.5 mbar with total plasma pressure of 30.75 mbar. This composition is selected based on previous experiments discussed in Section 3.3 in Fig. 3.4. The spectrograph of the plasma for different time interval is shown in Fig. 3.11. It shows that silica IV peak transition (in magnified image) increases till 2 to 3 mins and further decreases. However, the rate of decrease is not stiff as observed previously in the presence of Teflon as discussed in Figs. 3.6 and 3.7. Similarly, further experiments are conducted with different gas compositions as shown in Table 3.6.

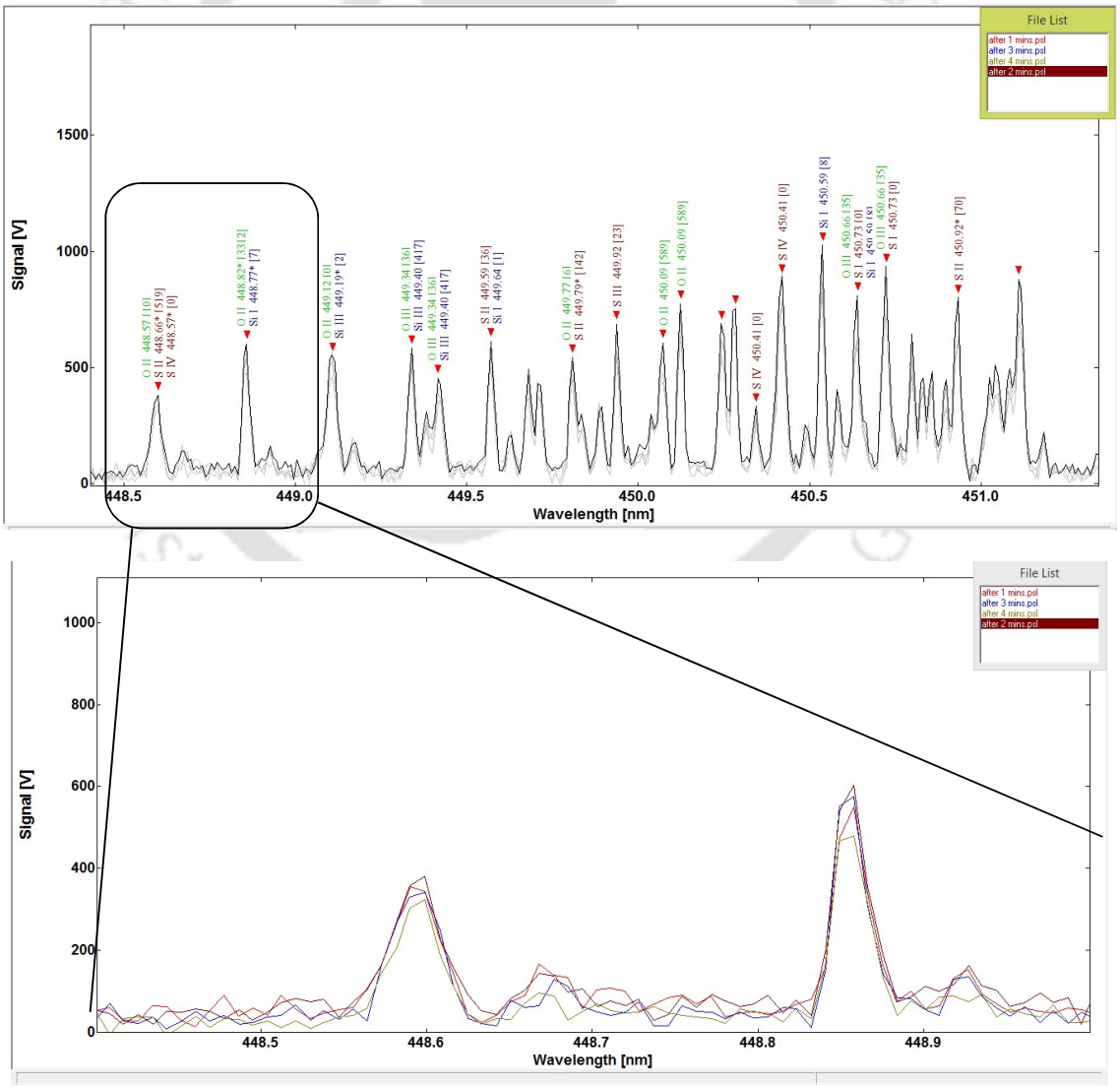

Fig. 3.11 Spectrograph of He 30 mbar, O_2 0.25 mbar and SF_6 0.5 mbar plasma for different

time interval

Table 3.6 Experiments with different gas compositions

Sl. No	Total pressure	*P_{He}	P_{O2}	P_{SF6}	Rate of increase in pressure (mbar/min)
1	31.5	30	1	0.5	0.039
2	30.75	30	0.25	0.5	0.080
3	30.98	30	0.25	0.5	0.067
4	28.4	27.26	0.22	0.8	0.100

*P_{He} – Partial pressure of He

From Table 3.6, it is observed that with the increase in total gas pressure, the rate of increase in pressure inside plasma chamber decreases during plasma polishing. The pressure rise inside closed plasma chamber is due to the formation of volatile SiF_4 molecule. Hence, rate of rise in pressure inside plasma chamber is directly proportional to MRR. Hence, lower value of total pressure inside plasma chamber is more advantageous for machining due to higher collision energy. Therefore, total pressure of 28.3 mbar consisting 27.26 mbar of He (96% by Vol.), 0.22 mbar of O_2 (0.8% by Vol.) and 0.9 mbar of SF_6 (3.2% by Vol.) has shown better result (Table 3.6). However, at 28.3 mbar pressure, the discharge is not very stable and difficult to get plasma initiation. Hence, the total pressure is further reduced to study MRR as discussed below.

Figure 3.12 shows the MRR with different total pressure of machining. The MRR is deduced from the weight loss analysis of the substrate after machining. It shows that MRR increases with increased pressure till 20 mbar and further reduces with pressure. Decrease in MRR with increased pressure beyond 20 mbar can be attributed to decreased collision energy. Whereas, increased MRR with the increase in pressure is attributed to increased chemical reactions, as the number of reactive SF_6 molecules also increases. As mentioned earlier in Table 3.6, the rate of pressure rise increases with the decrease in total pressure of operation. The rise in pressure is due to the presence of the SiF_4, CO and CO_2 gas which are formed during plasma processing. The SiF_4 gas formed during machining from the substrate is directly proportional to MRR, while CO and CO_2 gases are formed due to degradation of O-ring seal at low pressure.

Figure 3.13 shows the intensity of carbon monoxide with different total pressure and input power. The intensity of CO is attributed to the O-ring seal degradation during machining. Figure 3.13 suggests that O-ring seal degradation increases with decreased pressure and increased power. Hence, total pressure of operation is optimized to be 20 mbar with 40W input power.

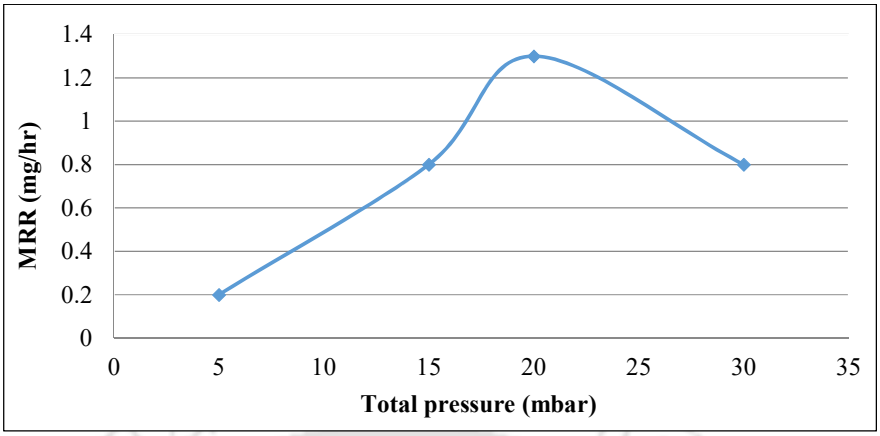

Fig. 3.12 Variation of MRR with total plasma pressure

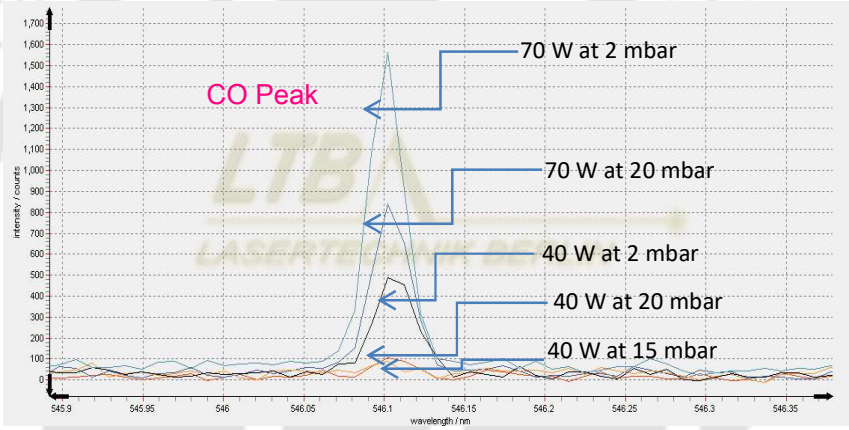

Fig. 3.13 Variation of carbon monoxide intensity at different total pressure and input power

3.3.2.3 Optimization of SF_6 to O_2 ratio

Experiments are carried out to optimize the ratio of SF_6 and O_2 composition at 20 mbar total pressure. The optimization is carried out by monitoring silicon oxidation states during plasma processing by optical emission spectrometer. Increase in intensity of Si II and Si III states during plasma processing has been correlated with the efficient plasma processing. Table 3.7 shows different experimental conditions as cases from 1 to 5 at constant total pressure of 20 bar and power of 40 W. In case 1, both SF_6 and O_2 are considered as 0.5 mbar. In case 3, the composition is same as case 2, but the chamber is decontaminated by evacuation. For cases 4 and 5, post decontaminated plasma chamber is considered.

Table 3.7 Plasma experiments with different gas compositions for constant total pressure and power

	Composition (mbar)			Duration (mins)	Temperature generated (°C)	Remark
	He	SF_6	O_2			
case 1	19	0.5	0.5	10	45	At higher O_2 concentration
case 2	19.25	0.5	0.25	10	45	Without de-contamination
case 3	19.25	0.5	0.25	20	49	Post decontamination
case 4	19.4	0.5	0.1	25	49	At low O_2 concentration
case 5	19.25	0.5	0.15	25	45	Post decontamination

The intensity of Si III transition with time for different cases (Table 3.7) are shown in Fig. 3.14. The reduction in intensity of the peaks for case 1 may be due the presence of more O_2, which reduces plasma energy. In case 2, the peak intensity increases and reaches to a maximum value up to 4 min and beyond that further decreases. It may be due the deposition of the silicon oxide polymer (due to excess O_2) or Sulfur polymer (due to the insufficient O_2). Hence, to identify the reason, the system is evacuated overnight to reduce the contamination in the system.

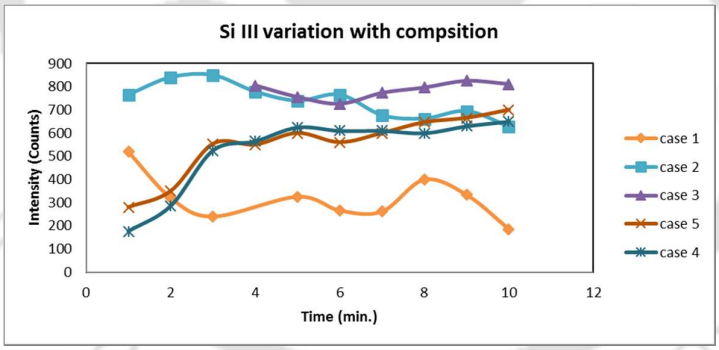

Fig. 3.14 Si III variation with composition

Figure 3.15 shows the variation of Si III intensity with time for cases 3, 4 and 5. Si III intensity increases slowly unlike case 2 which suggests that absence of contamination enhances reaction kinetics. Hence, reaction sustains beyond 10 mins also without reduction in Si III intensity. Hence, it confirms that reduction in Si III intensity in case 2 due to the formation of silicon oxide polymer.

Figure 3.16 shows the variation of Si II and Si III intensity for cases 3 and 5. It clearly suggests that intensity of Si II and Si III is higher during 8 to 20 mins of machining for case 3 than case 5. It also suggests that 1.25% (Vol. %) O_2 may be more efficient than 0.5%. Hence, to confirm the results further experiments are conducted for these two compositions.

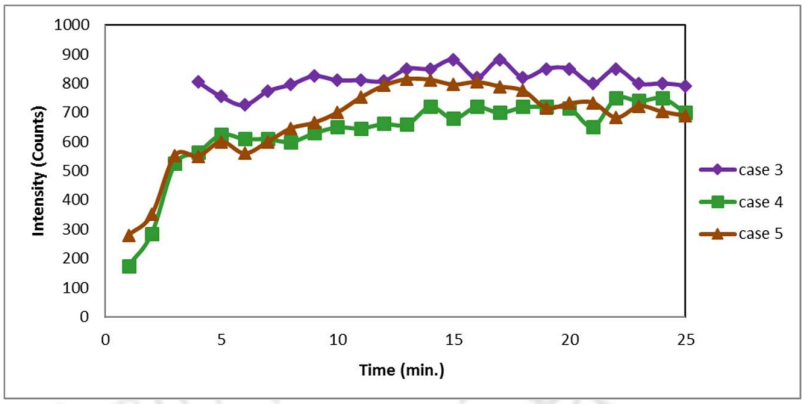

Fig. 3.15 Variation of Si III intensity for cases 3, 4 and 5

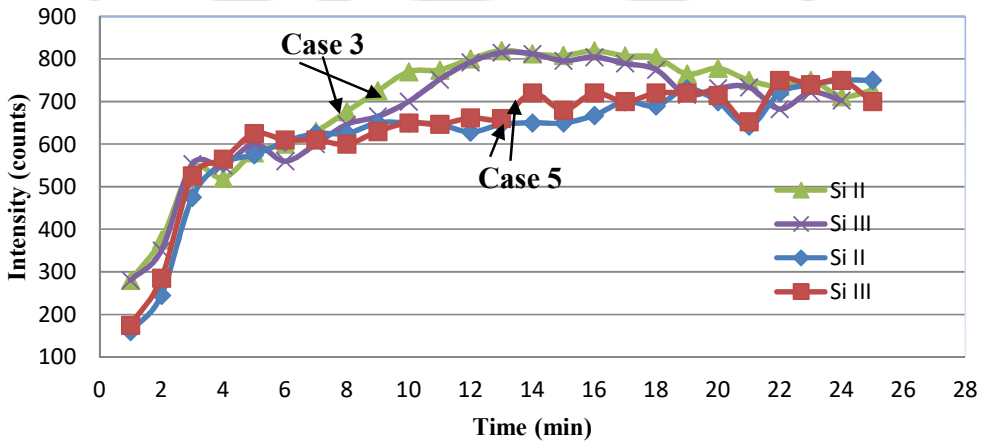

Fig. 3.16 Variation of Si II and Si III intensity for cases 3 and 5

Plasma processing is done at 20 mbar pressure and 40 W power, where uniform plasma distribution is obtained. Experiments are carried out to study the effect of SF_6/O_2 ratio on MRR as shown in Fig. 3.17. MRR is highest when the ratio of SF_6/O_2 is 2. The rate of material removal is 1.1 mg/hr. The mean MRR of 0.008 mm^3/min is achieved for optimised reactive gas mixture. The gas mixture selected after a series of experiments is He: 19.25 mbar, O_2: 0.25 mbar and SF_6: 0.5 mbar.

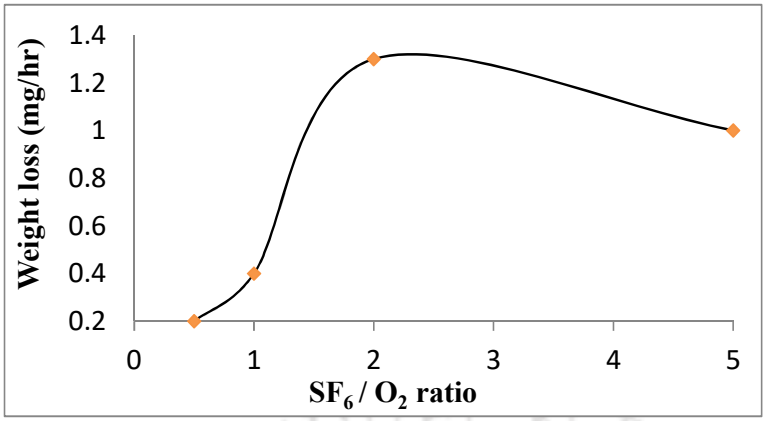

Fig. 3.17 Weight loss vs. ratio of SF_6 / O_2

For further experiments, each cycle duration is fixed to 20 minutes and the chamber is evacuated to flush out the volatile products. After that the chamber is refilled for next cycle of experiments. Multiple such cycles are performed and the silicon ion and SiF transitions are plotted with time in Fig. 3.18. The mean material removal rate of 0.008 mm^3/min is achieved for the given reactive gas mixture of 1% SF_6 and 0.5% O_2. Plasma chamber pressure also increases indicating the formation of volatile products for every 30 minutes of plasma operation.

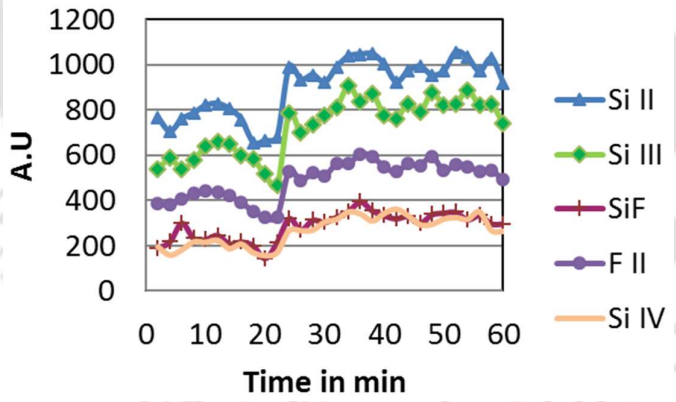

Fig. 3.18 Silicon ions and SiF transitions with time

Measurements (spectrum) are taken at different locations (excluding near chamber wall zones) to cover the entire volume of the chamber by shifting the location of the spectroscopy probe. After analyzing all the spectra at different locations within the plasma chamber for relative intensity of each species (I-rel), it is found that I-rel varies less than 5% indicating isotropic plasma action.

3.4 Surface finish analysis of substrate

Plasma polishing experiments are carried out for course machined (ultrasonic milling) substrate. The surface roughness profiles measured by Talysurf surface profiler before and after plasma polishing on coarse machined surface are shown in Figs. 3.19 (a) and (b), respectively. The coarse machined surface displays suspected surface cracks and poor surface waviness. 68% improvement in surface roughness and also distinct improvement in waviness (85%) of the surfaces are observed. Also, Rmr improves from 11.5% to 36% indicating more bearing area.

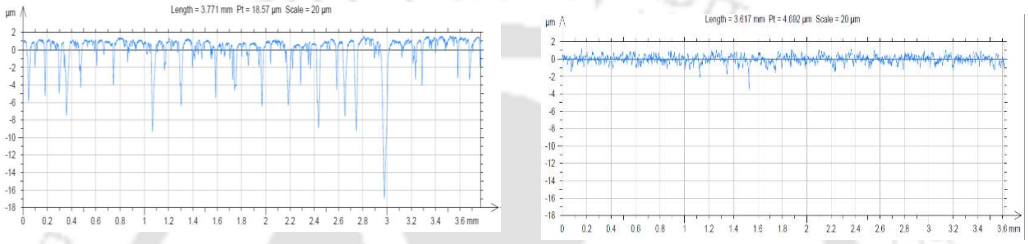

(a) (b)

Fig. 3.19 Surface profile (a) before (Ra= 1.099 µm, Rz=9.663 µm, Wa=0.234 µm, Rmr =11.5% and (b) after (Ra= 0.358 µm, Rz=3.379 µm, Wa=0.035 µm, Rmr=36.2%) plasma processing

3.4.1 Plasma polishing of fine machined substrate

Similarly, the fine machined (ultrasonic machining followed by diamond tool grinding) substrates are also finished by plasma. The surface profiles are obtained by using surface profiler and Atomic force microscope (AFM). Figures 3.20 (a) and (b) show the surface roughness profiles and Figs. 3.21 (a) and (b) show the AFM profiles before and after plasma polishing, respectively. About 30% improvement in surface roughness (Ra) is observed. However, better improvement around 60% is observed for waviness. The AFM profiles clearly show the presence of surface cracks in the fine machined surface and reduction of crack depth in the plasma processed surface apart from surface finish improvement.

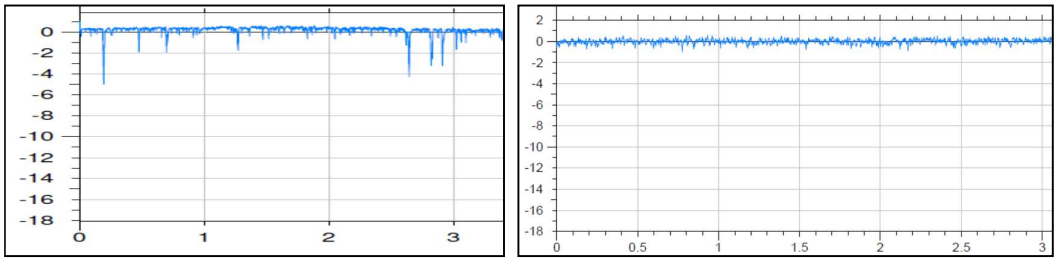

(a) (b)

Fig. 3.20 Surface profiles (a) before (Ra= 0.256 µm, Rz=5.352 µm, Wa=0.226 µm, Rmr=91.1%) and (b) after (Ra= 0.169 µm, Rz=1.386 µm, Wa=0.02 µm, Rmr=96.5%) plasma polishing on fine machined surface

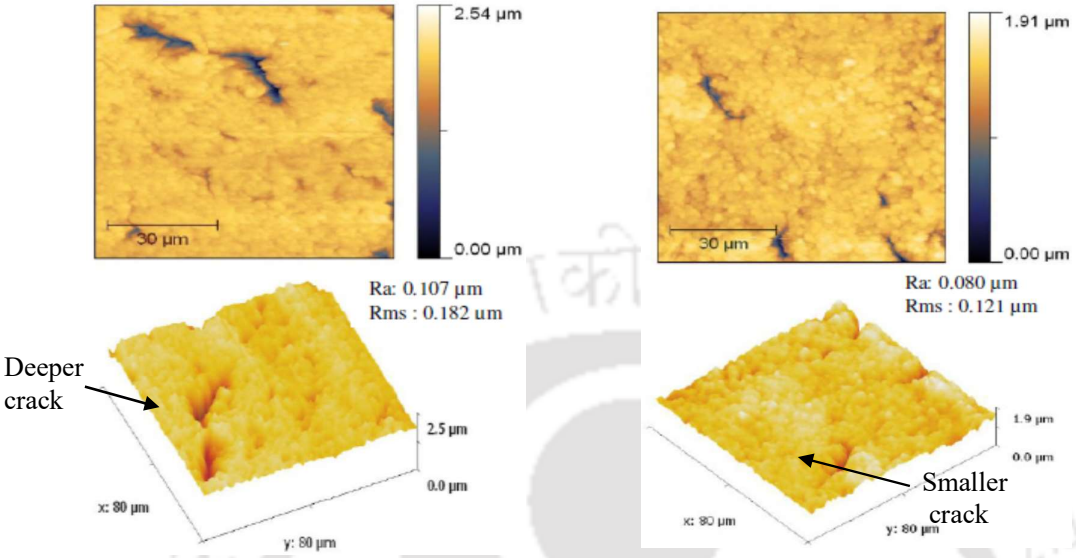

(a) (b)

Fig. 3.21 AFM surface profiles (a) before and (b) after plasma polishing on fine machined surface

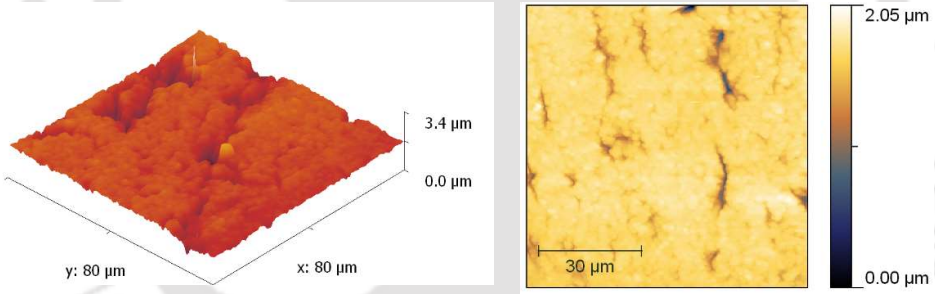

(a) (b)

Fig. 3.21a AFM micrographs of specimen (a) before and (b) after plasma processing

The magnified (100 X) image of the surface before and after plasma processing are shown in Fig. 3.22 (a) and (b), respectively. It clearly indicates that the micro cracks are reduced drastically (Fig. 3.22 (b)) after plasma processing.

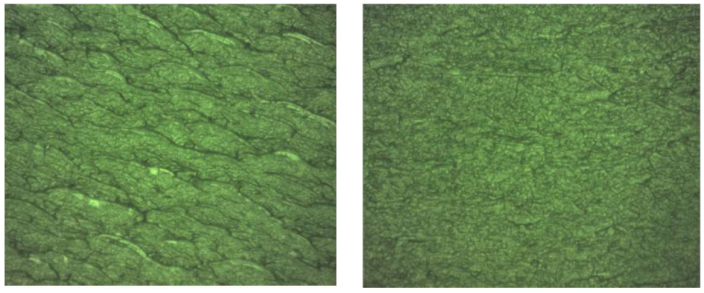

(a) (b)

Fig. 3.22 Magnified image (100X) of the specimen surface (1.5 x 1.5 mm^2) inspected (a) before and (b) after plasma processing

Figure 3.22a shows average surface roughness of various experiment specimen sets before and after plasma processing. Figure 3.22a suggests average surface roughness of various experiment specimen sets processed by plasma. All samples have shown reduction in average surface roughness value after plasma processing. As expected, reduction is maximum for rougher samples compared to smoother ones.

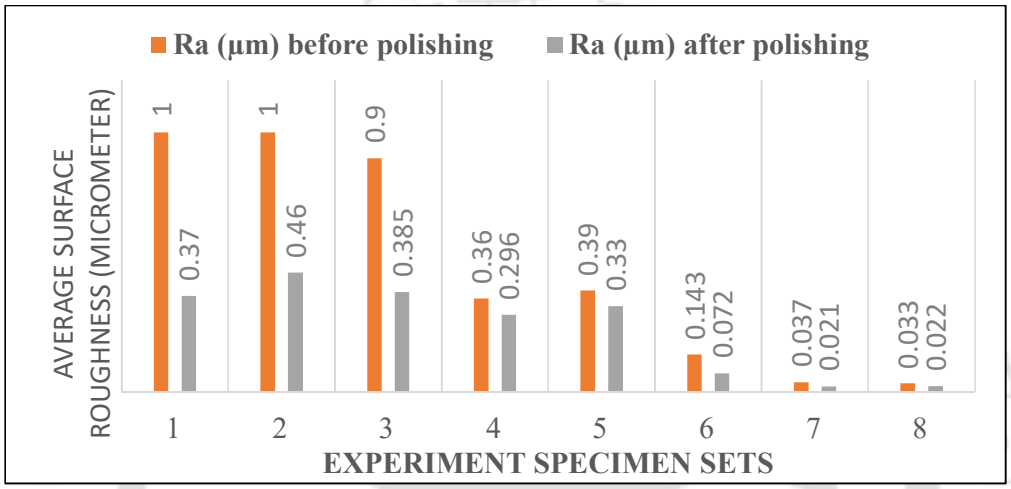

Fig. 3.22a Average surface roughness of various experiment specimen sets before and after plasma processing

3.4.2 Raman spectroscopic analysis

Raman spectroscopy is proven to be an efficient method for characterizing surface integrity in fused silica during fabrication and finishing operations. The spectrum of fused silica generally shows a broadband centered at around 440 cm^{-1} attributed to the Si-O-Si bond rocking and bending of SiO_4 tetrahedral. The Raman spectrum as shown in Fig. 3.23 also shows characteristic shoulder peak around 495 cm^{-1} and another peak around 606 cm^{-1}. These correspond to four and three-member siloxane rings formed due to the strain generated during conventional contact machining. Fig. 3.23 provides the comparison of Raman spectrum on fine machined specimen before and after plasma polishing.

In the Raman spectroscopy after post plasma polishing, the shoulder peak around 495 cm^{-1} is almost absent suggesting the absence of three-member siloxane ring. Also, the decrease in intensity of 606 cm^{-1} peak indicates the reduction in three-member strained

siloxane ring. The above observation confirms the reduction in surface and subsurface damaged layers in post plasma polishing.

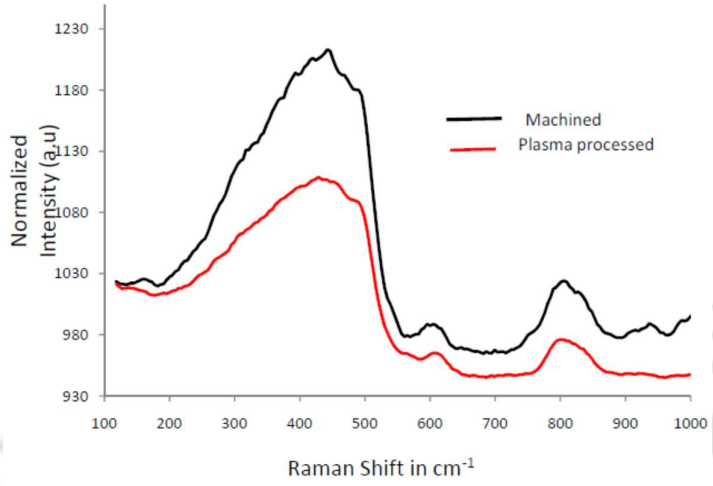

Fig. 3.23 Comparison of Raman Spectrum of fine machined surface of fused silica before and after plasma polishing

3.5 Summary

In this chapter, experimental investigation on atomistic isotropic material removal on fused silica surfaces is carried out to understand its material removal mechanism. Plasma characterization methodology by optical emission spectroscopy is effectively established. Isotropic plasma is established without heating the specimen beyond 50 °C. With He as processing gas and O_2 as reactive gas, surface modification is possible by medium pressure plasma. The surface finish improves and the surface waviness improvement is very distinct and effective in all machined specimens irrespective of their orientation with respect to the electrodes. The strained surface layer gets removed and surface integrity improves. Further, material removal is not effectively happening with O_2 alone as reactive gas to remove all surface cracks. A more reactive radical (such as fluorine) is to be present for effective material removal in the form of volatile compound of Si and fluorine. SF_6 gas is used to vaporise the fused silica surface continuously. A mixture ratio of He, O_2, and SF_6 is identified for the given plasma chamber to get a material removal rate of 0.008 mm^3/min while improving surface finish.

Chapter 4

SIMULATION OF PLASMA PROCESS

3.1 Introduction
3.2 System design and methodology
3.3 Preliminary experiments
3.3.1 Experiments with Teflon
3.3.2 Optimization of Plasma processing gases
3.3.2.1 Advantages of SF_6 gas over O_2 gas
3.3.2.2 Optimization of SF_6 gas concentration during plasma polishing
3.3.2.3 Optimization of SF_6 to O_2 ratio
3.4 Surface finish analysis of substrate
3.4.1 Plasma polishing on of fine machined substrate

4.1 Introduction

The primary aim of the present chapter is to identify the distribution of electron density and its uniformity as well as O_2 radical's distribution with respect to the shape of the chamber, position and shape of the electrodes using Comsol® Multiphysics, a FEM based software. Also, electron temperature is studied to confirm electron's temperature as benign to maintain "cold" plasma condition. Further, the Comsol® model is validated with experimental results of atomic spectroscopy data and analytical model. The following objectives are identified as;

- Investigate the effect of mixture of helium and oxygen gas on SiO_2 specimen inside plasma chamber by varying volume concentration and pressure of plasma gases.
- Study the effect of shape, size and position of specimen inside plasma chamber.
- Design the shape, size and position of electrodes of plasma chamber to get homogeneous distribution of reactive species and ions.

In the present case, a two dimensional frequency transient study under microwave plasma (MWP) is used for simulation. Electric field is setup using out of plane vector considering the signal in transverse electric mode. Reduced electron transport properties are considered to account for the heavy species transport. The pressure and temperature of the plasma are taken as 25 mbar and 300K, respectively and are considered to be constant throughout the operation of the plasma. Plasma setup is made considering the plasma to be static. The different species used for current simulation are, in atomic/molecular state: He and O_2, ions: He^+, e, O, O^-, O_2^+ and radicals: O_2a1d, O_2b1s, O1d, O1s, He^*. To study the plasma chemistry, the main reactions occurring inside the plasma chamber are shown in Table 4.1.

Table 4.1 Main reactions occurring inside plasma chamber

Electron impact reactions	**Heavy species transport Reactions**	**Surface reactions**
e+He => e+He	$He^*+ O_2 => O_2+ +He+ e$	$He^* => He$
$e+He => e+He^*$	$He+ + O_2 => O+ +O+ He$	$He+ => He$
$e+He => 2e+He+$	$He+ + O_2 => O_2+ +He$	$O_2+ => O_2$
$e+O_2 => 2e+O_2+$		$2O+ => O_2$
$e+O_2 => e+O_2a1d$		
$e+O2a1d => e+O_2$		
$e+O_2 => e+O_2b1s$		
$e+O_2b1s => e+O_2$		
$e+O_2 => e+ O +O$		
$e+O_2 => e+O+O1d$		
$e+O_2 => e+O+O1s$		

For each of the heavy species, the molecular weight, potential characteristic length and minimum potential energy are required to compute correct diffusivity and mobility. The initial number density for electron is considered as $1\times10^{17}/m^3$. Considering the plasma to be neutral consisting of ions and electrons, the initial number density and initial mole fractions of different species (ions and electrons) are to be equal. Since the radicals (excited species) are formed at a later part during reaction, hence, the initial mole fraction of the radicals are considered negligible i.e. $1\sim5\times10^{-8}$.

4.2 Computational domain and boundary conditions for cylindrical substrate

The geometry of the two dimensional computational domain as shown in Fig. 4.1 is prepared similar to the proposed experimental set up. The cross-sectional area of the setup is prepared into three domains i.e. dielectric, plasma and electrodes (Fig. 4.1). The electrodes are placed at the extreme boundaries on both left and right side of the setup. The setup dimensions considered as 55×40 mm^2 and the thickness of the dielectric chamber is 5 mm. A specimen of SiO_2 (quartz) is placed at the bottom of the chamber. The dimension of the specimen is 10×8 mm^2. A physics controlled mesh of finer nature is used to carry out the simulation. The mesh at the boundaries are made finer to accommodate the collision of the charged particles. Free triangular mesh is considered.

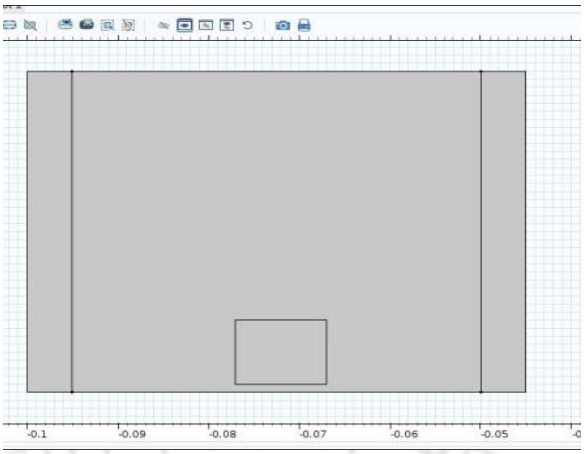

Fig. 4.1 2D Computational domain of the plasma chamber

The four boundaries of the plasma chamber are considered as the four walls in the model containing plasma within the domain. The four boundaries of the chamber are grounded so as the surface reactions to take place at the boundaries. The plasma is excited using a RF frequency powered to one electrode while another electrode opposite to the first one is grounded. Square wave RF signal is used for exciting the plasma and the power level considered is 40 W.

4.2.1 Simulation results and discussion

It is a transient analysis and steady state is reached before one second. The plasma conditions at 1s is taken for comparison study for all cases. The electron density and O_2 radials such as O1s, O_2b1s are studied. In Figs. 4.2 (a) and (b), the electron density is shown without and with the presence of a rectangular specimen, respectively inside the plasma chamber. The electron density varies from 1×10^{16} to 6×10^{16} $1/m^3$ for both the cases. However, the distribution profile is altered while the specimen is placed inside the chamber. Hence, it is understood that the shape and position of the fused silica influence the distribution of electron density inside the polishing chamber.

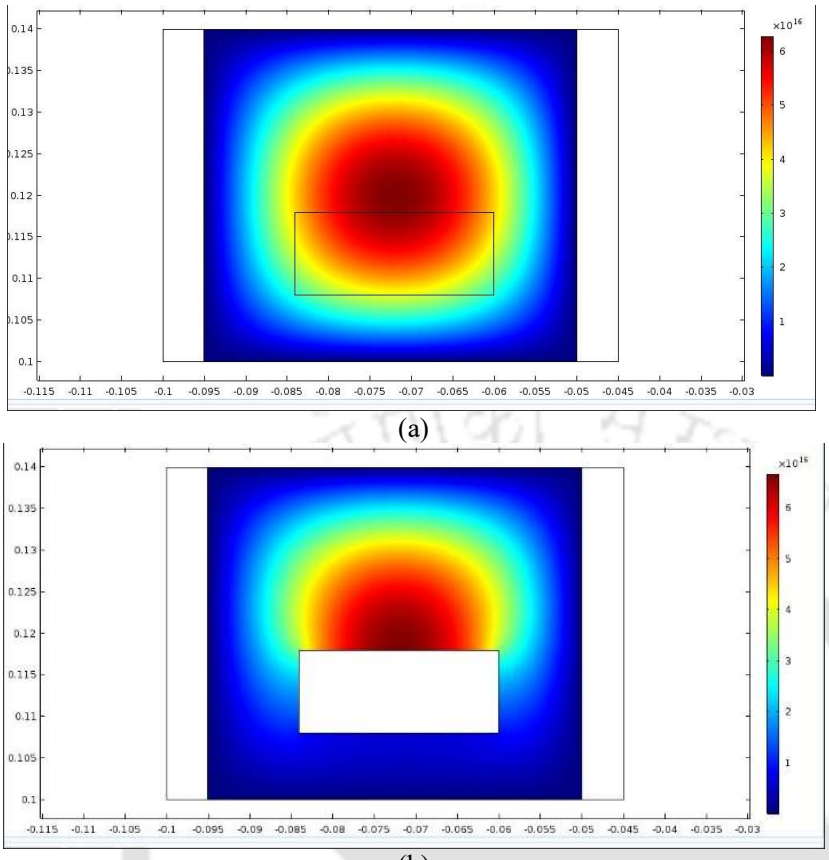

(a)

(b)

Fig. 4.2 Electron density (a) without and (b) with specimen inside plasma chamber

After that a cylindrical fused silica specimen of varying sizes with respect to the plasma chamber are placed inside the plasma chamber to understand the effect of specimen size inside the plasma chamber as shown in Fig. 4.3. The specimen sizes as shown in Figs. 4.3 (a), (b) and (c) are approximately three-fourth, half, and one-fourth of the chamber size, respectively. As shown in in Fig. 4.3 (a), the electron density distribution is not uniform when the specimen size is large compared to the cross section of the chamber. In other words, when the free volume is less, the electron density is lower and non-uniform. As the specimen size reduces from Fig. 4.3(a) to Fig. 4.3(c) i.e. free volume of the chamber increases, the uniformity of the electron density distribution improves distinctly and electron density also increases. The same is true for the distribution of O_2 radials such as O1s, O_2b1s (results not shown). However, there is no variation in the number density of radicals irrespective of the size of the specimen.

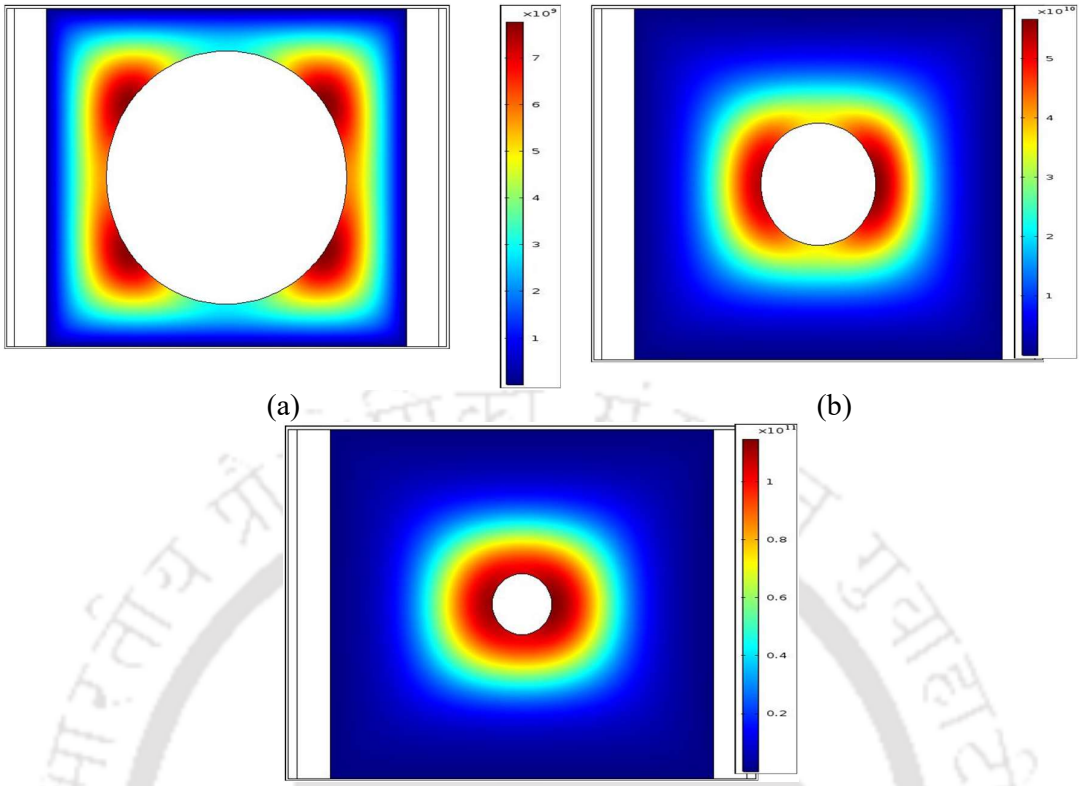

Fig. 4.3 Electron density when specimen sizes are (a) three-fourth, (b) half and (c) one-fourth of chamber size

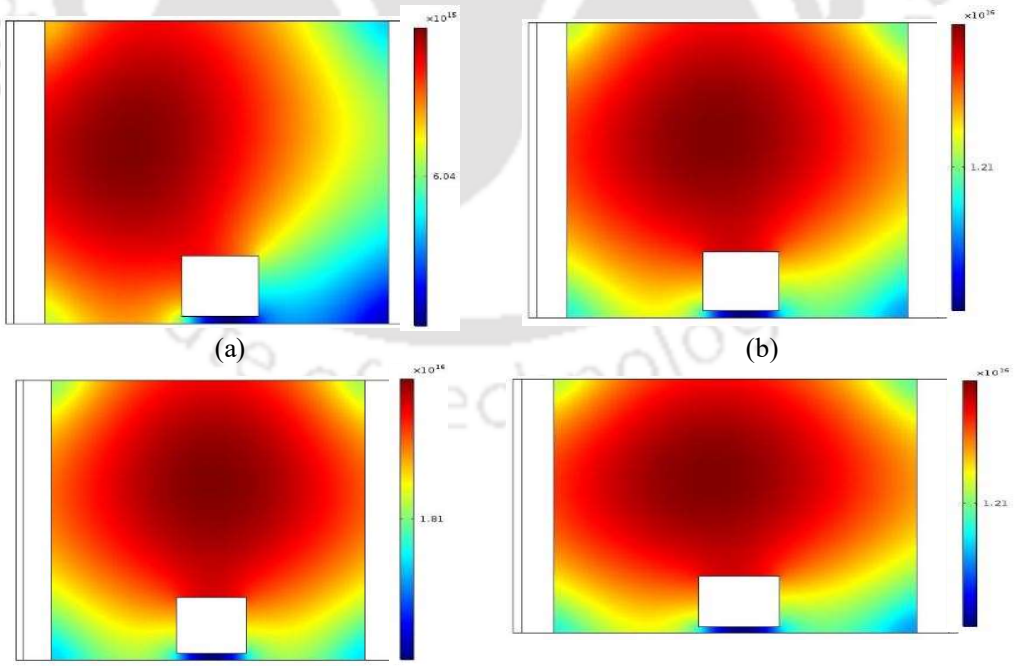

Fig. 4.4 Variation of O1s radical number density with increasing O_2 concentration (a) 1%, (b) 1.5 %, (c) 2% and (d) 5%

Figure 4.4 shows variation of O1s radical number density with increasing O_2 concentration (%) from 1 to 5%. From Fig. 4.4, it is observed that as the O_2% increases, the number density of O1s radicals increases. However, the distribution of O1s radicals is unsymmetrical with respect to the specimen up to at 1% and symmetrical at 2% and it loses its symmetrical distribution on further increase of O_2%. Therefore, 2% O_2 concentration may be optimum for processing fused silica components.

4.3 Simulation for hemispherical shell

Based on the Comsol® simulation results, the plasma chamber along with electrodes are modified to suit target specimen of hemispherical shell made of fused silica. Fig. 4.5 (a) shows the plasma chamber with two parallel electrodes with respect to the position of the HRG shell. Fig. 4.5 (b) shows the same plasma chamber with four sided electrodes. The corresponding distribution of O_2b1s radicals are shown in Fig. 4.6.

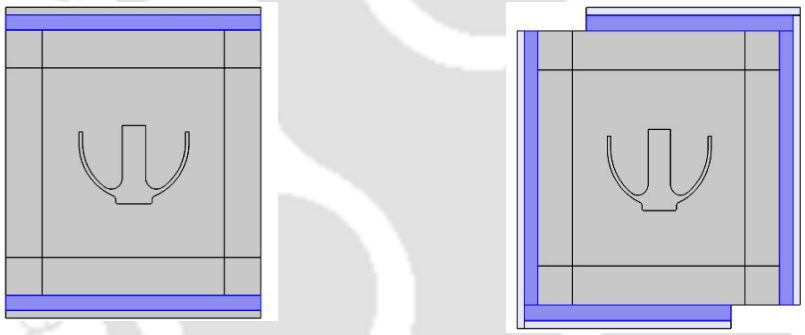

(a) (b)

Fig. 4.5 2D Computational domain of the plasma chamber with two (a) parallel electrodes at top and bottom and (b) L shaped four sided electrodes

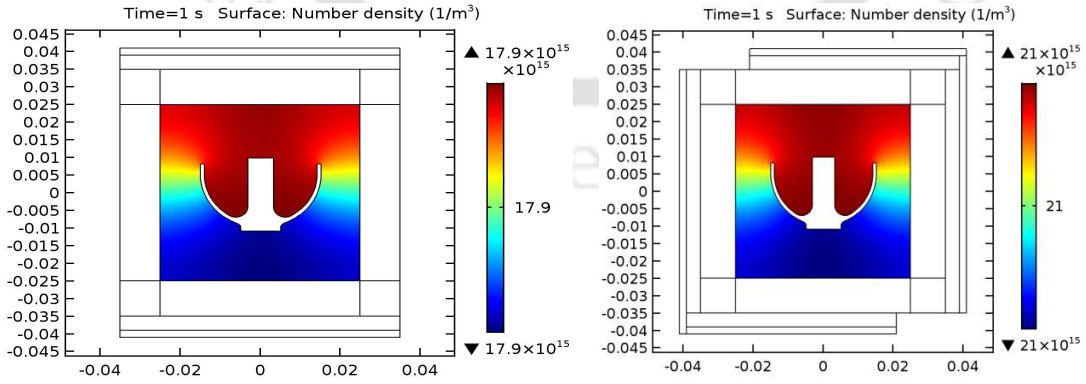

(a) (b)

Fig. 4.6 Distribution of number density of O_2b1s radicals inside plasma chamber with (a) two parallel electrodes at top and bottom, and (b) four sided electrodes

The number density of O_2b1s radicals is more by 18% for four sided electrode configuration than electrode placed at top and bottom. Hence, more material removal is expected while polishing with four sided electrodes. The primary objective of Comsol® simulation is to determine the O_2 radical density and its uniformity about the position of hemispherical shell as well as with the shape of the electrodes and chamber configuration. Previous study was carried out on flat fused silica sample. In this section, the hemispherical shell is used as a substrate. Electron temperature inside plasma chamber is studied to confirm cold plasma atmosphere during plasma processing. Also, Comsol® model is experimentally validated by using optical emission spectroscopy data. The following objectives of the Comsol® simulation are identified as

- To investigate the effect of hemispherical shell's position inside plasma chamber with the distribution of the reactive species.
- Also, to ascertain the electrode position and its shape for attaining homogeneous reactive species distribution.

4.3.1 Computational domain and boundary conditions

The geometry of the 2D computational domain is designed as per proposed experimental set up. The cross-sectional area of the set-up is distinguished into three domains such as electrodes, plasma and dielectric construction body. The electrodes are placed at (a) both top and bottom side and (b) L shaped electrodes covering four sides of the setup as shown in Fig. 4.7.

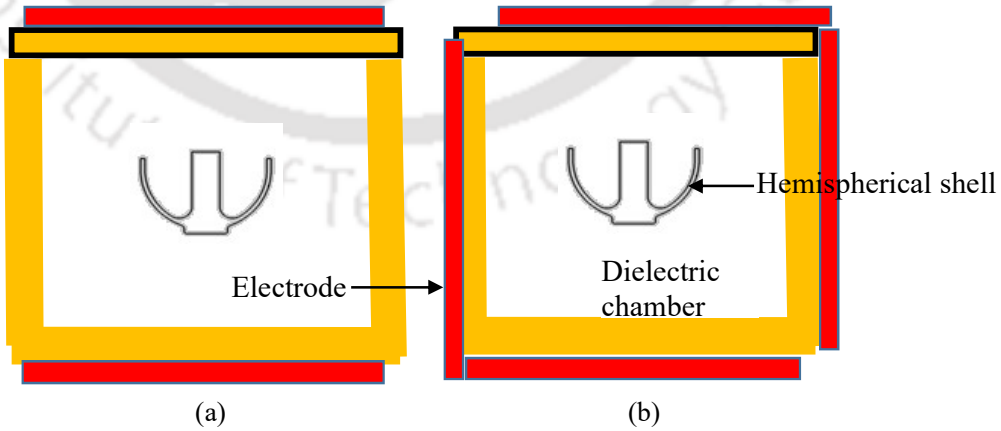

Fig. 4.7 2D Computational domain of the plasma chamber with hemispherical shell having two (a) top and bottom and (b) L shaped electrodes

The setup dimension is considered as 55×40 mm^2 and the dielectric thickness is taken as 5 mm. A hemispherical shell made of SiO_2 (i.e. fused silica) is kept at the middle of the chamber for simulation. Free triangular finer mesh is considered to carry out the simulation of the charge particle collision at walls and physics controlled reaction at the substrate interface. The plasma is contained within the four boundaries of the chamber considered as walls. These four walls are grounded for boundary surface reactions. RF frequency is applied to the one of the electrodes while other acts as ground for plasma excitation. In the present simulation, square wave RF signal is adopted for plasma excitation with 40 W power. Different transient analyses are adopted with various positions of the hemispherical shell with or without support with two different configurations of the electrodes as explained below.

4.3.2 Simulation results of hemispherical shell

Transient analysis is carried out using Comsol® and steady state is achieved within one second. Hence, in the present study, the condition of the plasma inside chamber is considered for 1s for all cases. Distribution of O_2 radicals i.e. O_2b1s are studied as discussed below. Radicals play active role in material removal process. Hence, uniform radial distribution surrounding hemispherical shell is required for uniform machining throughout the workpiece surface.

Figure 4.8 shows the O_2b1s radical density distribution inside plasma chamber while hemispherical shell is (a) centred in the chamber without support and (b) placed at the bottom of the chamber. From Comsol® simulation, it is observed that average radical density is similar for both the configurations. However, the distribution of reactive species is more uniform about the axis of the hemispherical shell while it is placed at the center of the plasma chamber (Fig. 4.8 (a)) than the other configuration (Fig. 4.8 (b)). As the positioning of the shell at the center of the chamber is not feasible, hence, it is placed at the center of the chamber with the help of a support. Natural choice of a support is dielectric material. However, as the dielectric material will also get eroded along with hemispherical shell during plasma processing, option of keeping a metallic stand is also studied.

Figure 4.9 shows the distribution of O_2b1s radicals inside plasma chamber while the hemispherical shell is supported by (a) metallic and (b) dielectric stand. The distribution of O_2b1s radicals is not uniform in both the configurations about the axis of the hemispherical shell. However, higher radical density is observed in case of dielectric stand than metallic one. This may be due to ion burial of the plasma on the surface of the metallic stand. Hence,

the supporting material is selected as dielectric fused silica. Also, more uniform and higher radical density is observed at the inner surface of the shell than outer surface. However, uniform radical distribution about the centre of the hemispherical shell is not achieved with top and bottom electrodes configuration. Therefore, to achieve uniform radical distribution, L shaped electrode configuration is studied further.

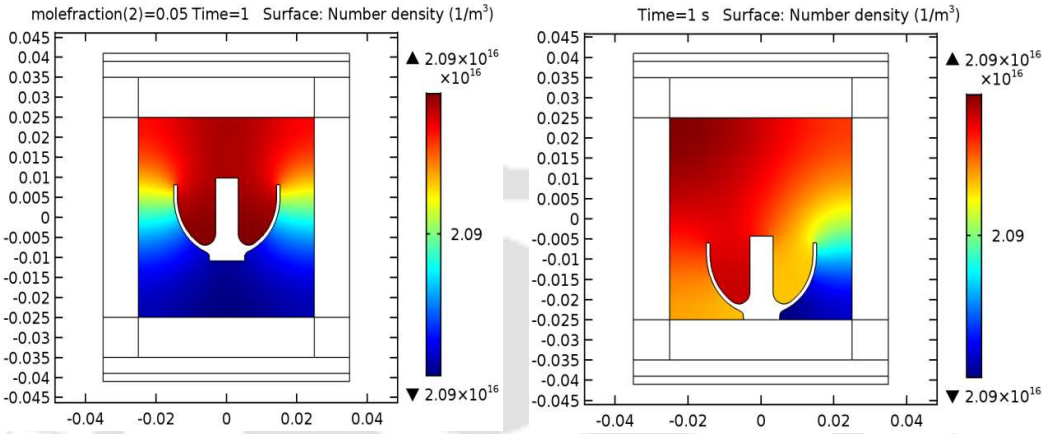

Fig. 4.8: Distribution of O_2b1s radical density inside plasma chamber while hemispherical shell is (a) centred in the chamber without support and (b) placed at the bottom

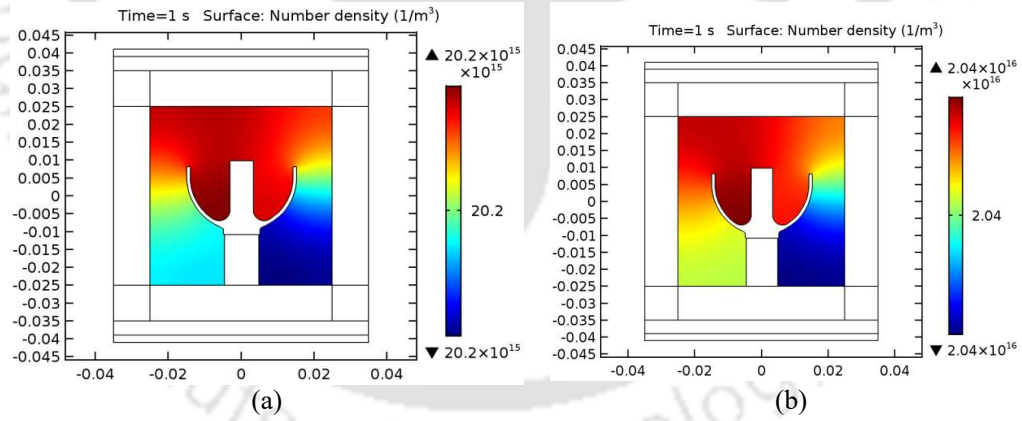

Fig. 4.9 Distribution of O2b1s radical density inside plasma chamber while hemispherical shell is supported by a (a) metallic and (b) dielectric stand

Figure 4.10 shows the O_2b1s radicals distribution inside plasma chamber with L shaped electrode configuration. It is observed from Fig. 4.10 that uniform radical distribution about hemispherical shell axis is not achieved also with L shaped electrodes. Hence, further modification which can be implemented for uniform radical distribution by changing configuration of the dielectric stand.

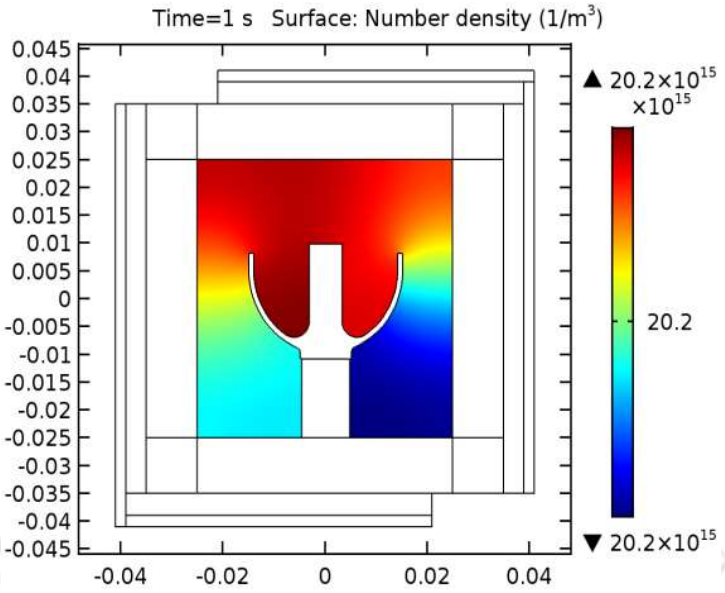

Fig. 4.10 Distribution of O2b1s radical density inside plasma chamber while hemispherical shell is supported by dielectric stand with L shaped electrode

Figure 4.11 shows the modified dielectric stand with two different electrode configurations (a) top and bottom and (b) L shaped electrodes. The distribution of O2b1s radicals having upside down hemispherical shell with modified dielectric stand is show in Fig. 4.11. It is observed from Fig. 4.11 that with both the electrode configurations having modified dielectric stand uniform radical distribution is observed about the axis of the hemispherical shell. Hence, from Comsol® simulation it can be concluded that with modified dielectric configuration uniform finishing throughout the workpiece surface can be achieved.

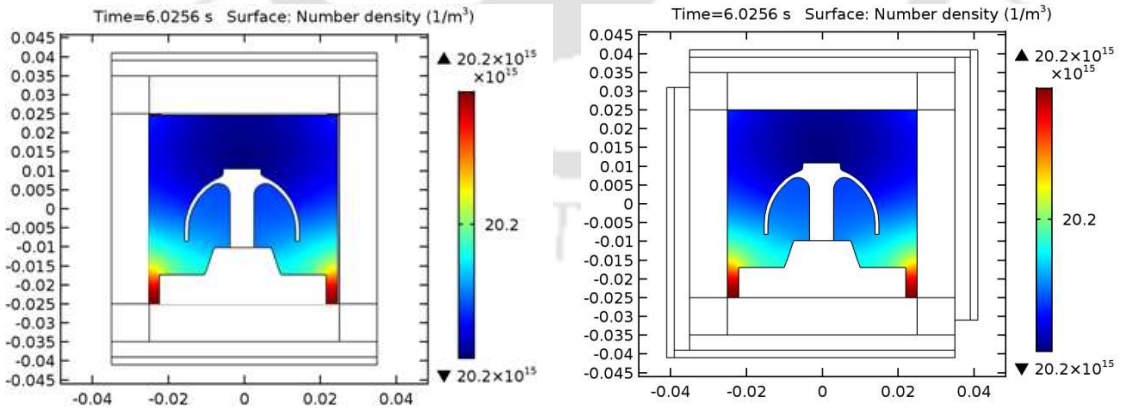

(a) (b)

Fig. 4.11 Distribution of O2b1s radicals having upside down hemispherical shell with modified dielectric stand for (a) top and bottom and (b) L shaped electrodes

4.4 Simulation for total reflecting prism

The geometry of the two dimensional computational domain as shown in Fig. 4.12 is prepared similar to the proposed experimental set up. The L shaped electrode covering four sides are placed at the extreme boundaries. A Total reflecting prism made of SiO_2 (fused silica) is taken at the middle of the chamber. A dielectric material used for centring substrate with respect to chamber for uniform plasma processing. The four boundaries of the plasma chamber are considered as the four walls in the model containing the plasma within the domain. The four boundaries of the chamber are grounded so as the surface reactions to take place at the boundaries. The plasma is excited using a RF frequency as a port applied to one electrode while another electrode opposite to the first electrode is grounded. Square wave RF signal is used for exciting the plasma and the power level considered is 40 W.

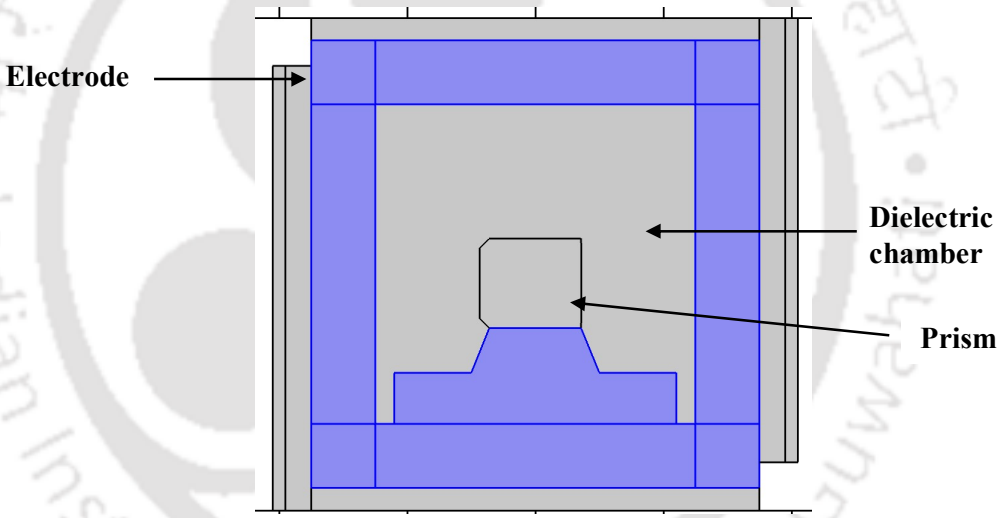

Fig. 4.12 A 2D Computational domain of the plasma chamber for total reflecting prism

4.4.1 Simulation results and discussion

The electron density, O_2 radials such as O1s, O_2b1s and electron temperature are studied. Fig. 4.13 (a) shows the electron density distribution in the chamber. Whereas Figs. 4.13(b) and (c) show the O1s and O_2b1s radical density distribution, respectively. From Fig. 4.13, it is observed that these distributions are uniform throughout the substrate. Hence, material removal is expected to be uniform during plasma polishing. Fig. 4.13 (d) shows the distribution of electron temperature during machining. It reveals that the temperature near substrate is 0.05 eV (550K) confirming cold plasma machining.

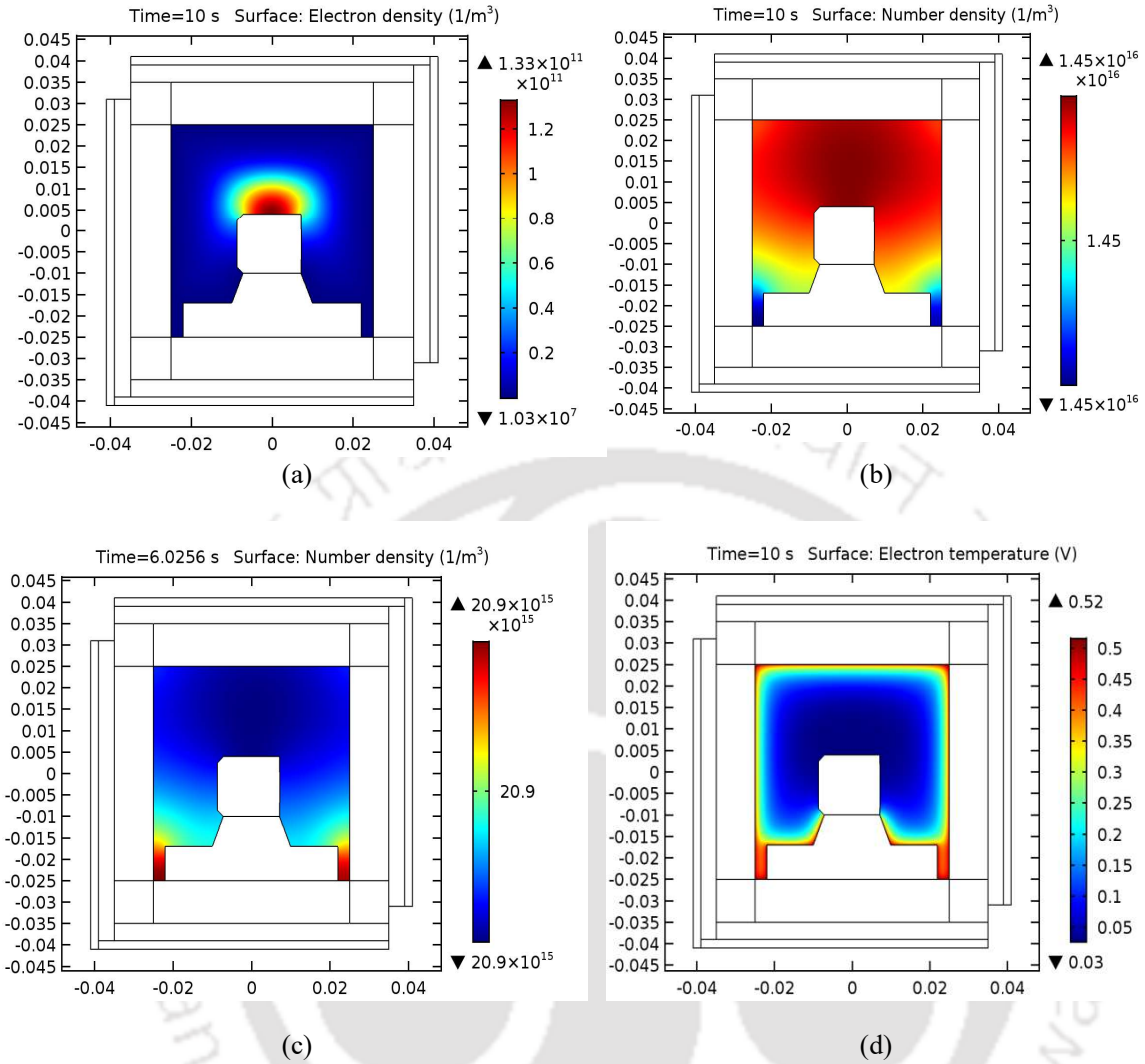

Fig. 4.13 (a) Electron density, (b) O1s Density, (c) O_2b1s density and (d) Electron temperature

4.5 Validation of simulation results

In the present study, the results obtained from Comsol® simulation is validated based on experimental spectroscopic measurement data of electron temperature for simulation of HRG shell using L shaped electrodes. In Fig. 4.14, the electron temperature in terms of electron volt (eV) is plotted for (a) top and bottom and (b) L shaped electrodes. One eV is equivalent to 11000 K. The electron temperature is obtained in two different positions inside plasma chamber. Position A is close to the shell and position B is close to the plasma chamber wall. The temperature observed at positions A and B from Comsol® simulation are shown in Table 4.2. To validate Comsol® model experimentally, optical emission spectroscopic (OES) method is adopted. According to atomic emission theory, the temperature of the plasma can be evaluated by spectral line ratio method (Zhu et al., 2009).

Also, optical emission spectroscopic method is convenient, inexpensive and non-intrusive. In the present study, the line ratio method of OES technique is adopted where emission line's intensity ratio is related to the temperature of the electron by a method called as collisional-radiative model (CRM) (Zhu et al., 2007). This method is generally used for medium and low pressure plasma (Kano et al., 2000 and Crinteal et al., 2009). The measured temperature obtained from the optical emission spectroscopy (OES) is a mean temperature of positions A and B since the data collected through spectroscopic probe from outside plasma chamber. The electron temperature is calculated as (Zhu et al., 2007)

$$T = \frac{(E_1 - E_2) \times \left(1/k\right)}{\ln\left(\frac{I_1}{I_2}\right) - \ln\left(A_1 g_1 \frac{\lambda_2}{A_2 g_2 \lambda_1}\right)} \tag{4.1}$$

where, A= Einstein's coefficient of respective transition, E= energy of transition, g= degeneracy of state, I= intensity of transition, λ= wave length. The value of the Boltzmann's constant (K) is equal to 1.38×10^{-23} J/K. The wave lengths considered here are λ_1=706.52 nm and λ_2=667.82 nm. The mean plasma electron temperature calculated from Eq. (4.1) is 1230K.

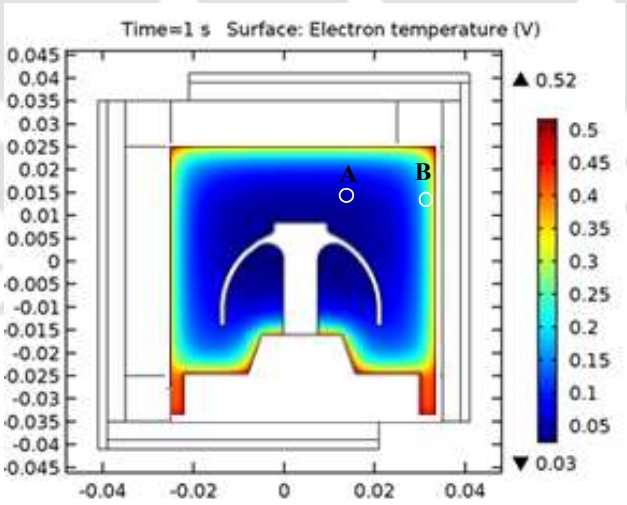

Fig. 4.14 Electron temperature distribution of hemispherical shell

Table 4.2 Measured plasma temperature from simulation and optical emission spectroscopy

Plasma temperature	**Simulation study**			**Spectroscopic method**
	Position A	Position B	Avg. Temp.	
	550 K	2200 K	1375 K	1230 K

Table 4.2 shows the comparison between electron temperature by both the methods. The average electron temperature of positions A and B obtained from Comsol® model (1350K) matches with the OES result (1230 K). It is to be noted that the position A during plasma processing represent shell interface electron temperature. This temperature calculated by Comsol® simulation is approximately 550 K. Hence, it can be considered as a 'cold plasma' process.

4.6 Summary

Finite element simulation of the plasma process is carried out using Comsol® to analyse the distribution of the radicals inside the plasma chamber with and without specimens and for the ratio of free volume to be total available volume of the chamber for uniform distribution of radicals. The ratio of processing gas and reactive gas is identified for optimum distribution of radicals. In the presence of hemispherical shell as well as prism, the four sided electrode provides higher density of radicals. The experimental set up is designed and built based on preliminary inputs from Comsol® analysis and four sided electrodes are used for shell processing. The simulation results are validated with experimentally measured electron temperature data using optical spectroscopy and analytical model. The average temperature calculated from simulation study is approximately 550 K which can be considered as 'cold plasma' process.

Chapter 5

PLASMA PROCESSING OF HEMISPHERICAL SHELL

5.1 Introduction
5.2 Preliminary experiments
5.2.1 Process optimization to improve MRR
5.3 Study of uniform plasma processing of hemispherical shell
5.4 Analysis of surface strain by Raman spectrometer
5.5 Summary

5.1 Introduction

The ultra-smooth-surface finish with negligible surface or sub-surface defect (SSD) is essential in inertial sensors which are state of the art in nature. It directly impacts sensor's performance. Mostly these inertial sensors are having complex freeform surfaces which are fabricated using fused silica. Conventionally these fused silica structures are manufactured through brittle machining using diamond coated tool in an ultrasonic milling machine followed by wet etching to remove surface cracks and SSD and further fine finishing. The chemical wet etching process significantly deteriorates surface finish as well as surface topography. To improve the surface topography, traditional ultraprecision grinding and lapping techniques are conceived. In order to attain surface finish in the nanometer level, conventional polishing techniques like magnetorheological polishing and chemo-mechanical polishing (CMP) methods are generally used. The contact finishing methods fail to be deterministic resulting in poor yield and thus high cost and effort. Therefore, in the present study, an alternative finishing technique to polish brittle components like glass is adopted. This method is aimed to remove material in the atomic scale from the surface of the component.

The hemispherical resonator shell as shown in Fig. 5.1, made of fused silica, is required to be polished in the nanometer level without imparting molecular level strains at the surface as well as sub-surface. The hemispherical shell mentioned above, in contrast to its name, the component has multiple surface profiles like cylindrical and tangential filleting apart from hemispherical shape all merged flawlessly. In other wards the shape is not defined by a single standard equation. In optical polishing methods when the surface of a component is not polishable with a form tool profile then such surfaces are called freeform. For this particular component, if hemispherical tool is used in conventional contact polishing methods, it fouls at location A and B for exterior polishing tool and fouls at C and D for interior polishing tool

(Fig. 5.1). Mechanical form tool comprising all the profiles does not work due to the demand of highly geometrical tolerances like concentricity and sphericity of about 2 µm as shown in Fig. 5.1. Therefore, the conventional contact type chemomechanical polishing methods fail to achieve required surface finish without degrading the surface geometry. Hence, the objective of the present chapter is to build up a finishing methodology for enhancing surface integrity of the freeform / complex surface without degrading the surface profile and form accuracy. Also, surface finishing of the hemispherical shell should be within sub-nanometer range without any subsurface damages. The hemispherical shell is fabricated by 5 axes ultrasonic milling machine. Due to the brittle nature of the fused silica, cracks are generated on the specimen during ultrasonic milling operation. Also, because of ploughing action during milling operation, surface and subsurface cracks are formed. Generally, the typical process followed to remove such defects is wet chemical etching. It effectively removes the surface strains, surface cracks and opens up / removes sub-surface damages. However, this process damages the surface profiles and degrades the surface finish. Conventional grinding and lapping processes can be adopted on planar surfaces to achieve nanometer level surface finish. However, these process also introduce subsurface damages due to its contact nature of material removal (Suratwala et al., 2006; Dong et al., 2014; Xiao et al., 2018 and Lin et al., 2016). For components like hemispherical shell having complex surface, the conventional CMP process cannot be adopted. However, these process also introduce subsurface damages due to its contact nature of material removal. Therefore, there is a need to develop a polishing process which replaces the role of wet chemical etching and CMP on components having freeform / complex surfaces like in hemispherical shell.

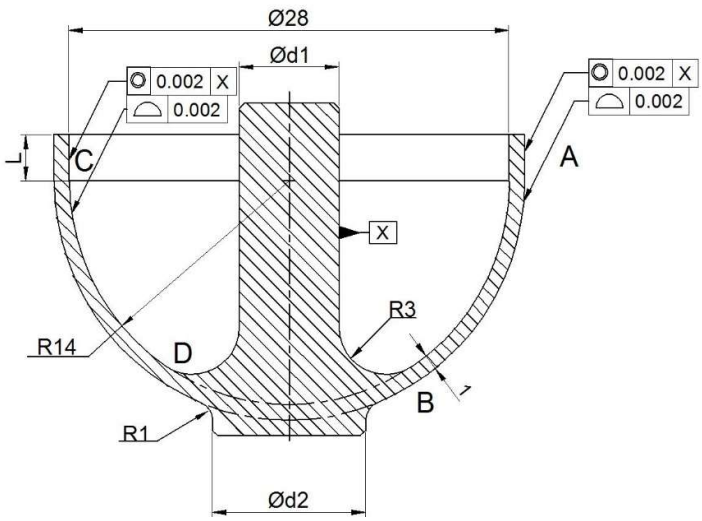

Fig. 5.1 Cross sectional view of a typical hemispherical shell (all dimensions are in mm)

The hemispherical shell shown in Figure 5.1 displays complex freeform surfaces which is to be polished uniformly in sub-nanometer range. Also, the surface integrity level i.e. surface topography and geometrical tolerances are to be highly maintained during polishing. Traditional contact methods cannot be adopted for machining of high quality precession optics where molecular level strain results in the degradation of functional parameter such as quality factor (Q) of hemispherical shell. Hence, the demand for an advanced non-contact type polishing is gowning day by day. Among the non-contact polishing methods plasma based machining is proved to be an effective technique for sub-nanometer finishing of brittle optics, thanks to its chemical interaction with the silicon based substrates.

Zhang et al. (2013) developed atmospheric pressure plasma polishing system for finishing of high quality optics. This study proved that chemical interaction is higher for convex surfaces than concave surfaces. Hence, the surface finish gets improvement during plasma processing. They observed the improvement in average surface roughness (Ra) with processing time and found that average surface roughness (Ra) decreases from 4.5 nm to 0.9 nm in 100 s. Na et al. (2015) studied the atmospheric pressure plasma processing of fused silica by dielectric barrier discharge plasma torch with different modes of discharge. They compared the material removal rate with different gas compositions and flow rates. They showed that depth of material removal increases with increased ratio of O_2/CF_4. Wang (2013) developed capacity coupled plasma torch for chemical machining of fused silica without inducing surface/ sub surface damage. He studied the key influential parameters effecting the material removal rate and developed a mathematical model for plasma processing. Yu et al. (2016) investigated a high temperature plasma jet with De-Laval nozzle used for correcting surface figure. This study utilized computational fluid dynamics for optimizing the design of inductive coupled plasma torch (Yu et al., 2016). Deng et al. (2014) adopted a novel plasma-assisted polishing (PAP) technique which was combined with the irradiation of atmospheric pressure water vapour plasma and polishing using soft abrasives. By this method surface roughness is decreased from 4.410 nm p-v and 0.621 nm root mean square (rms) to 1.889 nm p-v and 0.280 nm rms without inducing any crystallographic defects on silicon carbide surfaces (Deng et al., 2014). Gerhard et al. (2014) did plasma polishing of various optical media with a dielectric-barrier discharge (DBD) plasma at atmospheric pressure. They utilized symmetric shaped atmospheric pressure plasma source for plasma processing. They achieved 20% improvement in surface roughness for fused silica sample. The material removal in their process is not due to chemical reaction rather due to ion bombardment and de-excitation of argon species (Gerhard et al., 2013). Yao et al. (2013) studied chemical machining of multi-phase Zerodur material by using atmospheric

pressure plasma jet. They studied the improvement in surface roughness of mechanically lapped zerodur surface. They suggested the role of oxygen to improve the surface finish. Wang et al. (2009) developed novel plasma polishing process and studied the influence of various operational parameters on material removal. They concluded that material removal rate depends mostly on the flow rate of O_2 and SF_6. Paetzelt et al. (2013) studied the surface finishing of finely ground fused silica using a microwave-powered APP jet source. They used a mixture of argon and helium gas as a processing gas at a microwave power of 135 W. They found significant improvement in Ra of 0.64 nm with a surface heating to 1900 K. Zhang et al. (2008) achieved sub-nanometer range smooth surfaces on silicon workpiece by atmospheric pressure plasma methodology with fluorine as a processing gas. Similarly, Arnold et al. (2010) observed an improvement in surface roughness in case of plasma jet machining of silicon carbide (SiC) component. These non-contact type advanced atmospheric pressure plasma processes have been fruitfully established to attain sub-nanometer surface finish with negligible surface damage. However, these processes utilize small aperture plasma source for machining. Hence, these processes are not applicable for bulk machining of freeform complex shaped optics. Liu et al. (2009) studied the plasma polishing at low-pressure process in the range of 10^{-2} to 0.5 mbar and it is accomplished in minimizing the subsurface defect on complex freeform surface (Liu et al., 2009).

Unlike existing studies, the present work is intended to establish surface finishing methodology in atomic scale by utilizing medium pressure plasma processing. The present novel method of medium pressure plasma process is competent enough to polish entire freeform 3D surface simultaneously without the need of expensive mechanization system. In this study, it is targeted to develop an atomistic finishing process combining the best of low pressure plasma processing capabilities and high pressure plasma polishing abilities such as fine polishing and isotropic material removal. The process novelty is that it is capable of polishing simultaneously entire complex 3D surfaces including cavities where no tool or beam can reach.

5.2 Preliminary experiments

The main objective of the present process is to uniformly polish a complex shaped hemispherical shell which is fabricated from fused silica. Initial experiments are carried out on a planner fused silica substrate prior to hemispherical shell machining to optimize plasma parameters. The previous study shows that material removal rate (MRR) is sufficiently low. Hence, further experiments are conducted to improve the MRR without degrading the surface

finish i.e to obtain maximum MRR. MRR in a cold plasma process depends on surface chemical reaction of substrate with reactive gases which is facilitated and sustained by the electron collision energy. Chemical reaction of plasma with substrate interface depends on composition of reactive gases such as SF_6 and O_2 and processing gas i.e. He. The electron and ion collision energy depends on total chamber pressure and excitation power. Therefore, the parameters which determine the MRR are mixture ratio of gases, total pressure of plasma medium and RF excitation power. The experiments are carried out on a specimen of fused silica for a duration of 10 mins and MRR is calculated based on the mass loss of the specimen after plasma processing. From previous studies (Section 3.2.2.3), it is observed that material removal rate of the fused silica specimen is maximum with SF_6 to O_2 ratio of 2 at a total pressure of 20 mbar and excitation power of 40 W.

Table 5.1 shows MRR of fused silica substrate at different excitation power and total pressure. It is observed that there is no significant change in MRR with increased excitation power from 40 to 70 W. Due to increased power, the heat dissipation is increased resulting in increased rate of change in temperature inside plasma chamber. For a given plasma processing duration, the pressure inside the plasma chamber is increased due to this increased temperature. With increased pressure, electron collision energy decreases due to the reduction in mean free path which leads to insignificant change in MRR. With 20 mins experimental duration, there may be initial increase and further reduction in MRR which leads to no net change in MRR. Although there is an initial increase in MRR with power, it decreases later due to increase in pressure inside the plasma chamber which reduces MRR.

Table 5.1 MRR of fused silica substrate at different plasma excitation power and total pressure

Exp. No.	Composition (%)			Total Pressure (mbar)	Power (W)	MRR (mm^3/min)
	SF_6	O_2	He			
1	2.5	1.25	96.25	20	40	0.008
2	2.5	1.25	96.25	20	70	0.008
3	2.5	1.25	96.25	15	70	0.009

Hence, in subsequent experiment (Exp. No. 3, Table 5.1), total pressure of plasma chamber is reduced to achieve sustained and increased MRR at higher excitation power of 70 W. To our surprise, there is no distinct weight loss of the sample observed after plasma processing. However, the weight loss is observed after ultrasonic cleaning of the sample with deionised water, equivalent to an MRR of 0.009 mm^3/min which is also marginal. It suggests

that there is a deposition of certain polymers (O_2 or fluorine based polymers) on the substrate during plasma processing at higher power of 70 W and lower pressure of 15 mbar inhibiting further material removal. Due to that no improvement in MRR is observed. Hence, it is very clear that MRR cannot be increased for this particular chamber configuration by changing either total pressure or operating power. Therefore, for subsequent experiments, excitation power and total gas pressure are optimized as 40 W and 20 mbar, respectively for 20 mins cycle time.

Further experiments are conducted with multiple cycles at 40 W power and 20 mbar pressure. Each cycle consists of first filling of gases with required pressure and composition, next plasma processing for 20 mins duration, after that evacuation of gases from plasma chamber. Multiple experimental cycles are carried out with cumulative plasma processing time of 320 mins (i.e. 16 cycles) to achieve uniform thickness reduction of 1 μm from substrate surface with 0.008 mm^3/min MRR. The expected total material removal, at 0.008 mm^3/min MRR for 320 mins, is 2.56 mm^3. However, only about 1.63 mm^3 material is removed in 320 mins (i.e. 0.005 mm^3/min) which is 35% less than expected material removal. Hence, further experiments are conducted at regular time interval for a total duration of 120 mins and MRR is computed based on mass loss measured after removing the specimen from the plasma chamber.

Figure 5.2 shows that MRR is very low (0.004 mm^3/min) for initial 10 mins of plasma processing, after that it increases to a maximum value of 0.009 mm^3/min for 40 to 60 minutes and further decreases continuously. The initial low MRR is probably due to the presence of moisture at the specimen surface which hinders the plasma interaction with the specimen. The reduction in MRR beyond 60 mins is probably due to the deposition of certain polymers as stated earlier.

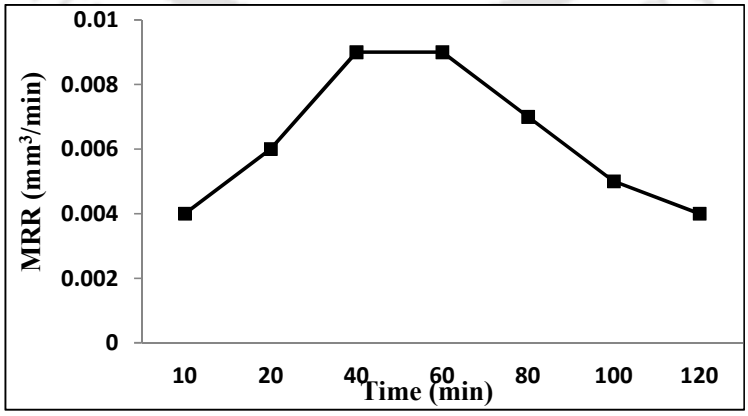

Fig. 5.2 MRR of the substrate at different time interval

5.2.1 Process optimization for improving MRR

In order to achieve a sustained MRR throughout the cumulative processing time, a pre and periodic post cleaning of the specimen surface are required without opening the chamber. Hence, various combinations of trial experiments i.e. processing sets are attempted by introducing plasma based surface cleaning as shown in Table 5.2. Plasma cleaning of the substrate is carried out at 6.5 mbar pressure with 92% He and 8% O_2 with different cleaning duration for individual processing set. Plasma processing is carried out at 40 W excitation power and 20 mbar total pressure with 96.25% He, 2.5% SF_6 and 1.25% O_2 for 10 mins processing cycle. Each cycle consists of filling of processing gases, plasma processing for 10 mins and evacuation of gases from the chamber. Each processing set consists of 20 mins cumulative plasma processing duration of the specimen. Each processing set consists of combinations of in-situ plasma cleaning and plasma processing.

Table 5.2 Different processing sets with different stages of plasma cleaning and plasma processing

Processing set	Description
1	Stage 1: Plasma cleaning for 6 minutes Stage 2: Plasma processing: Two cycles
2	Stage 1: Plasma cleaning for 12 minutes Stage 2: Plasma processing: Two cycles
3	Stage 1: Plasma cleaning for 16 minutes Stage 2: Plasma processing: Two cycles
4	Stage 1: Plasma cleaning for 10 minutes Stage 2: Plasma processing: Half cycle (5 mins) Stage 3: Plasma cleaning for 5 minutes Stage 4: Plasma processing for one cycle Stage 5: Plasma cleaning for 5 minutes Stage 6: Plasma Processing: Half cycle
5	Stage 1: 16 hours evacuation of plasma chamber Stage 2: Plasma cleaning for 10 minutes Stage 3: Plasma Processing for two cycles
6	Stage 1: Plasma cleaning for 10 minutes Stage 2: Plasma processing for two cycles

Figure 5.3 shows the MRR of the substrate for different processing sets. From Figure 5.3, it is observed that MRR is maximum for process set 4 i.e. about 5 times higher than the process set 1. With periodic conditioning after each machining, MRR can be increased about 300% (0.008 mm^3/min in earlier study to 0.026 mm^3/min in process set 4) as shown in Fig. 5.3.

Hence, it can be concluded that the conditioning of the substrate successfully removes the polymer deposition and helps in sustained material removal.

The maximum material removal is observed at processing set 4 (0.026 mm3/min). In processing set 4, multiple plasma cleaning is adopted in between shorter plasma processing time which effectively improved MRR. So, it is understood that with the optimized process parameters, higher MRR can be achieved by in-situ removal of polymer deposition formed during plasma processing for planar substrate of fused silica. Further, the optimized process parameters and processing set will be adopted for freeform polishing of hemispherical shell.

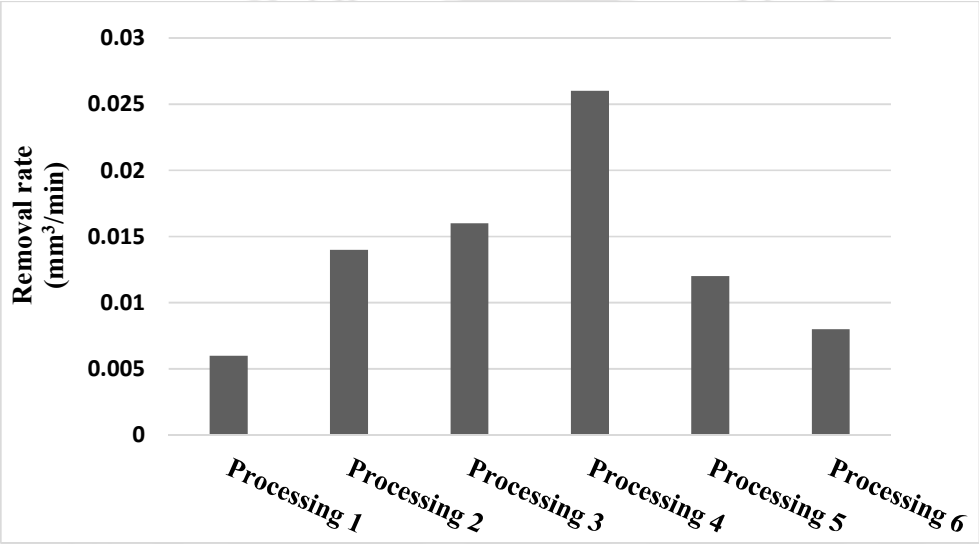

Fig. 5.3 MRR of the substrate at different processing sets

5.3 Study of uniform plasma processing of hemispherical shell

In the present study, the hemispherical shell (fabricated using ultrasonic milling operation) is plasma processed at optimized process parameters and processing set described in Section 5.2.1 to achieve uniform material removal from the entire surface. The shell has a characteristic of two identical natural frequencies of orthogonal mode shape as shown in Fig. 5.4. For an ideal perfect hemispherical shell, the frequency of modes is identical. Any non-uniformity such as surface irregularities and non-uniform mass / thickness distribution in the hemispherical profile of shell will result in frequency mismatch.

The thickness reduction due to plasma processing of shell is measured indirectly by measuring reduction in respective natural frequencies before and after plasma processing. The uniformity of material removal is monitored by analysing frequency mismatch between two orthogonal modes with the help of Laser Doppler Vibrometer (LDV). The shell surface quality

and surface integrity can be attributed through the quality factor (Q) which is calculated before and after plasma processing. The Q factor is defined as

$$Q = \Delta f / f \qquad (5.1)$$

where f is natural frequency and Δf is frequency difference at half power point. For as machined hemispherical shell, the two orthogonal modes of frequency are 6766.870 Hz and 6767.407 Hz with a frequency mismatch of 537 mHz and the Q is calculated as 1.3×10^5 as shown in Fig. 5.5(a). The hemispherical shell is plasma processed for cumulative time duration of 380 mins with top and bottom electrode configuration with optimized process parameters and process set. Similarly, the plasma processed hemispherical shell is analysed using LDV and the two orthogonal modes of frequency are measured as 6764.099 Hz and 6764.697 Hz as shown in Fig 5.5(b). Hence, the frequency mismatch is obtained as 598 mHz and the Q is calculated as 3.5×10^5. The material removal along thickness direction based on measured weight reduction during plasma processing is equivalent to 500 nm having linear MRR of 1.31 nm/min assuming uniform thickness reduction. However, the frequency mismatch after plasma polishing is increased to 598 mHz from 537 mHz (as machined) which indicates that the material removal is not uniform due to anisotropic polishing. The improvement of Q factor from 1.3×10^5 (as machined) to 3.5×10^5 (plasma processed) clearly suggests that the damaged surface layers are being removed and the surface integrity improves after plasma processing.

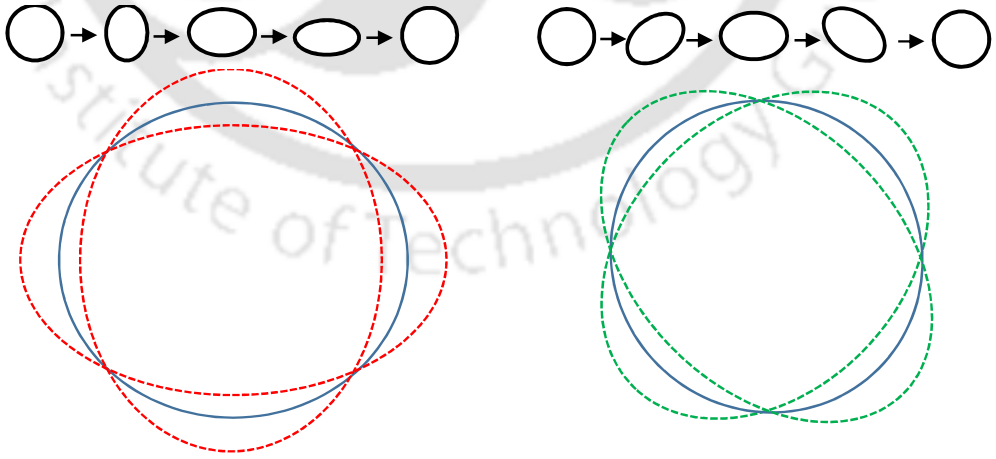

(a) (b)

Fig. 5.4 Vibration modes of hemispherical shell having two identical characteristics of natural frequencies in two mutually orthogonal mode shapes (a) Mode 1 and (b) Mode 2

The uniformity of plasma machining for capacitive coupled RF discharge strongly depends on the discharge chamber configuration. Hence, for a particular chamber design, uniform plasma machining depends mostly on the electrode configurations. Based on Comsol® analysis parallel electrodes at top and bottom are replaced by a pair L shaped electrodes for plasma processing of hemispherical shell as shown in Fig. 4.11(b). The hemispherical shell is further plasma processed for 760 mins. The reduction of wall thickness of hemispherical shell based on mass reduction is calculated as 2000 nm (with linear MRR of 2.63 nm/min). The linear MRR is increased by 100% using L shaped electrodes (Fig. 4.11(b)) as compared to top and bottom electrode configuration (Fig. 4.11(a)). This may be due to transverse firing of field resulting in energetic electrons with convergent fluxes in L shaped electrode configuration. This enhances the ionization rate as well as plasma density (Schmidt et al., 2013). Further plasma processed hemispherical shell is analysed using LDV and the two orthogonal modes of frequency are measured as 6750.83 Hz and 6751.32 Hz as shown in Fig. 5.6.

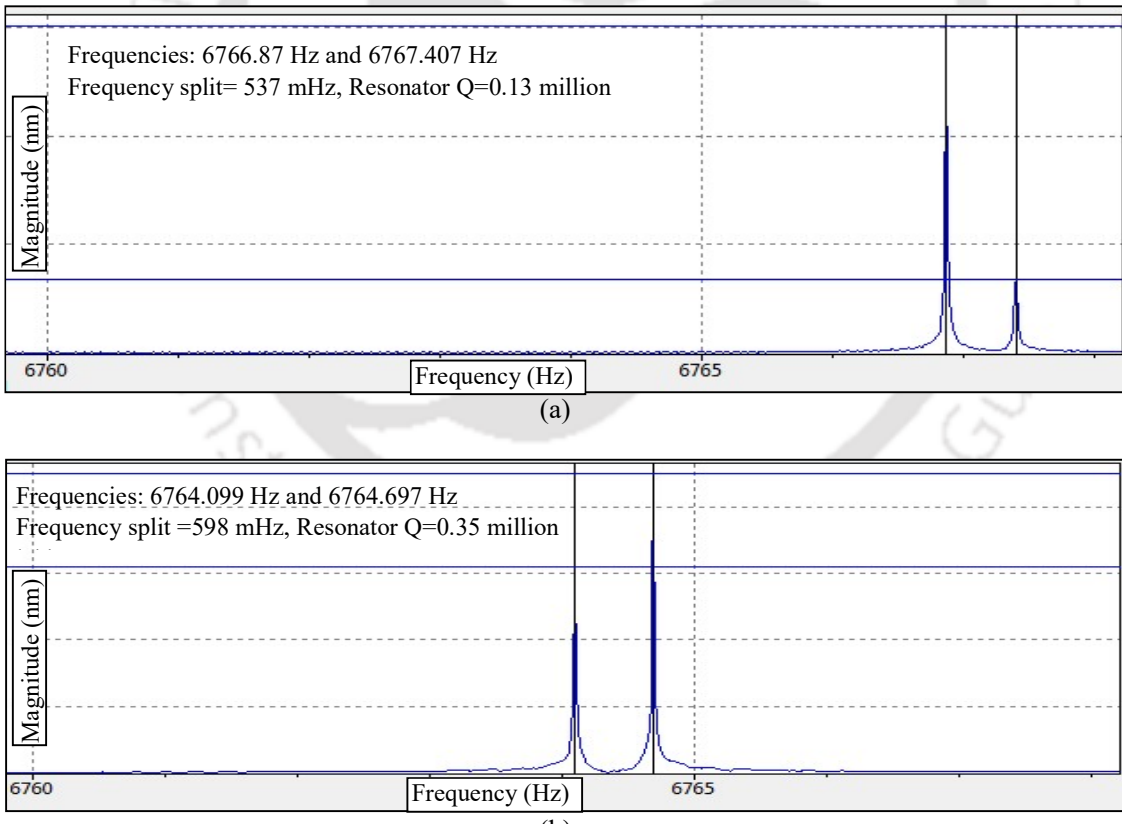

Fig. 5.5 Laser Doppler Vibrometer (LDV) frequency plots of hemispherical shell (a) before plasma processing (as machined) and (b) after plasma processing with top and bottom electrode configuration

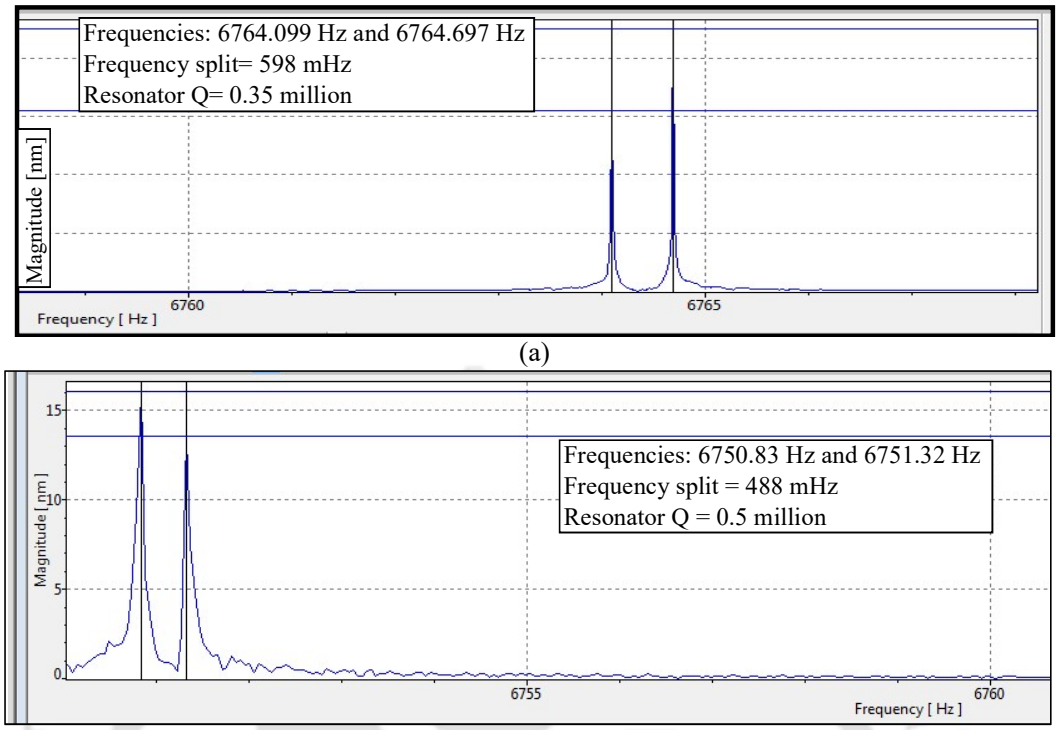

Fig. 5.6 Frequency plots (a) before and (b) after plasma processing with L shaped electrode configuration

Hence, the frequency mismatch is obtained as 488 mHz and the Q is calculated as 5×10^5. The frequency mismatch after plasma polishing is decreased significantly to 488 mHz from 598 mHz which indicates that material removal is uniform due to isotropic polishing. Also, the Q factor is improved to 5×10^5 in the present case from 3.5×10^5 in previously plasma processed hemispherical shell which shows the enhancement in surface integrity. The enhancement in surface integrity and improvement in Q are mostly due to the reduction in surface starin after plasma processing.

5.4 Analysis of surface strain by Raman spectrometer

The Raman spectrum is one of the efficient methods for understanding molecular network of fused silica (Chan et al., 2001). Hemispherical shell is analyzed using Raman spectroscopy before and after 2000 nm removal of hemispherical shell by plasma processing. The Raman spectrum of the shell is shown in Fig. 5.7. It shows that there is a significant improvement in Raman spectrum after plasma processing. The peak at about 440 cm^{-1} corresponds to Si-O-Si angle in the silica network and its width and area suggests the Si-O-Si angle distribution. Whereas, two characteristic bands centered at 495 cm^{-1} and 605 cm^{-1} are

formed due to in-phase breathing motion of oxygen atoms in puckered four- and planner three-member ring structures, respectively. These bands correlate the surface strain of the substrate generated due to machining.

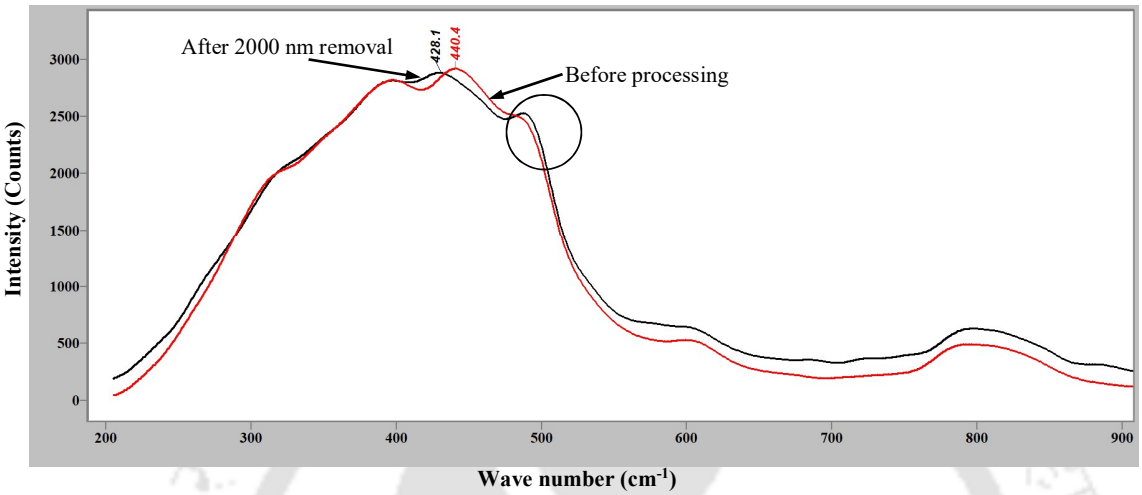

Fig. 5.7 Raman spectrum of hemispherical shell before and after processing

From Fig. 5.7, it is observed that there is a significant shift (about 12 cm^{-1}) in six-membered Si-O-Si linkage towards high energy suggesting decrease in damaged low energy bonds of the hemispherical shell after plasma processing. Similarly, there is a reduction in strained 4-membered ring as highlighted in Fig. 5.7 signifying reduction in structural defects.

Table 5.3 shows the area under Raman spectrum before and after plasma processing. It suggests that line intensity ratio of 6-membered ring to 4-membered ring increases about 200% (156 to 353) after plasma processing. It signifies the reduction in strain bonds and improvement in surface integrity. Hence, there is an enhancement of Q after plasma processing analyzed by LDV.

Table 5.3 Area under Raman peaks before and after processing

	440 cm^{-1}	**495 cm^{-1}**	**Ratio of 440/495**
Before processing	351993.7	2253.3	156
After processing	728120	2060	353

The hemispherical shell is processed for multiple sessions of plasma polishing cycles. It is machined for 48 hours with cumulative plasma processing cycles. The photograph of the hemispherical shell after plasma processing is shown in Fig. 5.8. The visual patches in the shell

are mainly generated because of ultrasonic machining for shaping the job. This concern will be addressed separately in the milling process which is beyond the scope of present work. The surface finish of the hemispherical shell is analyzed with Brooker's contour surface profilometer. The area surface roughness profiles before and after plasma processing are given in Figure 5.9 (a) and (b), respectively. The improvement in area surface roughness is observed as 22 nm (after plasma processing) from 37 nm (before processing). Hence, the primary objective to polish the hemispherical shell uniformly up to the nanometer level is achieved by plasma processing.

Fig. 5.8 hemispherical shell of fused silica after plasma polishing

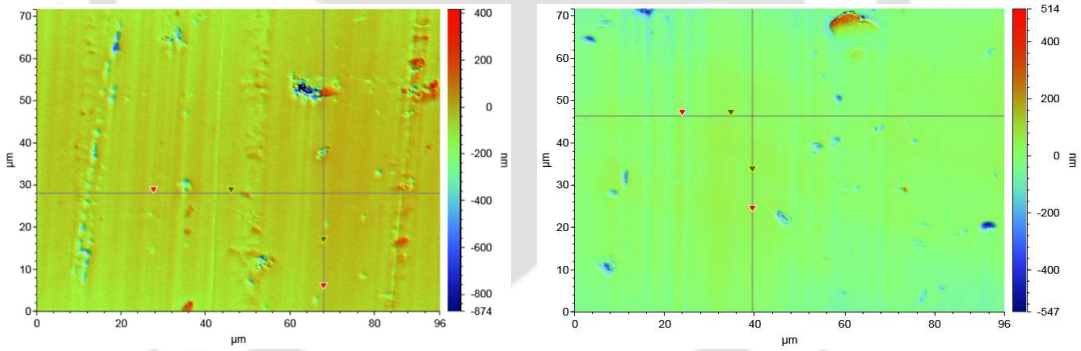

(a) (b)

Fig. 5.9 Area surface roughness plot of hemispherical shell (a) before (Ra=37 nm and Rq=53 nm) and (b) after (Ra=22 nm and Rq=33 nm) plasma processing

5.5 Summary

In this chapter, medium-pressure plasma polishing technique is adopted for uniform polishing of freeform hemispherical shell. The laser Doppler vibrometer method is successfully used for analysis of post plasma processing to verify uniform material removal over entire hemispherical shell by analysing frequency mismatch between two mutually orthogonal modes of frequency. Uniform and isotropic plasma machining is ascertained by 18% reduction in frequency mismatch between two orthogonal modes. About 300% improvement in material

removal rate is observed by optimizing process flow as well as electrode configuration. Significant improvement in Q factor of hemispherical shell is achieved which suggests the enhancement of surface integrity and the reduction of surface and sub-surface defects. Raman spectroscopy analysis provides clear evidence of reduction in strain bonds after plasma processing.

Chapter 6

PLASMA PROCESSING OF TOTAL REFLECTING PRISMS

6.1 Introduction
6.2 Experimental design
6.3 Surface inspection methodology
6.4 Surface characterization
6.5 Characterization of chemical Network
6.6 Results and discussion
6.7 Summary

6.1 Introduction

The geometrical precision, surface finish and surface integrity requirements of optical elements used in navigation grade inertial sensors such as Gyros and Accelerometers is extremely demanding. Surface integrity of this optics has direct impact on the performance and life of these sensors. The ISRO Ring Laser Gyro uses Total Internal Reflecting (TIR) prisms as corner reflectors. The surface integrity in terms of the chemical network on surface vis-a-vis the bulk of these prisms plays a crucial and decisive role in the performance of these Gyros. The TIR prisms are manufactured from 3D homogenous fused silica material shown in Fig. 6.1. Apart from high precision angles and dimensions requirement, the surface finish requirement is very fine and is of the order of less than 5 Å. The surface finish requirement is better than 5 Å on all surfaces with 'zero' surface cosmetic defects and detectable subsurface defects at selective locations. In order to meet the above requirements, customised chemo-mechanical polishing (CMP) methods are developed and surface finish of 2-3 Å is achieved consistently. White light inspection, for zero surface cosmetic defects, typically provides a yield of 85% from every batch. However, when these prisms are inspected by Laser light for surface and sub-surface damage, the yield drops to 5-15% due to detection of subsurface damages highlighted by laser light scattering indicating non-deterministic process. Even some of the screened prisms on exposure to low flounce He-Ne laser and/or spontaneous emission from He-Ne plasma continuously for longer periods (more than 5000 hours), the transmissibility degrades. Around 50% reduction in output power of the gyro devise is observed with time. This degradation is attributed to undetected chemical network disruption, subsurface damage and cracks not visible easily (Li et al., 2011 and Wang et al., 2011). On continuous exposure to these surfaces to low flounce laser and He-Ne plasma, they suffer

from reduction in transmissibility and output power due to colour centre formation and associated change in refractive index at the surface. Fused silica optical surfaces degrade due to the presence of chemical imperfection which occurs during fabrication/generated because of environmental effect (Demos et al., 2000 and Shen et al., 2005).

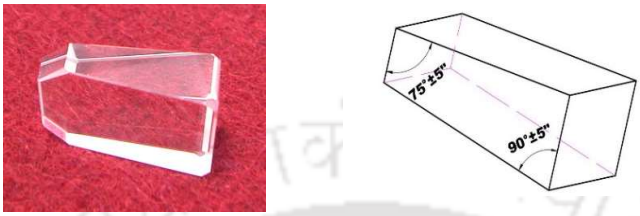

(a) (b)

Fig. 6.1 (a) Photograph and (b) line diagram of TIR prism

To understand and appreciate the challenges in nanofinishing of these prisms, it is essential to understand the chemistry of brittle damage, surface/sub-surface cracks generation and plastic deformation, that can occur on the surface of hard brittle materials (glass ceramics, fused silica etc.) when the surfaces are precision ground, lapped and polished. The typical defects on fused silica specimen is depicted in Fig. 6.2.

With the level of technology maturing in manufacture of 3D homogenous fused silica (SiO_2), the extrinsic defects are almost absent. However, the intrinsic defects or network imperfections on the surface and subsurface caused by the machining / polishing are still challenging. Subsurface defects of optical materials generated in contact machining processes are poised of micro-cracks, ultra-fine scratches, residual stresses and so on. Therefore, the subsurface damaged layer is different in chemical network composition from other regions and stress state (Hamza et al., 2002). Subsurface damage (SSD) i.e. subsurface micro cracks, affects transmission performance, laser-induced damage threshold and operational life of optical elements (Hamza et al., 2002 and Genin et al., 2001). SSD can reduce laser damage threshold, increase mechanical weakness and enhance absorption due to trapped material in the cracks, and then induce macroscopic damage to optics (Li et al., 2010 and Menapacea et al., 2002). In order to avoid degradation of the final quality of optical substrates, SSD must be minimized or eliminated by optimization of finishing processes.

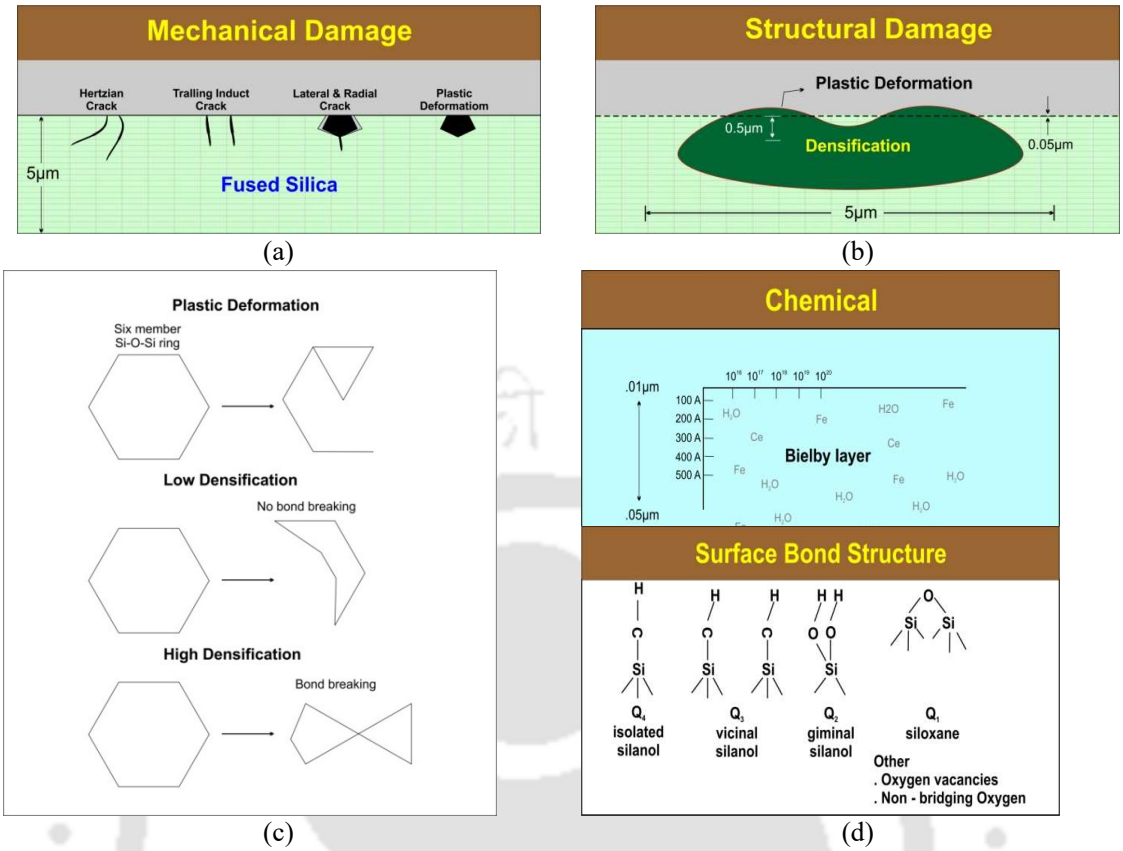

Fig. 6.2 Typical (a) mechanical, (b & c) structural and (d) chemical defects on fused silica specimen

If the amount of material removal is controlled and reduced to a certain level, as seen in CMP processes, only ductile damages (plastic deformation, densification) or surface hardening remain (Yoshiyama et al., 1998). Apart from these defects there are numerous mechanical, chemical and structural effects which cause atomic level surface and subsurface degradation.

The manufacturing process of optical surface has been developed significantly to improve lifetime of fused silica optics. Smooth surfaces can be realized by the magnetorheological finishing (MRF) process, but this process will introduce Fe contaminants on the surface, which has a detrimental impact on the Laser Induced damage threshold (LIDT) (Suratwala et al., 2011). Hydrofluoric (HF) acid etching is proved to be one of the effective traditional post processing methods for improving optical damage threshold (Zhi et al., 2012 and Liu et al., 2014). However, etching causes re-deposition and surface roughness deterioration for precision optics (Li et al., 2017; Peng et al., 2014 and Xu et al., 2018).

Above studies clearly suggest that high quality optics with the required surface finish and defect free surface chemical bond structure, cannot be achieved with reasonable

yield, by the contact polishing processes. If the material removal amount can be further reduced with a non-contact polishing method and controlled at the molecular or atomic level, both structural and chemical damage free surface and subsurface can be achieved. Ion beam sputtering can realize smooth surface by inducing low damage and little stress on the substrate without re-deposition of contamination layers (Xu et al., 2016; Kamimura et al., 2003 and Negres et al., 2007). However, this process is not deterministic to eliminate the damages completely.

The motivation behind the present work is to develop a non-contact polishing process (a) to enhance the yield in laser light inspection by removing the damaged surface layer while maintaining the surface finish achieved, (b) improving the life time of prisms under continuous exposure to low flounce laser or plasma radiation by restoring the virgin chemical bond structure of fused silica on the surface and subsurface. Therefore, a non-contact atomistic manufacturing technique is developed as a finishing process.

The types of defects and the damage mechanics of fused silica irradiated with different wavelengths of UV, deep UV and low flounce laser have been well studied (Burakov et al., 2007; Wang et al., 2006; Gerhard et al., 2013 and Dev et al., 2016). Coupling cracks with densified material creates still lower threshold material. If CMP processes only covers and fills in the region, lower threshold materials may still remain. Only in a contact polishing process like CMP re-deposition or re-adhesion at crack tip results in very fine surface finish but the chemical structure level defects remain. For fine CMP processed surfaces having surface roughness of 5Å, the depth of defects is predicted by Yao et al. (2010) of the order of less than 60 nm. Therefore, if a non-contact process can remove uniformly a fine layer of material, most of the subsurface defects can be removed.

6.2 Experimental design

The TIR prisms are selected from two different batches which have undergone two independent customized CMP processes. Specimen A is from pad based CMP and specimen B is from pitch based CMP methods. Both the specimens passed through white light inspection. However, laser light inspection revealed scatter indicating atomic level defects.

6.3 Surface inspection methodology

Generally, many non-destructive methods are evolved to analyse the surface cracks or foreign particle inclusion by using scattered light (Sakata et al., 2014). However, micro

cracks buried under surface cannot be detected. A novel stress induced light scattering method is developed to detect the micro cracks of 60 microns in size (Sakata et al., 2017; Xu et al., 2008 and Galeener et al., 1983). Crack size diminishes for the ultra-fine surfaces. Therefore, this method cannot be used for the sub-micron cracks. In this study, a novel laser light scattering method is adopted using 632.8 nm wavelength Laser. This method consists of square shaped optical jig having three TIR prisms placed at the three corners of the square enclosed by He–Ne plasma source, laser will generate while placing the inspected prism at the fourth corner. The generated 633 nm laser passes through the prism and highlights the scatter site greater than the wavelength. It is to highlight inclusions and cracks of submicron size.

The surface roughness (Ra) of specimen A is 0.25 nm and specimen B is 0.162 nm. The prisms are plasma processed as per the optimized recipe for specified time period to remove around 60 nm material uniformly which is deduced from the weight of the material.

6.4 Surface characterization

The target surface is characterised with Taylor–Hobson Talysurf surface profiler. The surface profile is analysed with extracting the profile, Ra values and the Power Spectral Density (PSD) of the profile. The utility of PSD is that it contains statistical information that is unbiased by the particular scan size and pixel resolution chosen by the operator. The PSD of a surface is a mathematical tool that decomposes a surface into contributions from different spatial wavelengths or spatial frequencies (Duparre et al., 2002). Mathematically, PSD is the Fourier transform of the autocorrelation function of the signal, which contains just the power (height/depth) across a range of wave vectors. This allows identification of the spatial wave lengths that are present in the signal. Higher spatial wave lengths represent shape or optical figure (deviation of the surface from a desired shape). Lower spatial wave lengths represent the roughness of the surface. For most isotropic surface, the PSD increases from low to high spatial wave lengths. The manner in which depends on the process by which the surface is made.

6.5 Characterization of chemical network

Raman spectroscopy is one of the efficient methods for characterizing the structural modification in fused silica. Broad bands are observed in Raman spectroscopy reflects the coupled vibration modes of the fused silica network (Xu et al., 2008). Characteristic Raman

peak centred at 440 cm^{-1} is related to the Si-O-Si angle in the silica network and its width and area suggests the Si-O-Si angle distribution (Galeener et al., 1983). The SiO_2 network is ideally 6-member structure as shown in Fig. 6.3(b). However, the generation of 4-member and 3-member structures on fused silica surface is very common due to mechanical strains developed during contact polishing. Two characteristic bands centred at 495 cm^{-1} and 605 cm^{-1} are formed due to in-phase breathing motion of oxygen atoms in puckered four- and planner three-member ring structures as shown in Figs. 6.3 (c) and (d), respectively (Galeener and Geissberger, 1983). Intensity and area under these bands reflect the disruption of the tetrahedron Si-O network and densification of the fused silica material (Liu et al., 1997). With increased number of these rings results in a decrease in overall bond angle and increased density.

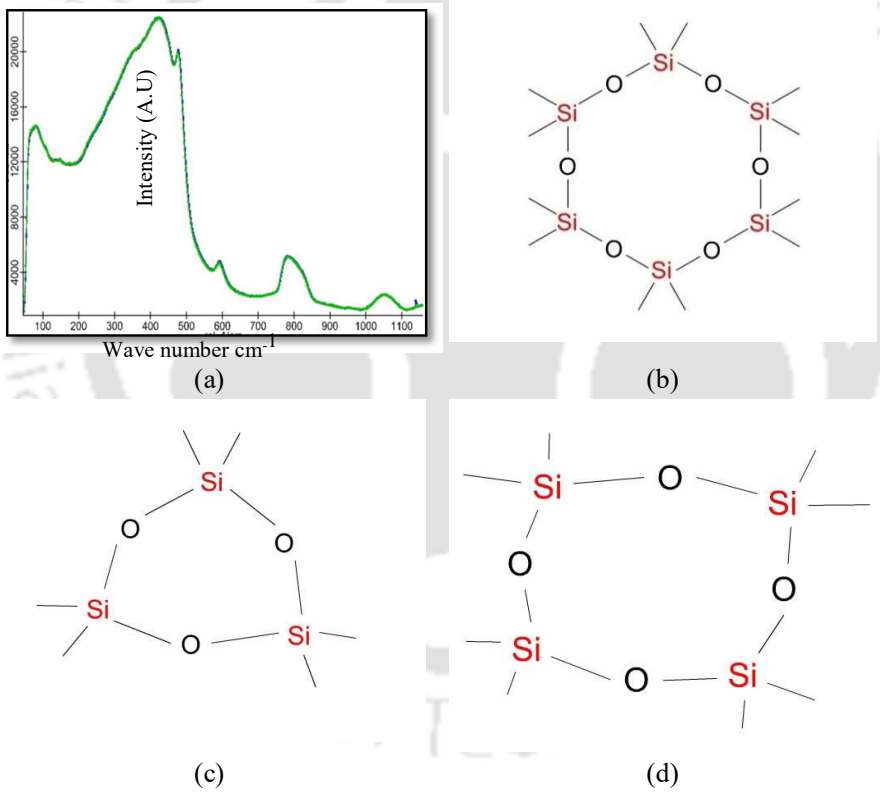

Fig. 6.3 Typical Raman Spectrum of fused silica, (b) six membered peak at 440 cm^{-1}, (c) three membered ring at 605 cm^{-1} and (d) 4-membered ring at 490 cm^{-1}

Intensity and area under these bands reflects disruption of the tetrahedron Si-O network and densification of the fused silica material (Schenkerand et al., 1997). An increase in the number of these rings results in a decrease in overall bond angle and increase in density. To quantify the results, the area under the 440 cm^{-1} peak with respect to area under the 605 cm^{-1} peak is plotted. The 605 cm^{-1} peak is more suitable for quantitative analysis than

the 490 cm^{-1} peak, since the later peak strongly overlaps with the main 440 cm^{-1} peak. Area under the respective peaks have been calculated by using Gaussian fit as shown in the following section for different prisms before and after plasma processing. The optimum iteration is done to minimize the error residue.

6.6 Results and discussion

TIR optics after plasma polishing is analysed by EDX for quantifying contaminations during plasma processing. Figures 6.4(a) and (b) show that EDX image and elemental concentration of TIR optics after plasma processing. Absence of fluorine and sulphur contamination on the optics suggests that there is no contamination developed on the optics after plasma processing. However, negligible amount of carbon found on the optics, may be due to the presence of cleaning solvent traces on the substrate.

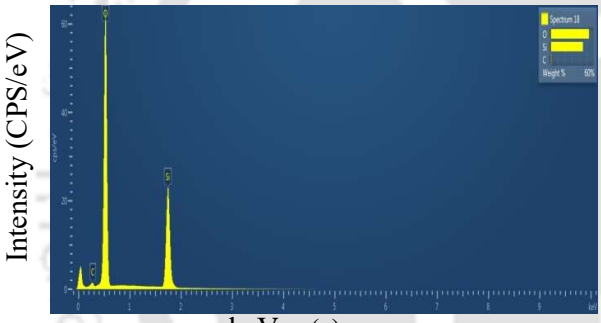

(a)

Element	Wt%	Standard deviation
C	1.0	0.09
O	53.70	0.17
Si	45.30	0.17

(b)

Fig. 6.4 (a) EDX image of TIR optics and (b) elemental concentration of contamination

The 605 cm^{-1} peak is more suitable for quantitative analysis than the 490 cm^{-1} peak. Since the latter peak strongly overlaps with the main 440 cm^{-1} peak. Area under the respective peaks has been calculated by using Gaussian fit as shown in Figs. 6.5, 6.6, 6.7 and 6.8 for optics A and B before and after plasma processing. To quantify the results, the area under 440 cm^{-1} peak with respect to the area under the 603 cm^{-1} peak are plotted in Figs. 6.5 and 6.6, respectively for specimen A and in Figs. 6.7 and 6.8, respectively for specimen B. Figures 6.5 and 6.6 show the Raman spectrum of optics A at peaks (a) 440 cm^{-1} and (b) 603 cm^{-1} before and after plasma polishing, respectively. Similarly, Figs. 6.7 and 6.8 show the Raman spectrum of optics B at peaks (a) 440 cm^{-1} and (b) 603 cm^{-1} before and after plasma polishing, respectively. Table 6.1 shows the area and ratio of Raman spectrum peaks before and after plasma processing for both optics A and B. It shows that ratio improves from 81 to 111 and from 80 to 110 for pre to post plasma processing of optics A and B, respectively

which indicates the reduction in 3-member chain. Therefore, the reduction in 3-member structure suggests removal of damaged and strained layers from the optics.

Table 6.1 Area and ratio of Raman spectroscopy peaks before and after plasma processing

Optics	Before plasma processing			After plasma processing		
	Area under 440 cm^{-1}	Area under 603 cm^{-1}	Ratio	Area under 440 cm^{-1}	Area under 603 cm^{-1}	Ratio
A	61493	754.7	81	57683	517	111
B	61300	813	75	65178	652	100

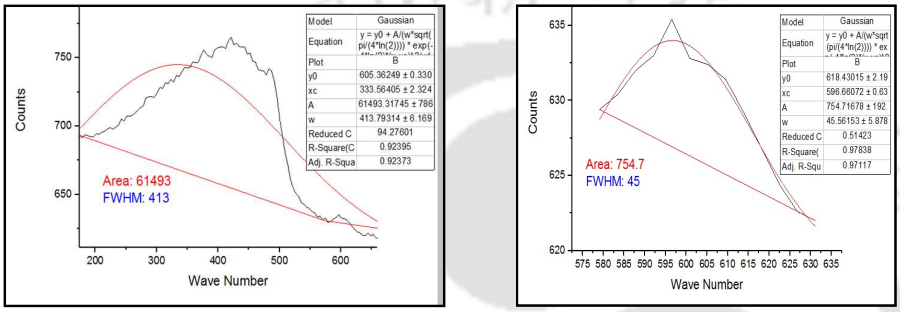

(a) (b)

Fig. 6.5 Raman spectroscopy of optics A before plasma polishing at peak (a) 440 cm^{-1} and (b) 603cm^{-1}

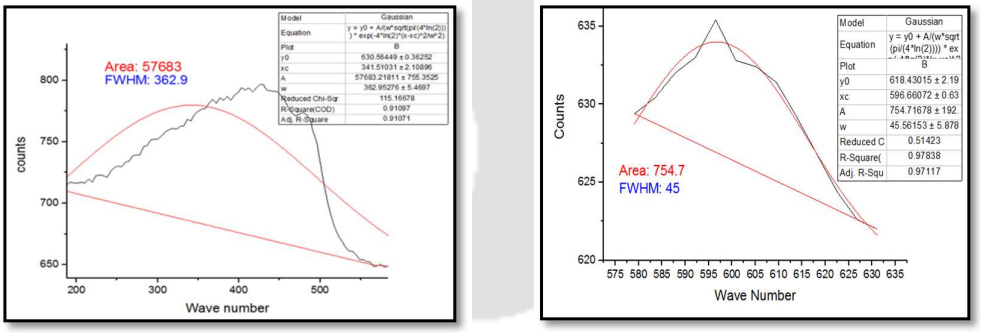

(a) (b)

Fig. 6.6 Raman spectroscopy of optics A after plasma polishing at peak (a) 440 cm^{-1} and (b) 603cm^{-1}

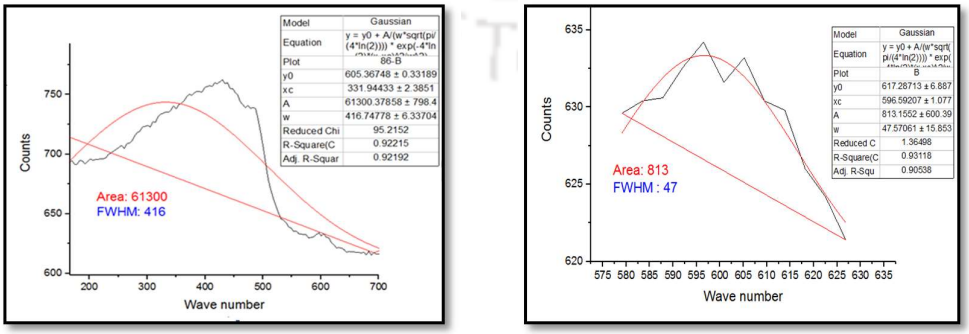

(a) (b)

Fig. 6.7 Raman spectroscopy of optics B before plasma polishing at peak (a) 440 cm^{-1} and (b) 603cm^{-1}

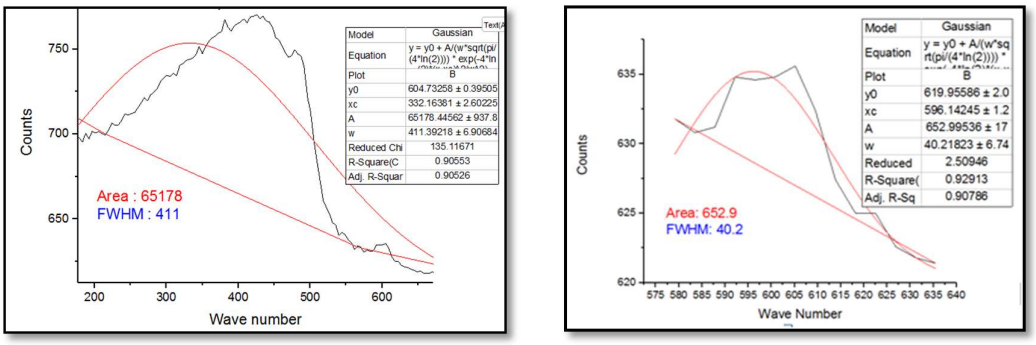

(a) (b)

Fig. 6.8 Raman spectroscopy of optics B after plasma polishing at peak (a) 440 cm^{-1} and (b) 603 cm^{-1}

Figures 6.9 and 6.10 show the (a) PSD and (b) area surface roughness profiles of Optics A. The surface finish marginally degrades from 0.25 nm to 0.33 nm after plasma polishing but still within the requirement of 0.5 nm. However, the PSD at higher wavelengths is reduced to 0.3 nm^2 after plasma polishing from 1.6 nm^2 clearly indicates the improvement in surface figure. Figures 6.11 and 6.12 show the surface profiles of Optics B before and after plasma polishing, respectively. The surface finish marginally degrades from 0.16 to 0.37 nm, but still less than 0.5 nm requirement. Also, for specimen B, the PSD at higher wavelengths is reduced to 0.25 nm^2 after plasma polishing from 1.5 nm^2.

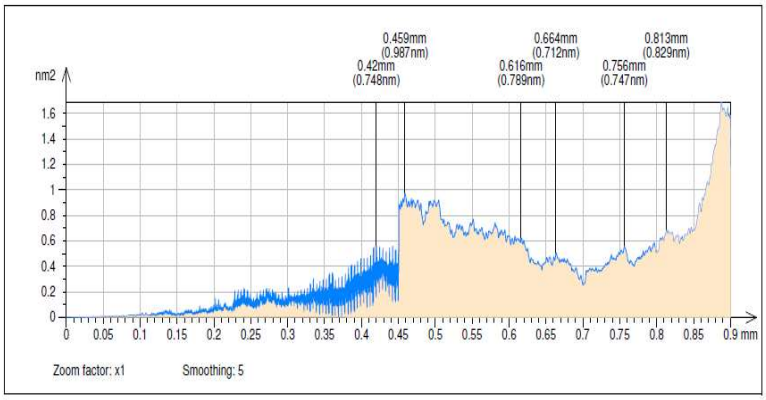

(a)

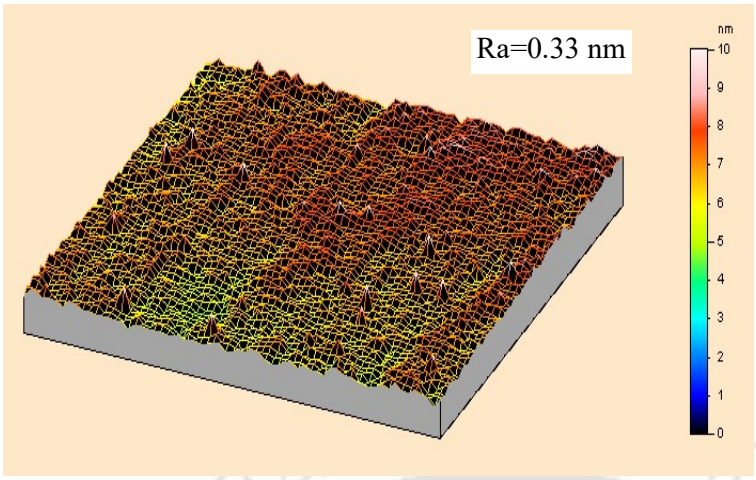

(b)

Fig. 6.9 (a) PSD of surface profile and (b) area surface roughness profile of CMP finished Optics A before plasma polishing

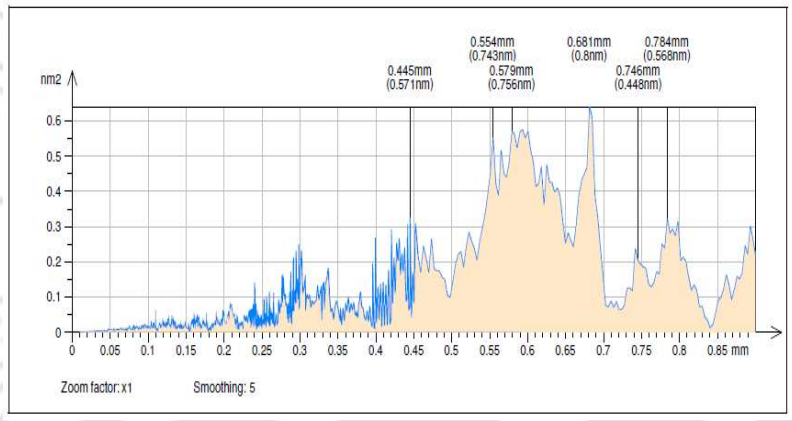

(a)

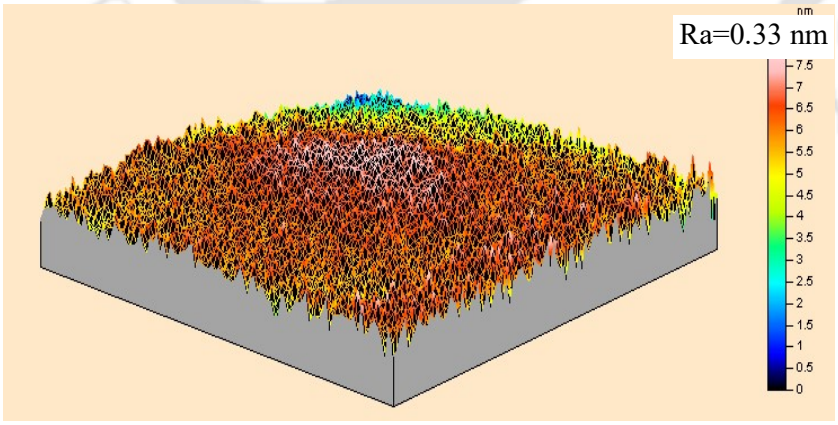

(b)

Fig. 6.10 (a) PSD of surface profile and (b) area surface roughness profile of CMP finished Optics A after plasma polishing

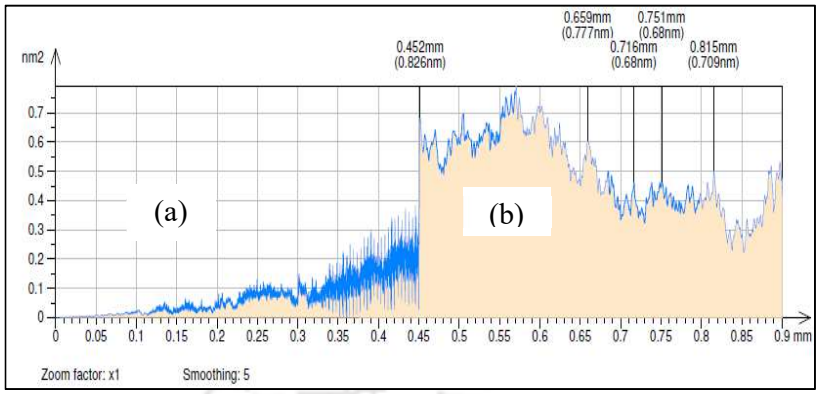

(a)

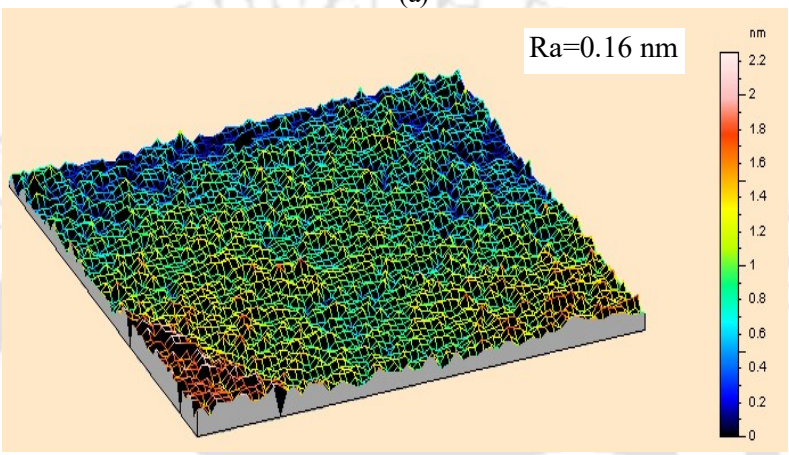

(b)

Fig. 6.11 (a) PSD of surface profile and (b) area surface roughness profile of CMP finished Optics B before plasma polishing

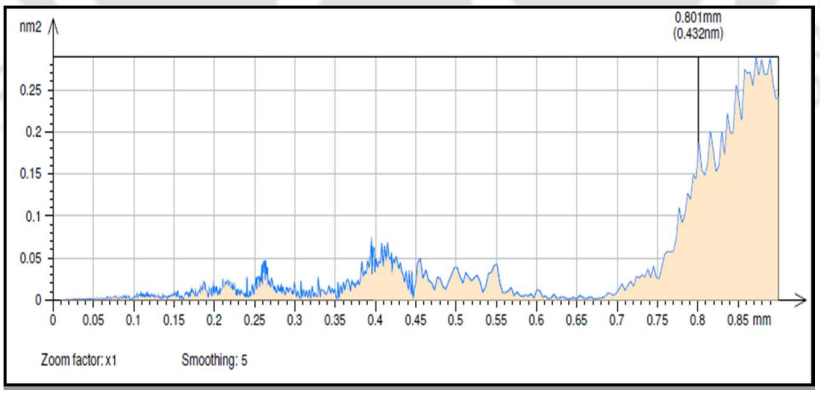

(a)

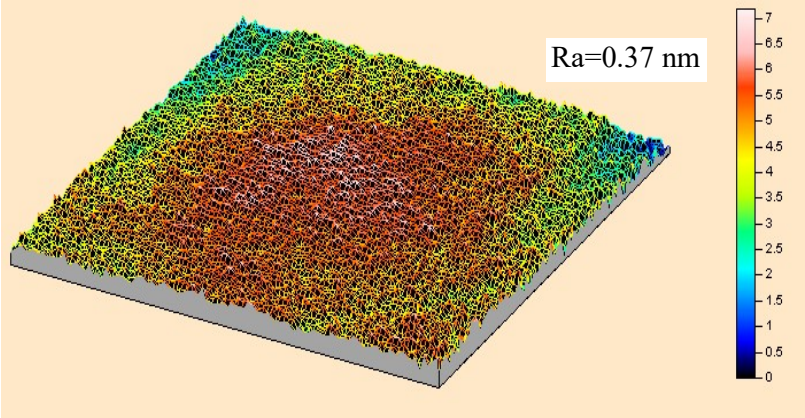

(b)

Fig. 6.12 (a) PSD of surface profile and (b) area surface roughness profile of CMP finished Optics B after plasma processing

Figure 6.13(a) shows the laser light inspection set up and zoomed view of Optics A (Figs. 6.13(b) and (c)). Laser light inspection has revealed that the plasma polishing has removed the defects totally for specimen A (Fig. 6.13(c)). However, for specimen B (Fig. 6.14(b)), similar inspection indicates reduction with one defect remaining with lesser severity. The results clearly indicate that the defective surface is being removed by fine plasma polishing which improves surface integrity.

Figure 6.15 shows the reflected output power from gyro device assembled with TIR optics before and after plasma processing. The output reflected power of the device is a function of gyro output power. Significant decrease in reflected power is observed for the device realized with TIR optics which is not plasma processed having laser illuminated defects. The horizontal line is the threshold line beyond which the device stops working due to the decrease in output gyro power. TIR optics without plasma processing reached to the threshold line at around 15000 hrs. Further, the defective TIR optics is plasma processed and most of the defects gets eliminated as shown in Figs. 6.13(b) and 6.14(b) due to the improvement in surface chemistry. Now, the device is realized with modified / plasma processed TIR optics and it is observed that it performs well without reduction in reflected power up to 9000 hrs of continuous operation (Fig. 6.15). The linear trend line suggests that the life of the optics increases significantly after plasma processing and may reach to the target of 50000 hrs.

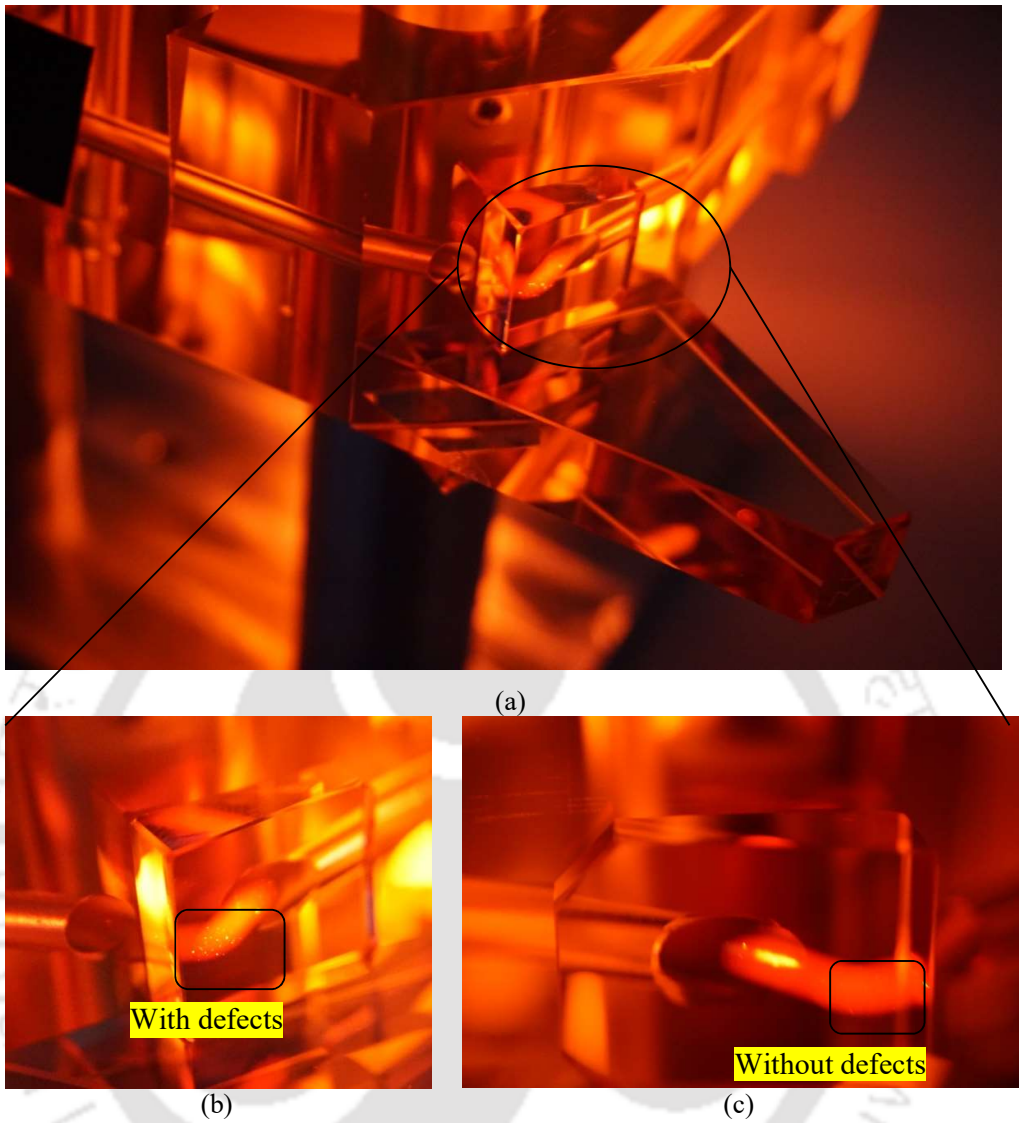

(a) (b) (c)

Fig.6.13 (a) Laser light inspection set up and zoomed view of specimen A (b) before and (c) after plasma polishing

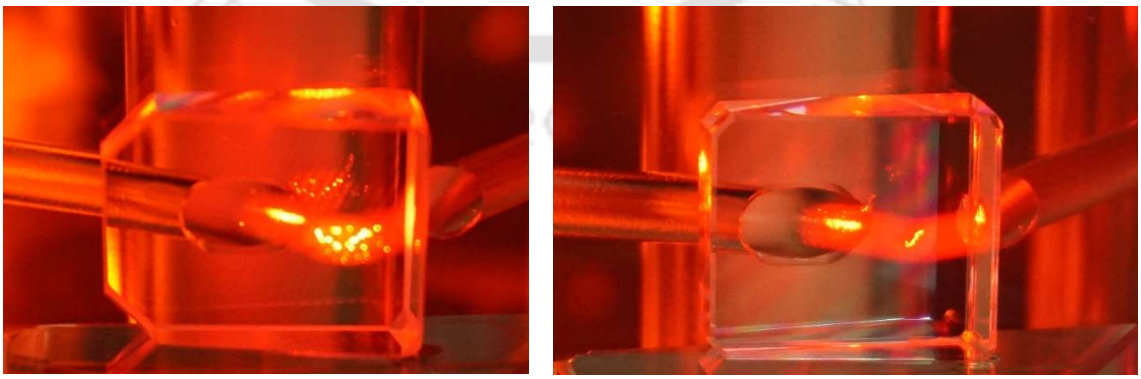

(a) (b)

Fig. 6.14 Laser light inspection of Optics B (b) before and (c) after plasma polishing

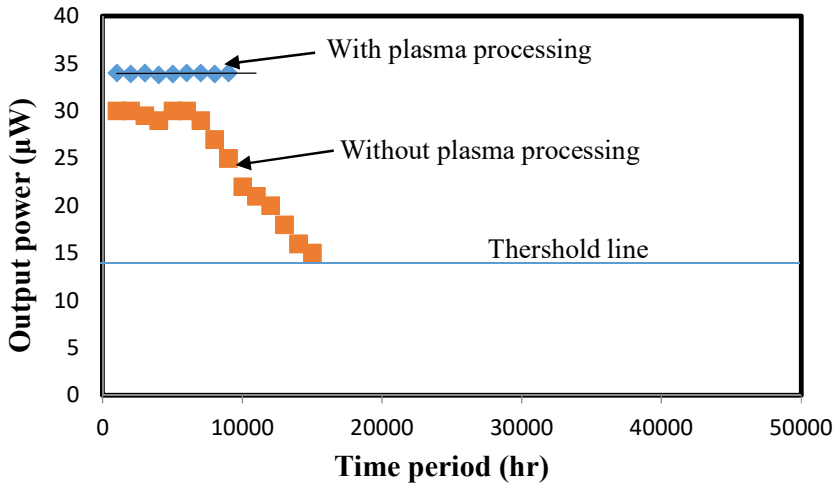

Fig. 6.15 Reflected output power variation of gyro device with time period

6.7 Summary

Chemical bond / structural network of fused silica prism is characterised and is analysed by Raman spectroscopy. The increase in ratio of area under 440 to 605 cm^{-1} confirms that the chemical bond structure of the surface is becoming more like bulk material and atomic level surface and sub-surface defects reduced distinctly. Even though marginal degradation of surface finish from 2 to 3 Å units is observed the surface figure has improved substantially as indicated by the reduction of PSD of higher wavelengths. Laser light inspection has revealed that the plasma polishing has removed the subsurface damage. A non-contact atomistic plasma polishing method is conceived, polishing set up designed and developed, process fine-tuned and implemented as super finishing process to remove molecular or atomic level defects in fine finished TIR prisms.

Chapter 7

CONCLUSIONS AND SCOPE FOR FUTURE WORK

7.1 Conclusions

7.1.1 Characterization techniques adopted

7.1.2 Preliminary experiments
7.1.3 Simulation of plasma process
7.1.4 Plasma processing of hemispherical shell
7.1.5 Plasma processing of total internal reflecting prisms
7.2 Scope for further work

7.1 Conclusions

A non-contact type atomistic medium plasma polishing method is conceived, polishing set up is designed and developed which is capable of polishing complex shaped glass or fused silica components up to a size of 40 mm diameter. The process is developed by conducting experiments on fused silica planar specimens. Optical emission spectroscopy based correlation model is developed to monitor material removal mechanism. The developed process with intermediate in-situ plasma cleaning is adopted for polishing hemispherical resonator shell which is a Gyro component. The process is fine-tuned and implemented as superfinishing process on prisms to remove molecular or atomic level defects which is already fine finished by ultra-high finishing process such as chemo-mechanical polishing.

The novelty of this process is that it combines the merits of isotropic etching by low pressure plasma and chemical vaporization by atmospheric pressure plasma process. The process is capable of simultaneously polishing entire complex 3D surfaces including cavities where no tool or beam can reach.

7.1.1 Characterization techniques adopted

- Optical emission spectroscopy is used to characterise the plasma and study the material removal and plasma-surface interaction mechanism. It is used as a tool to monitor the polishing process.
- Atomic Force Microscopy (AFM) is used for characterising surface finish and Raman spectroscopy to extensively evaluate surface integrity before and after plasma processing to confirm the efficiency of the finishing process.

7.1.2 Preliminary experiments

- Plasma polishing chamber is designed and built with zerodur material with an optical window. Components up to 40 mm diameter can be processed in this chamber.
- Stable plasma with processing gases such as He and Ne and reactive gases such as O_2 and SF_6 up to 30 mbar pressure is achieved by using dielectric barrier capacitive coupled RF discharge.
- Atomic emission spectroscopy is used to identify the relative density of the excited species in the plasma and monitor the various oxidation states of silica. A correlation model is established with respect to material removal rate and oxidation states of silica Si II and Si III.
- With Helium as processing gas and oxygen alone as reactive gas, surface modification is possible by medium pressure plasma. On machined fused silica surface, improvement in surface roughness is up to 68% with He-O_2 plasma while there is 85% improvement in surface waviness.
- It is identified that reactive radicals such as Fluorine are essential for sustained material removal. SF_6 is selected as reactive gas for plasma processing.
- The ratio of processing gas Vs. reactive gases and the ratio among reactive gases also are identified.
- Further surface finish improvement is achieved with He-SF_6-O_2 gas mixture plasma with a material removal rate of 0.008 mm^3/min.
- Helium as plasma processing gas and oxygen and Teflon as a source of fluorine also was studied but discontinued due to carbon contamination. However, SF_6 as fluorine sources is observed to be more practical and useful.
- Atomistic material removal has also enabled reduction in surface residual stresses and surface cracks thereby enhancing the surface integrity.

7.1.3 Simulation of plasma process

Simulation of the plasma process using FEM based software module i.e. Comsol® is used to analyse the distribution of the radicals inside plasma chamber with and without specimens. Further analysis for the ratio of free volume to the total available volume of the plasma chamber for uniform distribution of radicals is also carried out.

- The optimum position of planar specimen, hemispherical shell and prism inside the plasma chamber is identified for effective distribution of radicals and is adopted in experiments.
- The shape and size of electrodes outside plasma chamber are varied to get homogenous distribution of reactive species and ions. In the presence of hemispherical shell component, the four sided electrode (i.e. L shaped) provides higher density of radicals.
- The simulation results are validated with experimental measured electron temperature data using atomic spectroscopy and analytical model.
- The average temperature calculated from simulation study is approximately 550 K which can be considered as 'cold plasma' process.

7.1.4 Plasma processing of hemispherical shell

A typical gyro component, the hemispherical resonator shell, is made of fused silica having complex free form surfaces. The main objective is to uniformly polish the hemispherical resonator shell which is fabricated by a rotary ultrasonic milling process.

- A combination of plasma polishing and intermediate cleaning process is arrived to have sustained polishing of the hemispherical shell. Sustained material removal rate of 0.026 mm^3/min is achieved during this process.
- The uniformity of material removal is ensured with reduction of frequency mismatch of hemispherical shell and surface integrity by enhanced Q factor after each plasma processing using Laser Doppler Vibrometer. Uniform and isotropic plasma machining is ascertained by 18% reduction in frequency mismatch between two orthogonal modes.
- Significant improvement in Q factor of hemispherical shell is achieved which suggests the enhancement of surface integrity and the reduction of surface and sub-surface defects.
- After multiple level of plasma processing, 22 nm surface roughness (Ra) is achieved.
- The molecular network of fused silica is studied using Raman spectrometer. The Raman spectroscopy analysis provides clear evidence of reduction in strain bonds after plasma processing. There is significant reduction of puckered four-member and three-member ring structures indicating reduction of surface strain caused by milling process.

- Compared to existing methods, the present plasma processing technique induces very low substrate heating.

7.1.5 Plasma processing of total internal reflecting prisms

The subsurface damages (SSD) which are not observable in white light inspection become more observable with laser light inspection resulting in poor yield of CMP finished TIR prisms for a laser Gyro application. The developed plasma processing method has been successfully applied as super finishing process for prisms already finished by chemo-mechanical contact polishing process.

- Chemical bond / structural network of fused silica optics is characterized and is analyzed by Raman spectroscopy. The increase in ratio of area under 440 to 605 cm^{-1} confirms that the chemical bond structure of the surface is becoming more like bulk material and atomic level surface and sub-surface defects are reduced distinctly.
- Improvement in surface figure is achieved as indicated by reduction of PSD of higher wave length (waviness) even though there is marginal degradation of surface finish from 2 to 3 Å (Ra).
- Laser light inspection of post plasma polishing revealed that the plasma polishing has removed / minimized the sub surface damages.
- The plasma polished prisms when used in gyro, has shown increased life span without reduction of laser intensity which is observed with CMP finished prisms.
- The developed plasma process is able to remove brittle damage, filled up surface / subsurface cracks and plastic deformation caused by the chemo-mechanical polishing.

7.2 Scope for further work

In the presently developed plasma process, the processing and reactive gases are filled inside the chamber to the required compositions and pressure for polishing of the components. The gas mixture composition and pressure inside plasma chamber changes with time due to the release of volatile by-products such as SiF_4 and SiO_2 gases.

- Periodic plasma cleaning of both plasma chamber and component surface is mandated to ensure continued polishing (material removal). If there is a provision of continuous replenishing and purging of processing and reactive gases, then the polishing process will be continuous. Studies of continuous replenishment of plasma gases are essential to establish this process as an industrial process.

- It is observed in mechanically machined hemispherical shell that the damaged layer exists till 20 to 30 µm. Therefore, complete elimination of these damaged layers is not possible with the presently developed plasma process. Hence, modification in the present plasma process is essential for improving material removal rate.
- The plasma polishing can be optimized as a pre-process for thin film coating and tailoring of surface energy suitable for required application.

REFERENCES

1. Achim, J. L; Eric, G; Thwaite, F. L; Jean, B. M. (1992) Polishing study using Teflon and Pitch Laps to produce flat and supersmooth surfaces. *Applied Optics 1992, Vol. 31, No. 10:* 1472-82.
2. Arnold, T; Boehm, G; Eichentopf, I; Janietz, M; Meister, J; Schindler, A. (2010) Plasma Jet Machining - A novel technology for precision machining of optical elements. *Vakuum in Forschung und Praxis*, 22: 10–16.
3. Burakov, M; Bulgakova, N.M; Stoian, R. (2007) Spatial distribution of refractive index variations induced in bulk fused silica by single ultra short and short laser pulses. *Journal of Applied Physics*, 101 (4) Article ID043506.
4. Chan, J. W; Huser, T; Risbud, S; Krol, D. M. (2001) Structural changes in fused silica after exposure to focused femtosecond laser pulses. *OPTICS LETTERS*, 26 (21): 1726-1728.
5. Chang, Y.P; Hashimura, M; Dornfield, D.A. (2000) An Investigation of Material Removal Mechanisms in Lapping with Grain Size Transition. *Journal of Manufacturing Science and Engineering*, 122: 413-419.
6. Coburn, J.W; Winters, H. F. (1979) Ion and electron-assisted gas-surface chemistry-An important effect in plasma etching. *Journal of Applied Physics*, 50: 3189-3196.
7. Crinteal, D; Czarnetzki, U; Iordanova, S; Koleva, I; Luggenhölscher, D. (2009) Plasma diagnostics by optical emission spectroscopy on argon and comparison with Thomson scattering. *J. Phys. D: Appl. Phys.*, 42: 045208, doi:10.1088/0022-3727/42/4/045208.
8. Demos, S.G; Burnham, A; Wegner, P. (2000) Surface defect generation in optical materials under high fluence laser irradiation in vacuum. *Electron. Lett.*, 36: 566-567.
9. Dev, D; Krishna, E; Das, M. (2016) A Novel Plasma assisted atomistic surface finishing on freeform surfaces of fused silica. *International Journal of Precision Technology*, 6: 262–276.
10. Dev, D; Krishna, E; Das, M. (2018) Novel finishing process development for precision complex shaped hemispherical shell by bulk plasma processing Precision

Product Process design and Optimization, Lecture notes on Multidisciplinary Industrial Engineering: 313-335.

11. Dong, Z. C; Cheng, H. B; Ye, X; Tam, H. Y. (2014) Subsurface damage of fused silica lapped by fixed-abrasive diamond pellets. *Applied Optics*, 53(26): 5841-5849.
12. Duparré, A; Ferre-Borrull, J; Gliech, S; Notni, G; Steinert, J; Bennett, J. M. (2002) Surface characterization techniques for determining the root-mean-square roughness and power spectral densities of optical components. *Appl. Opt.* 41: 154-171.
13. Gadelmawla, E. S; Koura, M. M; Maksoud, T.M. (2002) Roughness parameters. *Journal of Materials Processing Technology*, 123 (1): 133-145.
14. Galeener, F.L; Geissberger, A. E. (1983) Vibrational dynamics in Si-substituted vitreous SiO2, *Physical Review B*, vol. 27 (10): 6199–6204.
15. Galeener, F.L; Leadbetter, A.J; Stringfellow, M.W. (1983) Comparison of the neutron, Raman, and infrared vibrational spectra of vitreous SiO2, GeO2, and BeF2. *Physical Review B*, vol. 27 (2): 1052–1078.
16. Genin, F.Y; Salleo, A; Pistor, T.V; Chase, L.L. (2001) Role of light intensification by cracks in optical breakdown on surfaces. *J.Opt. Soc. Am.*, 18 (10): 2607–2616.
17. Gerhard, C; Weihs, T; Luca, A; Wieneke, S. (2013) Polishing of optical media by dielectric barrier discharge inert gas plasma at atmospheric pressure. *Journal of the European Optical Society - Rapid Publications*, 8: 13081-13085.
18. Gerhard, C; Weihs, T; Luca, A; Wieneke, S. (2013) Polishing of optical media by dielectric barrier discharge inert gas plasma at atmospheric pressure. *Journal of the European Optical Society - Rapid Publications*, 8: 13081-13085.
19. Gessenharter, A; Riemer, O; Brinksmeier, E (2003) ASEE ELD Nashville Annual Conference. Proceedings of the 18th ASPE, Nashville, June 22-25 2003.
20. Gillman, B. E; Tinker, F (1999) Fun facts about pitch and the pitfalls of ignorance. SPIE 3782:72-79.
21. Grebenshchikov, I. (1931) Keram i Steklo, 7:36.
22. Griem, H. R. (1964) Plasma Spectroscopy. New York: McGraw-Hill.
23. Griem, H. R. (1997), Principles of Plasma Spectroscopy. Cambridge University Press: Cambridge, UK.
24. Hamza, A.V; Siekhaus, W.J; Rubenchik, A.M; Feit, M; Chase, L,L; Savina, M; Pellin, M.J; Hutcheon, I.D, Nostrand, M.C; Runkel, M; Choi, B.W; Staggs, M; Fluss, M.J. (2002) Engineered defects for investigation of laser-induced damage of fused silica at 355 nm, *Proc. SPIE*, 4679: 96–107.

25. Izumitani, T. (1988) Optical glass. American Institute of Physics, New York.
26. Jain, R.K; Jain, V.K; Dixit, P.M. (1999) Modelling of Material Removal and Surface Roughness in Abrasive Flow Machining Process. *International Journal of Machine Tools and Manufacture*, 39: 1903-1923.
27. Jairath, R; Desai, M; Stell, M; Telles, R; Scherberbrewer, S (1994) Consumables for the chemical mechanical polishing (CMP) of dielectrics and conductors. Mat. Res. Soc. Symp. Proc., San Francisco, 337:121.
28. Jean M. B; Joseph J. S; Yukio S; Yoshiharu, N. (1983) Float polishing of optical materials. *Applied Optics, Vol. 26*, No. 4: 696-703.
29. Jin, H.L; Wang, B; Zhang, F.H. (2010) Effect on surface roughness of zerodur material in atmospheric pressure plasma jet processing. *Proceedings of SPIE - The International Society for Optical Engineering*, 7655.
30. Kamimura, T; Akamatsu, S; Yamamoto, M. (2003) Enhancement of surface-damage resistance by removing a subsurface damage in fused silica, in Laser-Induced Damage in Optical Materials. *Proceedings of SPIE,* 5273: 244–249.
31. Kano, K; Suzuki, M; Akatsuka, H. (2000) Spectroscopic measurement of electron temperature and density in argon plasmas based on collisional-radiative model. *Plasma Sources. Sci. Technol*., 9: 314, doi:10.1088/0963-0252/9/3/309.
32. Kim, W. B; Lee, S. H; Min, B. K (2005) Surface Finishing and Evaluation of Three-Dimensional Silicon Microchannel Using Magnetorheological Fluid. J. Manuf. Sci. Eng. 126: 772-728, https://doi.org/10.1115/1.1811113.
33. Komanduri, R; Lucca, D. A; Tani, Y. (1997) Technological advances in Fine Abrasive Processes. *Annals of CIRP*, 46: 545-596.
34. Kordonski, W; Jacobs, S. (1996) Model of Magnetorheological Finishing. *Journal of Intelligent Material Systems and Structures*, 7 (2): 131-137.
35. Kubota, A; Shinbayashi, Y; Hidekazu, M; Sano, Y; Inagaki, K; Yuzo, M; Yamauchi, K. (2006) Investigation of the Surface Removal Process of Silicon Carbide in Elastic Emission Machining. *Journal of Electronic Materials*, 36 (1): 92-97.
36. Leach, R. K. (2010) Introduction to metrology for micro- and nanotechnology. Elsevier publication.
37. Leistner, A. J (1976) Teflon polishers: Their manufacture and use. Appl. Opt. 15: (2).

38. Leistner, A. J; Thwaite, E. G; Lesha, F; Bennett, J. M. (1992) Polishing study using Teflon and pitch laps to produce flat and supersmooth surfaces. *Applied Optics*, 31: 1472-1482.
39. Li, X; Ling, L; Hua, X; Fukasawa, M; Oehrlein, G. S; Barela, M; Anderson, Harold M. (2002) Effects of Ar and O_2 additives on SiO_2 etching in C_4F_8-based plasmas. *Journal of Vacuum Science &Technology A*, 21: 284-293.
40. Li, Y; Liu, Z; Xie, R; Wang, J; Xu, Q. (2010) The surface layer of fused silica finished by various polishing techniques. *Symposium on Photonics and Optoelectronic* (SOPO): 1–6.
41. Li, Y; Wu, Y. B; Zhou, L; Guo, H; Cao, J; Fujimoto, M; Kemmochi, M (2012) Investigation into Chemo-Mechanical Fixed Abrasive Polishing of Fused Silica with the Assistance of Ultrasonic Vibration. Key Engineering Materials, 523 – 524.
42. Li, Y; Yuan, Z; Wang, J; Xu, Q. (2017) Laser-induced damage characteristics in fused silica surface due to mechanical and chemical defects during manufacturing processes, *Optics & Laser Technology*, 91: 149–158.
43. Li, Y; Zheng N; Li, H; Hou, J; Lei, X; Chen, X; Yuan, Z; Guo, Z; Wang, J; Guo, Y; Xu, Q. (2011) Morphology and distribution of subsurface damage in optical fused silica parts: bound-abrasive grinding. *Appl. Surf. Sci*., 257: 2066–2073.
44. Liu, F.X; Qian, J.Y; Wang, X.L; Liu, L; Ming, H. (1997) UV irradiation-induced defect study of GeO2-SiO2 glasses by Raman spectroscopy. *Physical Review B*, vol. 56 (6): 3066–3071.
45. Liu, H; Ye, X; Zhou, X; Huang, J; Wang, F; Zhou, X; Wu, W; Jiang, X; Sui, Z; Zheng, W. (2014) Subsurface defects characterization and laser damage performance of fused silica optics during HF-etched process. *Opt. Mater.*, 36 (5): 855–860.
46. Liu, W; Wang, D; Hu, M; Wang, Y; Liang, H; Hang, L. (2009) Roughness evolution of fused silica during plasma polishing processes. 4th *International Symposium on Advanced Optical Manufacturing and Testing* Technologies: *Advanced Optical Manufacturing Technologies*, 7282.
47. Lochte-Holtgreven, W. (1968) Plasma Diagnostics. Amsterdam: North-Holland.
48. Loveless, T.R; Williams, R.E; Rajurkar, K.P. (1994) A study of the effects of abrasive flow finishing on various machined surfaces. *Journal of Materials Processing Technology*, 47: 133-151.
49. Marr, G. (1968), Plasma Spectroscopy. Elsevier Publishing Company: Barking, UK.

50. Menapacea, J.A; Penetrantea, B; Golinib, D; Slomba, A; Millera, P.E; Parham, T; Nicholsa, M; Petersona, J. (2002) Combined advanced finishing and UV-laser conditioning for producing UV-damage-resistant fused-silica optics. *Proc. SPIE*, 4679: 56.
51. Na, L; Qiang, X; Peng, Z; Bo, W (2015) Atmospheric Pressure Plasma Processing of Fused Silica in Different Discharge Modes. *Plasma Science and Technology*, 17: 567-573.
52. Namba, Y; Tsuwa, H (1987) Ultra-Precision Float Polishing Machine. Annals of the CIRP, Vol 36:1.
53. Negres, R.A; Burke, M.W; Sutton, S.B; De Mange, P; Feit, M.D; Demos, S.G. (2007) Evaluation of UV absorption coefficient in laser-modified fused silica. *Applied Physics Letters*, 90 (6) Article ID 061115.
54. Paetzelt, H; Böhm. G; Arnold, T. (2013) Plasma jet polishing of rough fused silica surfaces. *Proceedings to euspen 13th International Conference*: 19–22.
55. Peng, W.Q; Guan, C.L; Li, S.Y. (2014) Efficient fabrication of ultra-smooth and defect-free quartz glass surface by hydrodynamic effect polishing combined with ion beam figuring. *Opt. Express*, (22): 13951–13961.
56. Preston, F. (1930) J Soc Glass Tech, 14:127.
57. Przyklenk, K. (1986) AFM- a process for surface finishing and deburring of workpieces with a complicated shape by means of an abrasive laden medium. ASME, New York, PED, 22: 101-110.
58. Rauschenbach, B; Frost, F; Ziberi, B; Schindler, A. (2008) Surface engineering with ion beams: from self-organized nanostructures to ultra-smooth surfaces. *Applied Physics, A* 91: 551–559.
59. Rhoades, L.J. (1988) Abrasive Flow Machining. *Manufacturing Engineering*, 1: 75-78.
60. Rhoades, L.J. (1991) Abrasive flow machining - a case study. *Journal of Materials Processing Technology*, 28: 107-116.
61. Sakata, Y; Sakai, K; Nonaka, K. (2014) Stress-induced light scattering method for the detection of latent flaws on fine polished glass substrates. *Rev. Sci. Instrum.*, 85 (8): 083303-1.
62. Sakata, Y; Terasaki, N; Nonaka, K. (2017) Development of a novel non-contact inspection technique to detect micro cracks under the surface of a glass substrate by

thermal stress-induced light scattering method. *Optics & Laser Technology*, 90: 80-83.

63. Schenkerand, R.E; Oldham, W.G. (1997) Ultraviolet-induced densification in fused silica, *Journal of Applied Physics*, vol. 82 (3): 1065–1071.
64. Schmidt N, Schulze J, Schüngel E, Czarnetzki U (2013) Effect of structured electrodes on heating and plasma uniformity in capacitive discharges. J. Phys. D: Appl. Phys. 46: 505202, doi: 10.1088/0022-3727/46/50/505202.
65. Seok, J; Kim, Y.J; Jang, K.I; Min, B. K; Lee, S.J (2007) A study on the fabrication of curved surfaces using magnetorheological fluid finishing. Int J Mach Tool Manu. 47: 2077-2090.
66. Shen, J; Liu, S; Yi, K; He, H; Shao, J; Fan, Z. (2005) Subsurface damage in optical substrates. *Optik* 116: 288–294.
67. Skoog, D. A; Holler, F. J; Crouch, S. R. (2006) Principles of instrumental analysis. 6th ed. Cengage Learning.
68. Suratwala, T.I; Miller, P.E; Bude, J.D; Steele,W.A; Shen, N; Monticelli, M.V; Feit, M.D; Laurence, T.A; Norton, M.A; Carr, C.W; Wong, L.L. (2011) HF-based etching processes for improving laser damage resistance of fused silica optical surfaces. *J. Am. Ceram. Soc.*, 94 (2): 416-428.
69. Suratwala, T; Wong, L; Miller, P; Feit, M. D; Menapace, J; Steele, R; Davis, P; Walmer, D. (2006) Sub-surface mechanical damage distributions during grinding of fused silica. *Journal of Non-Crystalline Solids*, 352: 5601-5617.
70. Sutton, S (2004) Development of new synthetic optical polishing pitches", OSA Technical Digest Series Optical Society of America.
71. W. Xu, X. Lu, Guoshun Pan, Yuanzhong Lei, Jianbin Luo "Ultrasonic flexural vibration assisted chemical mechanical polishing for sapphire substrate" Applied Surface Science 256 3936–3940, 2010.
72. Wang, B; Zhang, J; Dong, S. (2009) New development of atmospheric pressure plasma polishing. *Chinese Optics Letters*, 7: 537-538.
73. Wang, B; Zhao, Q. L; Wang, L. P; Dong, S. (2006) Application of Atmospheric Pressure Plasma in the Ultrasmooth Polishing of SiC Optics. *Materials Science Forum*, 532-533: 504-507.
74. Wang, D. F (2013) study on Atmospheric Pressure Plasma Processing of Fused Silica. *Advanced Materials Research*, 706-708: 270-273.

75. Wang, D; Liua, W; Wub, Y; Hang, L; Yu, H; Jin, N. (2011) Material removal function of the capacitive coupled hollow cathode plasma source for plasma polishing. *Physics Procedia,19*: 408–411.
76. Wang, J; Li, Y; Han, J; Xu, Q; Guo, Y. (2011) *Eur. Opt. Soc. Rapid Publ*., 6: 11001-11016.
77. Whitehouse, D. J. (1994) Handbook of surface metrology. 1st Ed., institute of physics: Bristol.
78. Wilson, S. R; Mcneil, J. R (1987) Neutral ion beam figuring of large optical surfaces. Proc. SPIE 818: 320-324.
79. Xiao, H; Chen, Z; Wang, H; Wang, J; Zhu, N. (2018) Effect of grinding parameters on surface roughness and subsurface damage and their evaluation in fused silica. *Optics Express*, 26(4): 4638-4655.
80. Xie, Y, Bhushan, B (1996) Effects of particle size, polishing pad and contact pressure in free abrasive polishing. Wear, 200: 281–295.
81. Xu, M; Dai, Y; Zhou, I; Peng, X; Chen, S; Liao, W. (2018) Evolution mechanism of surface roughness during ion beam sputtering of fused silica. *Applied Optics*, 57 (20): 5566-5573.
82. Xu, M; Dai, Y; Zhou, L; Shi, F; Wan, W; Xie, X; Sui, T. (2016) Investigation of surface characteristics evolution and laser damage performance of fused silica during ion-beam sputtering. *Optical Materials*, 58: 151-157.
83. Xu, S; Zu, X; Jiang, X. (2008) The damage mechanisms of fused silica irradiated by 355 nm laser in vacuum. *Nuclear Instrument sand Methods in Physics Research B: Beam Interactions with Materials and Atoms*, vol. 266 (12-13): 2936–2940.
84. Yaguo, Li; Jian, W. (2009) Surface characteristics of an optical component manufactured with a polyurethane lap. *Applied Optics Vol. 48, No.* 4: 737-42.
85. Yao, Y.X; Wang, B; Wang, J.H; Jin, H.L; Zhang, Y.F; Dong, S. (2010) Chemical machining of Zerodur material with atmospheric pressure plasma jet. *CIRP Annals-Manufacturing Technology*, 59: 337-340.
86. Yoshiyama, J; Genin, F.Y; Salleo A; Thomas, I; Kozlowski, M.R; Sheehan, L.M. (1998) Effects of polishing, etching, cleaving and water leaching on the UV laser damage of fused silica. *Proc. SPIE*, 3244: 331-40.
87. Yu, N; Jourdain, R; Gourma, M; Shore, P. (2016) Analysis of De-Laval nozzle designs employed for plasma figuring of surfaces. *Int J Adv Manuf Technol*, 87: 735–745.

88. Zhang, J; Li, B; Wang, B; Dong, S. (2013) Analysis on formation mechanism of ultra-smooth surfaces in atmospheric pressure plasma polishing. *International Journal of Advanced Manufacturing Technology*, 65: 1239-1245.
89. Zhang, J; Wang, B; Dong, S. (2008) Application of atmospheric pressure plasma polishing method in machining of silicon ultra-smooth surfaces. *Frontiers of Electrical and Electronic Engineering*, 3: 480-487.
90. Zhi, Z; Xiaotao, Z; Xiaodong, J; Xia, X; Jin, H; Xinda, Z; Chunhong, L; Wanguo, Z; Li, L. (2012) Effect of HF etching on the surface quality and laser-induced damage of fused silica. *Opt. Laser Tec.*, 44: 1039-42.
91. Zhu, X; Pu, Y. (2007) A simple collisional-radiative model for low-pressure argon discharges. *J. Phys., D: Appl. Phys*. 40: 2533, DOI: 10.1088/0022-3727/40/8/018.
92. Zhu, X; Pu, Y; Balcon, N; Boswell, R. (2009) Measurement of the electron density in atmospheric-pressure low-temperature argon discharges by line-ratio method of optical emission spectroscopy. *J. Phys. D: Appl. Phys*. 42: 142003, doi:10.1088/0022-3727/42/14/142003.

List of Publications

Papers published in Journals:

1. D. Sam Dayala Dev, Enni Krishna, Manas Das, "A Novel Plasma assisted atomistic surface finishing on freeform surfaces of fused silica, International Journal of Precision Technology, (2016) 6 (3/4), 262-276.
2. D. Sam Dayala Dev, Enni Krishna, Manas Das, Development of a non-contact plasma processing technique to mitigate chemical network defects of fused silica with life enhancement of He-Ne laser device, Optics and Laser Technology, 113 (2019) 289-302.

Papers communicated to Journals:

1. D. Sam Dayala Dev, Enni Krishna, Manas Das, "Design and development of a novel plasma processing technique for uniform nano-polishing of freeform hemispherical shell", International Journal of Advanced Manufacturing Technology.
2. Enni Krishna, D. Sam Dayala Dev, Manas Das, "Cost effective uniform plasma machining of fused silica shell by induction of conditioning gas (Machining Science and Technology, Taylor and Francis).

Papers published in conference proceedings:

1. D Sam Dayala Dev, Enni Krishna, Manas Das, "Development of novel finishing process for precision freeform / complex shaped glass components by bulk plasma processing". AIMTDR 2016, College of Engineering, Pune.
2. D Sam Dayala Dev, Enni Krishna, Manas Das, "A Novel Plasma Assisted Atomistic Surface Finishing on Free Form Surfaces of Fused Silica" COPEN 9-2015, IIT Bombay.
3. Enni Krishna, D Sam Dayala Dev and Manas Das, Induction of conditioning and its optimization in non-conventional plasma machining process of fused silica, International Conference on Recent Innovations and Developments in Mechanical Engineering (IC-RIDME 2018), National Institute of Technology Meghalaya, Shillong, Meghalaya, November 8-10, 2018 (Paper ID 349).
4. Enni Krishna, D Sam Dayala Dev and Manas Das, Simulation for uniform plasma processing of hemispherical shell, 2nd International Conference on Computational Methods in Manufacturing, ICCMM 2019, Indian Institute of Technology Guwahati, March 8-9, 2019 (Paper ID 71).

Published book chapter:

1. D Sam Dayala Dev, Enni Krishna, Manas Das, "Novel Finishing Process development for Precision Complex-Shaped hemispherical shell by Bulk Plasma Processing", Precision Product-Process Design and Optimization, Springer (Selected Paper from AIMTDR 2016, Editors: S.S. Pande and U.S. Dixit), (2018), 313-335.

Book chapter (review completed)

1. D Sam Dayala Dev, Enni Krishna, Manas Das, “Induction of Conditioning gas and its Optimization in Non-Conventional Plasma Machining Process of Fused Silica”, Springer Book Series, Lecture Notes in Mechanical Engineering (Selected Paper from IC-RIDME 2018, NIT Meghalaya, Shillong).